THE RADIATION-DRIVEN WINDS AND X-RAY EMISSION OF MASSIVE STARS

David Cohen
Department of Physics and Astronomy
Swarthmore College

Véronique Petit and Stan Owocki (Delaware), Rich Townsend (Wisconsin), Asif ud-Doula (Penn St.), Gregg Wade (RMC), Jon Sundqvist (Leuven), Maurice Leutenegger (GSFC)

Jackie Pezzato (Swarthmore '17), Zequn Li (Swarthmore '16), Emma Wollman (Swarthmore '09)

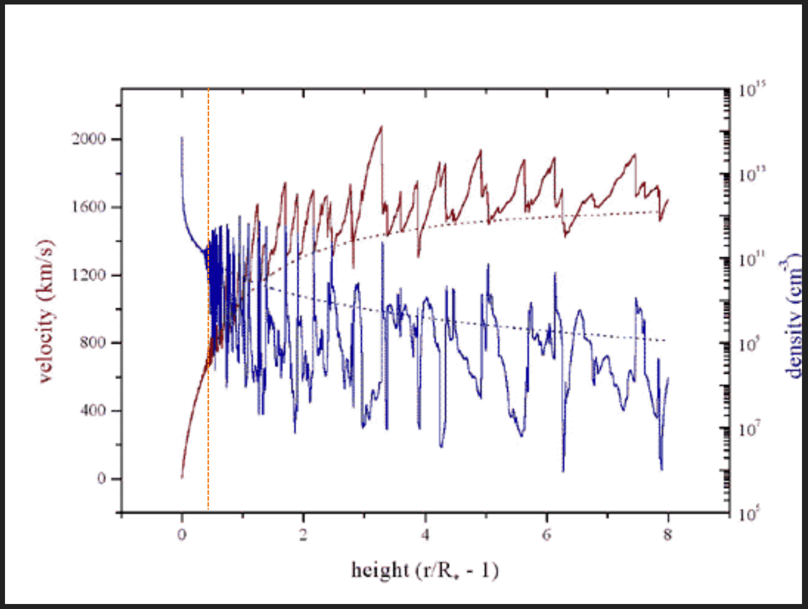

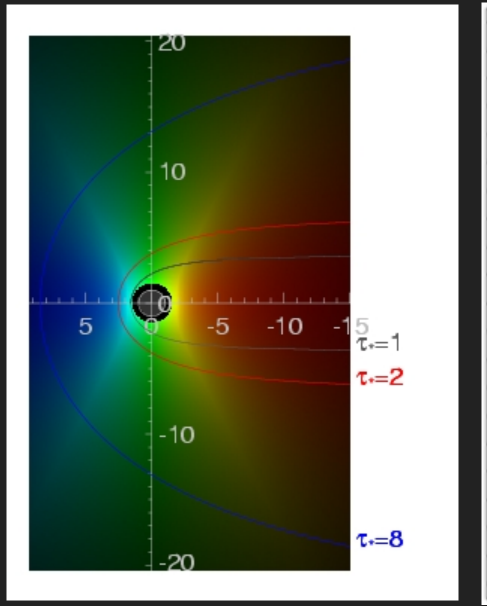

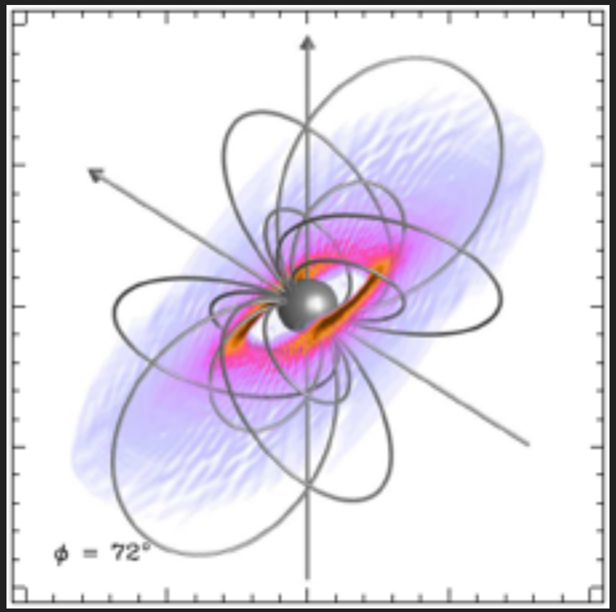

O STARS ARE STRONG X-RAY SOURCES

Carina Nebula

HD 93129A (O2If*)

Chandra/X-ray

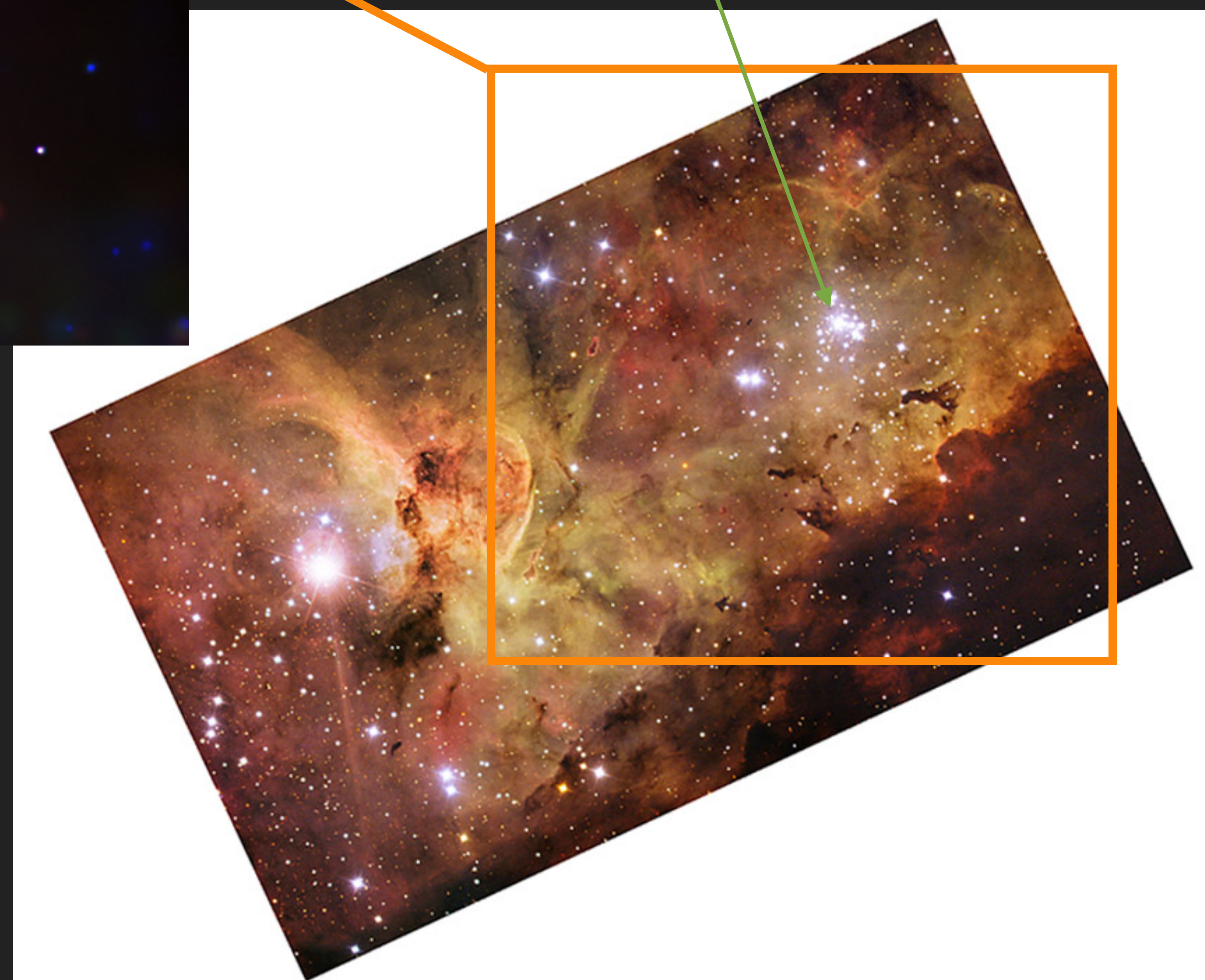

ESO/optical-IR

O STARS ARE DEFINED BY THEIR TREMENDOUS LUMINOSITIES

mass ~ 50 M_{sun}

luminosity ~ 10^6 L_{sun}

surface temperature ~ 45,000 K

Orion: the bright, blue stars are O stars

O STARS ARE DEFINED BY THEIR TREMENDOUS LUMINOSITIES

mass ~ 50 M_{sun}

luminosity ~ 10^6 L_{sun}

surface temperature ~ 45,000 K

Orion: the bright, blue stars are O stars

O STARS ARE DEFINED BY THEIR TREMENDOUS LUMINOSITIES

luminosity ~ 10^6 L_{sun}

O STAR RADIATION-DRIVEN WINDS

O stars are also defined by their strong, radiation-driven stellar winds

NGC 6888 Crescent Nebula - Tony Hallas

O STAR RADIATION-DRIVEN WINDS

UV absorption spectroscopy: P Cygni profile

ζ Pup (O4 supergiant): $\dot{M}$ ~ few 10^{-6} M_{sun}/yr

C IV 1548, 1551 Å

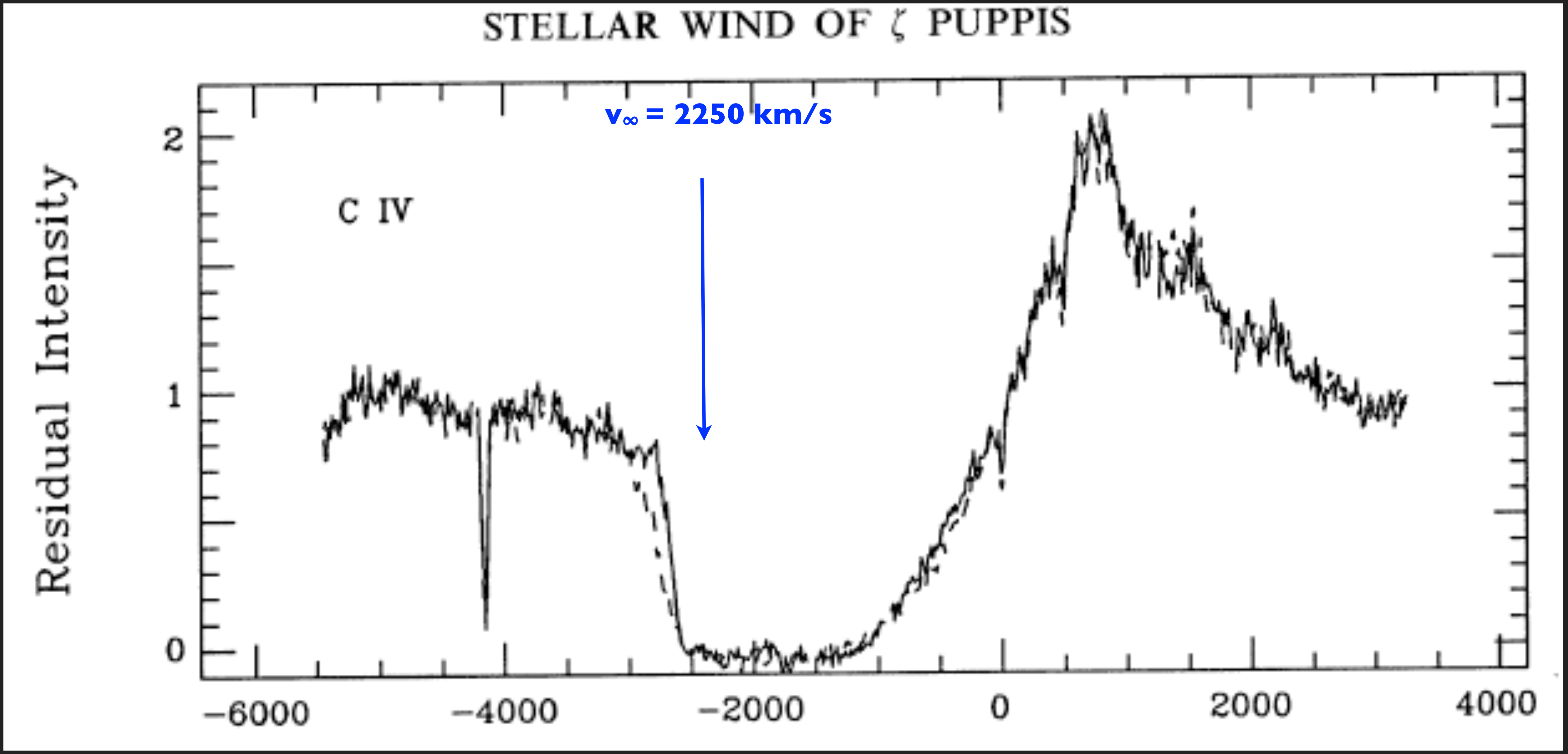

Velocity (km/s)

Prinja et al. 1992, ApJ, 390, 266

O STAR RADIATION-DRIVEN WINDS

UV absorption spectroscopy: P Cygni profile

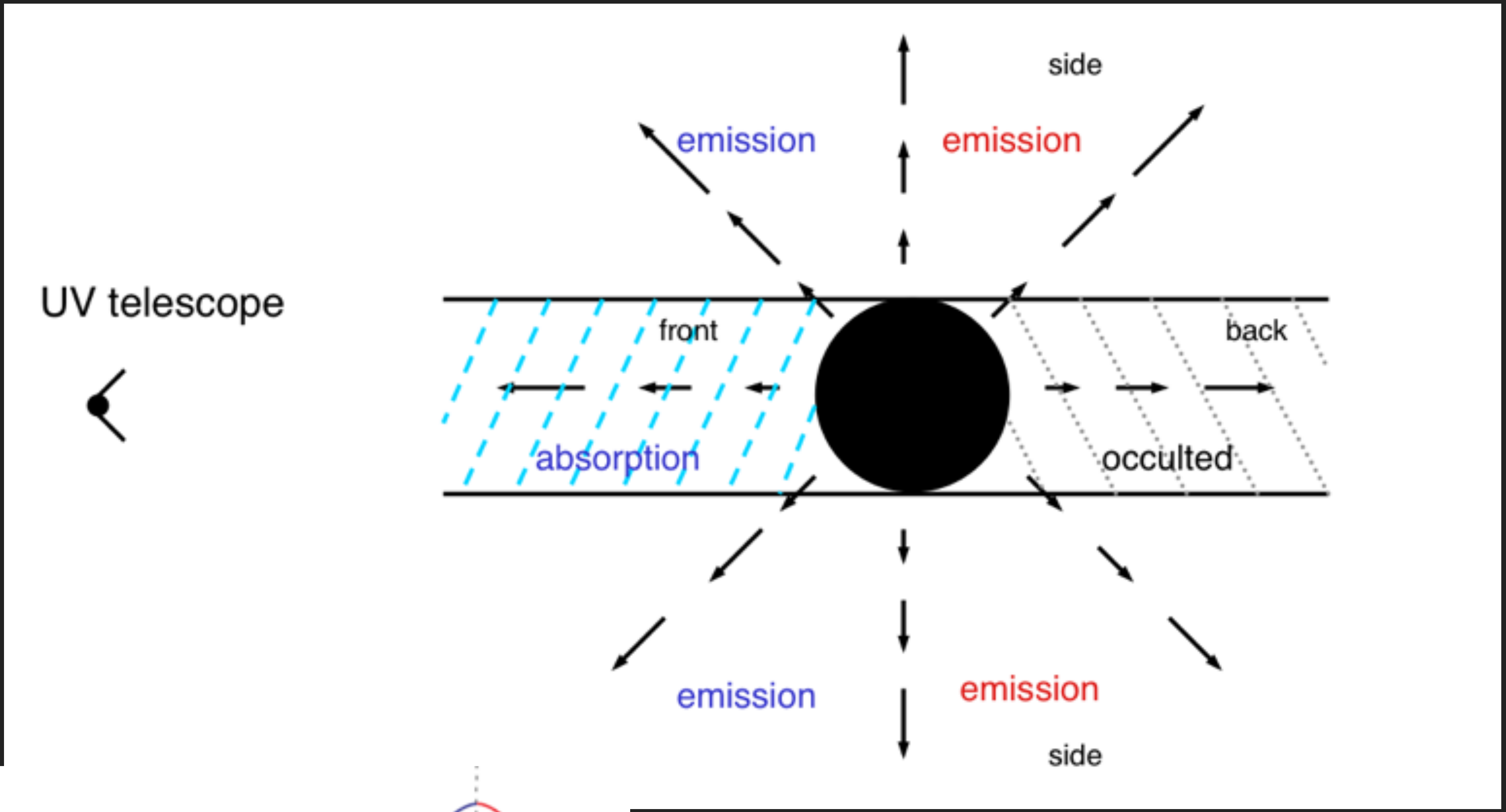

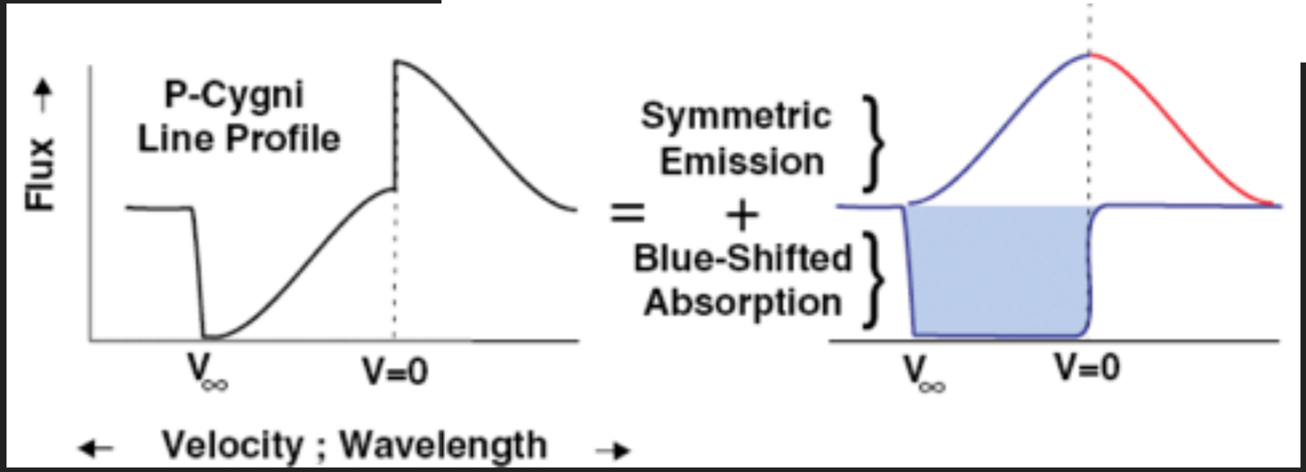

O STAR RADIATION-DRIVEN WINDS

UV absorption spectroscopy: P Cygni profile

ζ Pup (O4 supergiant): $\dot{M}$ ~ few 10^{-6} M_{sun}/yr   C IV 1548, 1551 Å

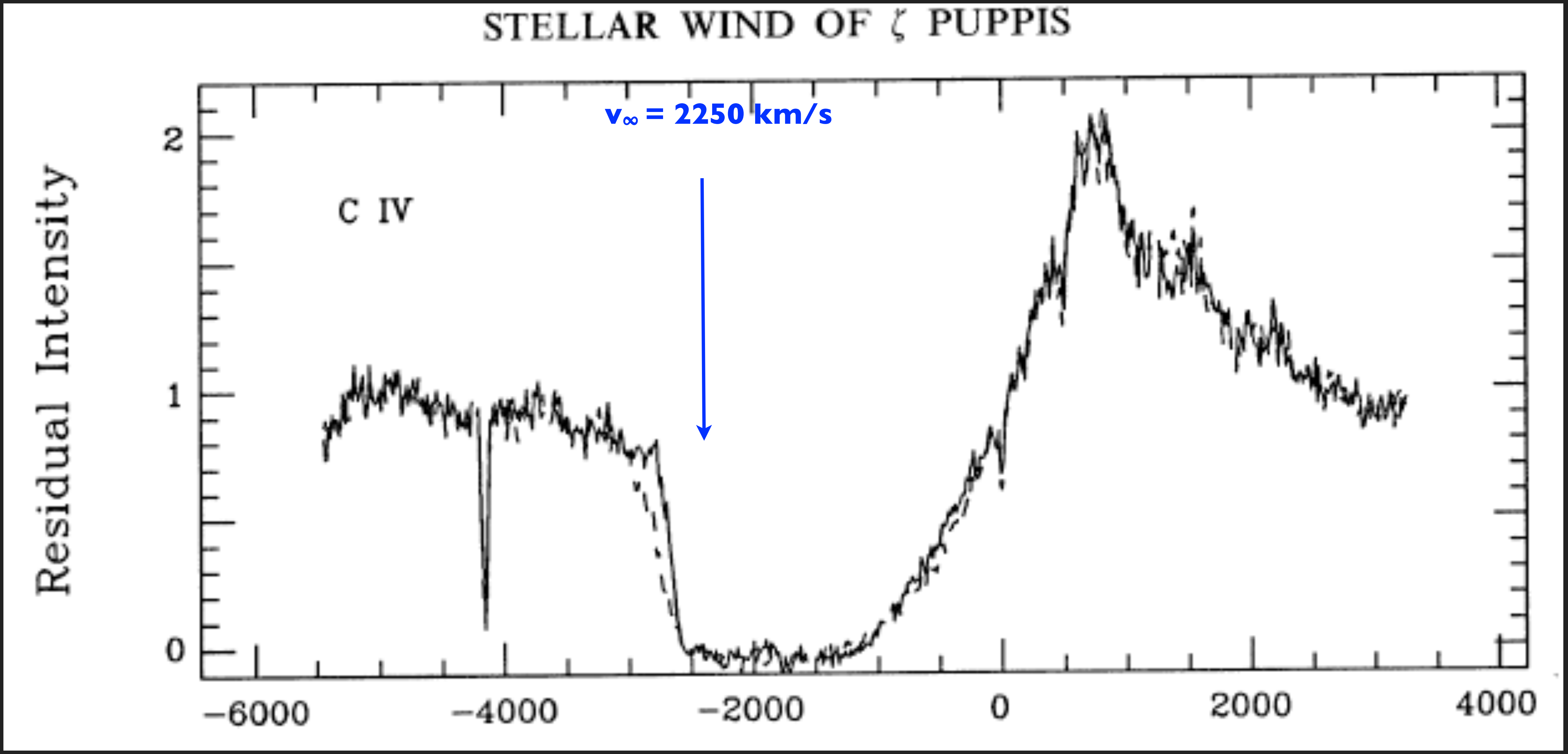

Velocity (km/s)

Prinja et al. 1992, ApJ, 390, 266

X-RAYS ARE PRODUCED BY EMBEDDED WIND SHOCKS (EWS)

intrinsic instability of radiative driving, Line Deshadowing Instability (LDI), leads to shock-heating of the wind

http://astro.swarthmore.edu/~cohen/presentations/ifrc3_xmbko1.e-2.gif

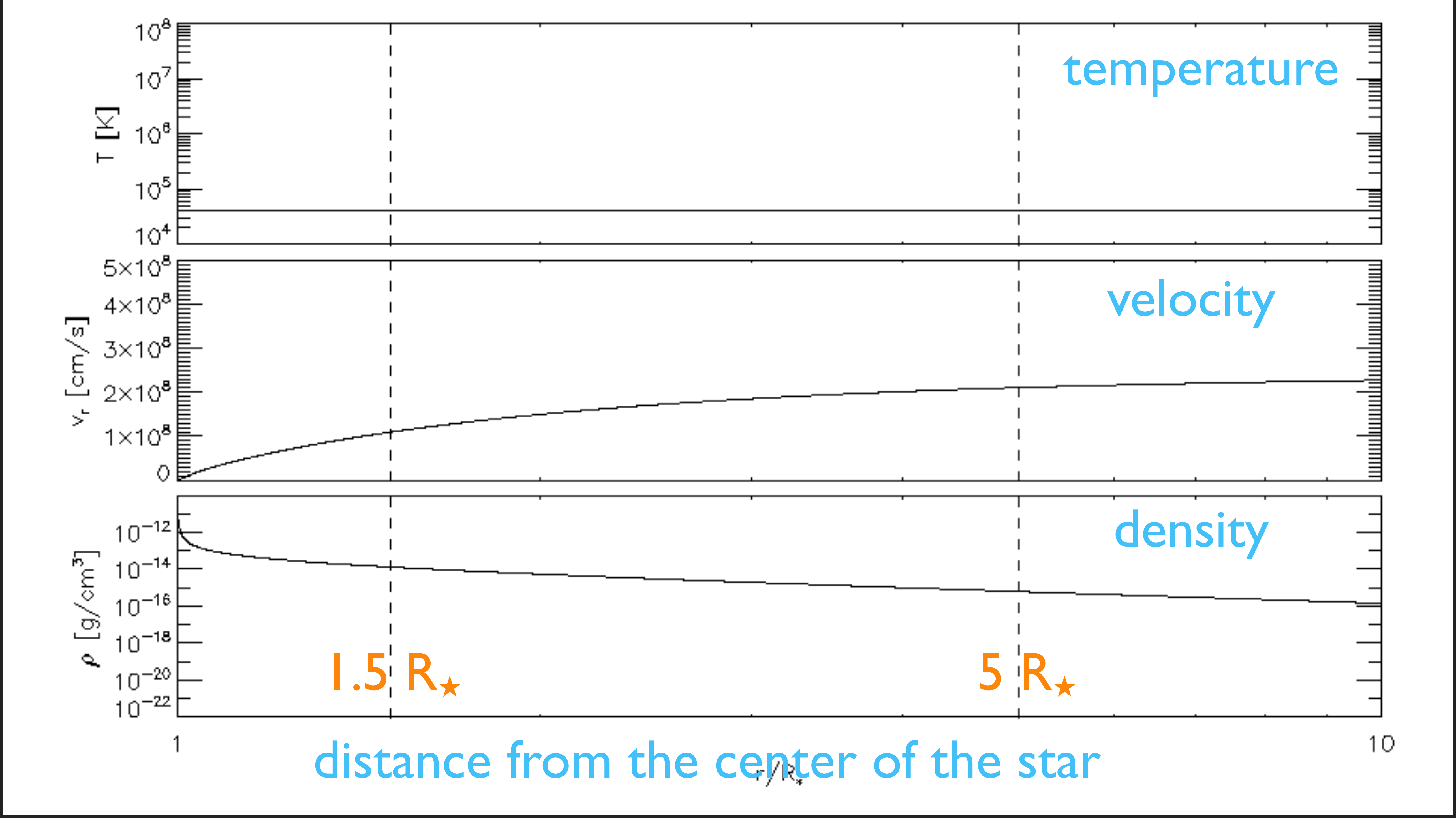

X-RAYS ARE PRODUCED BY EMBEDDED WIND SHOCKS (EWS)

A shock is a discontinuity where flow kinetic energy is converted to heat

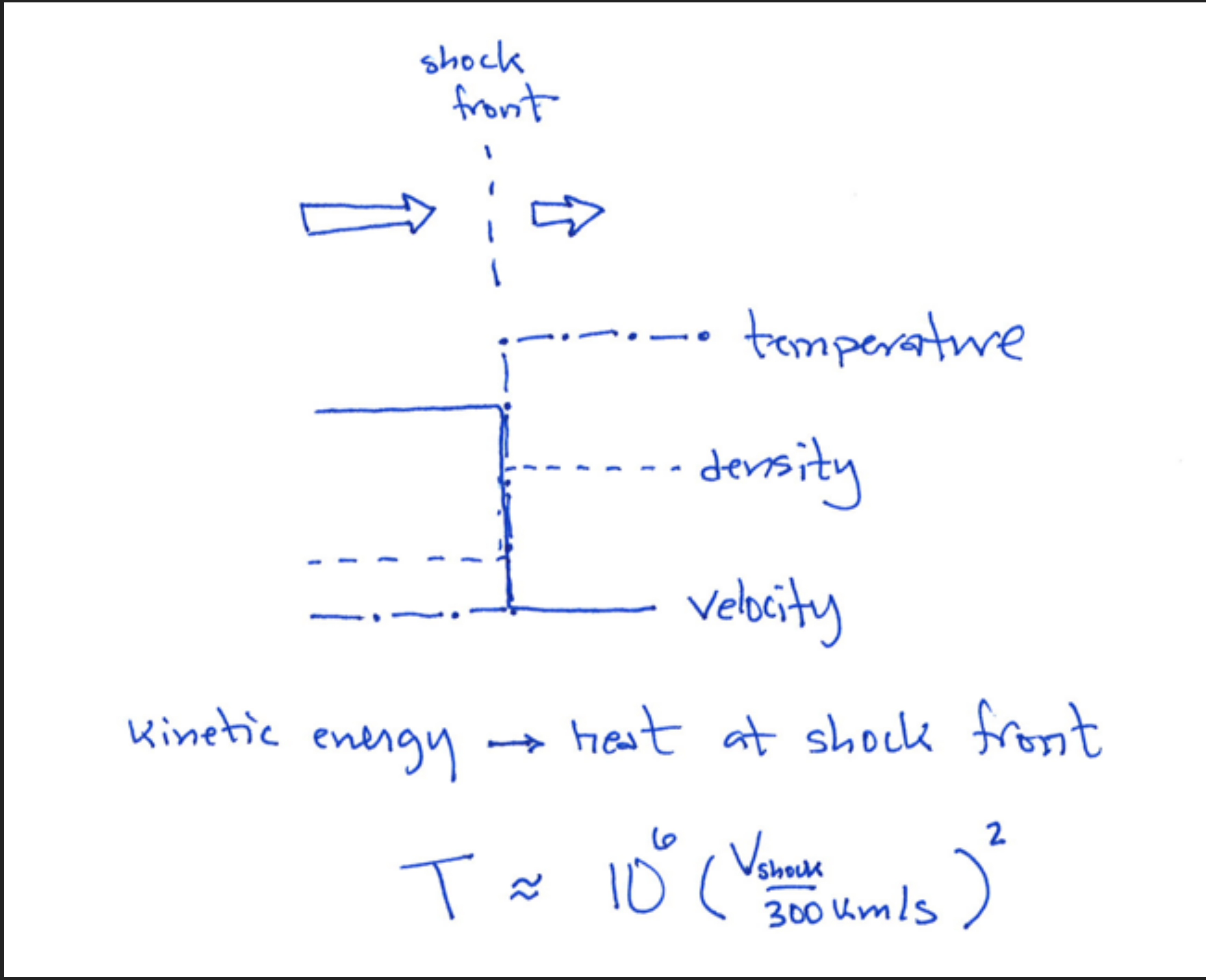

X-RAYS ARE PRODUCED BY EMBEDDED WIND SHOCKS (EWS)

Numerous shock structures distributed above $r \sim 1.5\ R_\star$

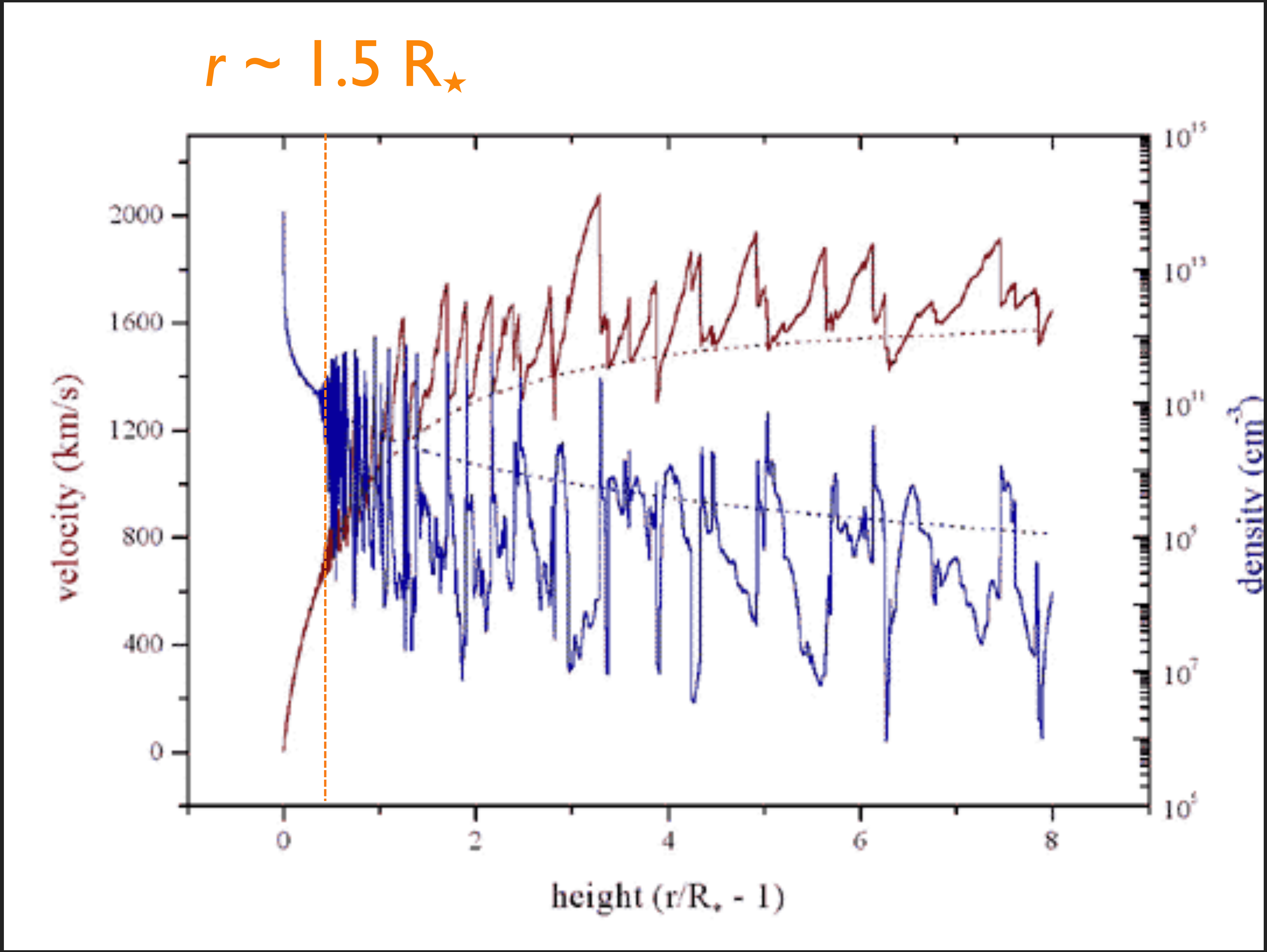

X-RAYS ARE PRODUCED BY EMBEDDED WIND SHOCKS (EWS)

V_{shock} ~ 300 km/s : T ~ 10^6 K

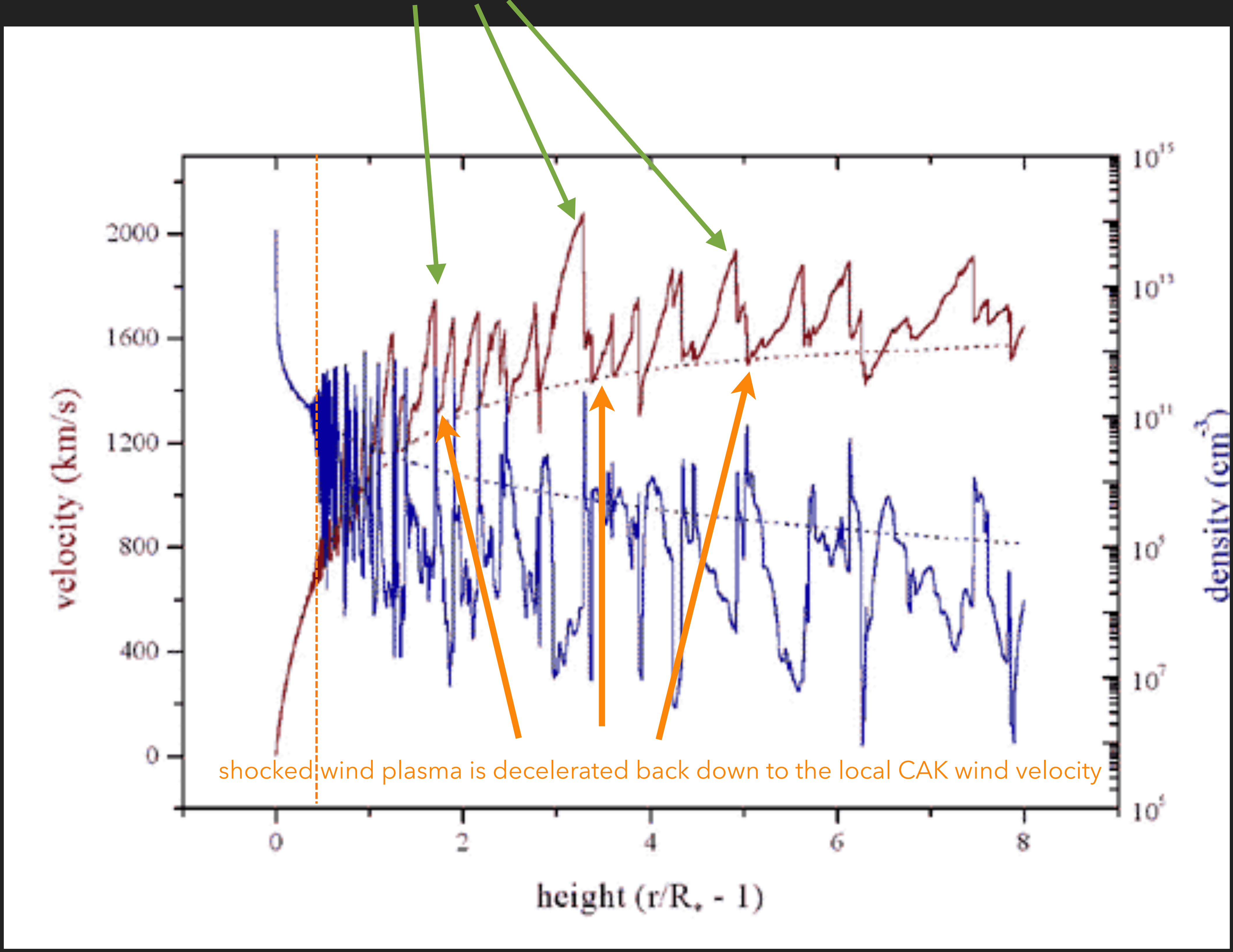

X-RAYS ARE PRODUCED BY EMBEDDED WIND SHOCKS (EWS)

Shocked plasma is moving at $v \sim 1000$ km/s

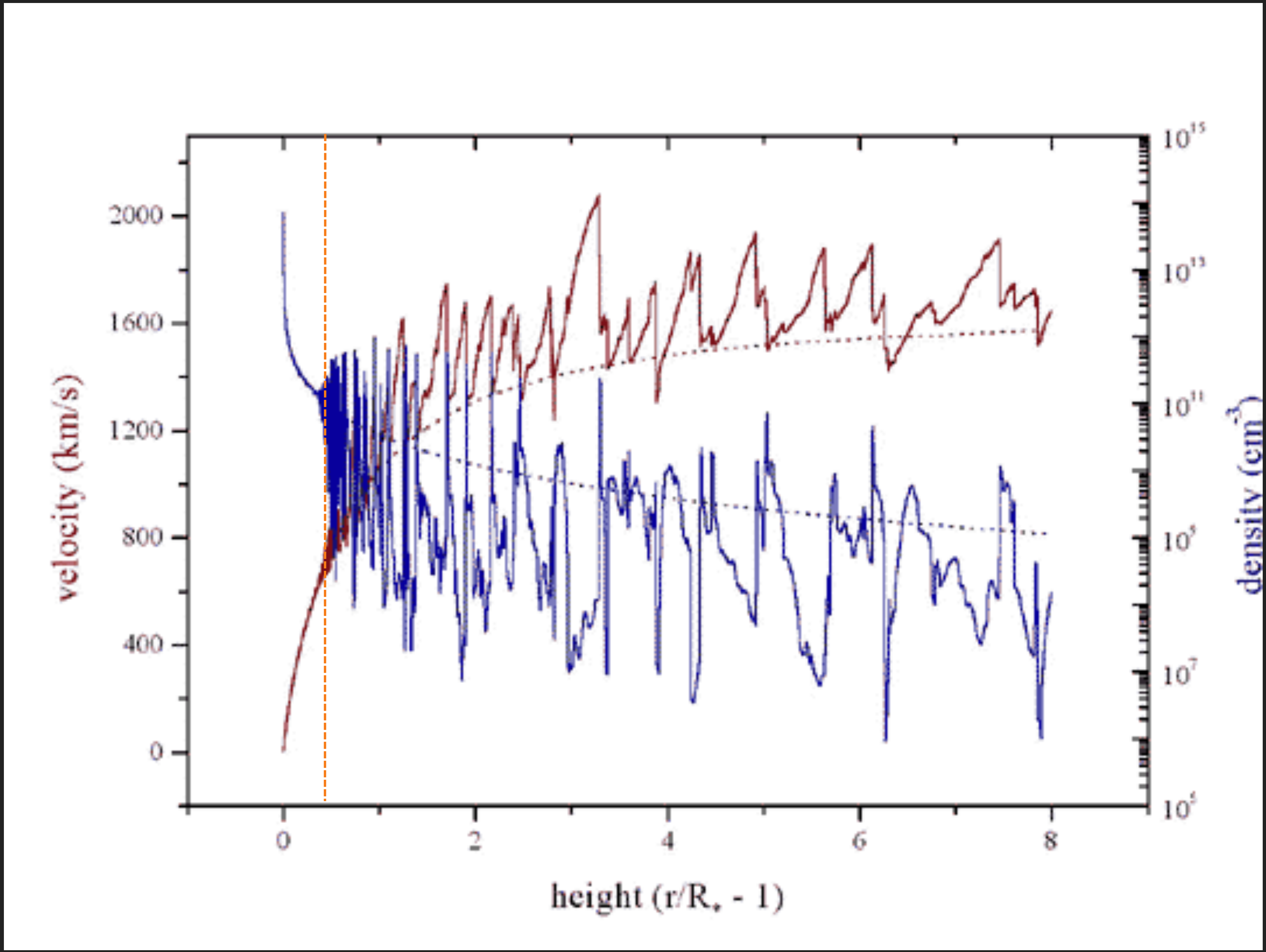

X-RAYS ARE PRODUCED BY EMBEDDED WIND SHOCKS (EWS)

X-ray emission lines should be **Doppler broadened**

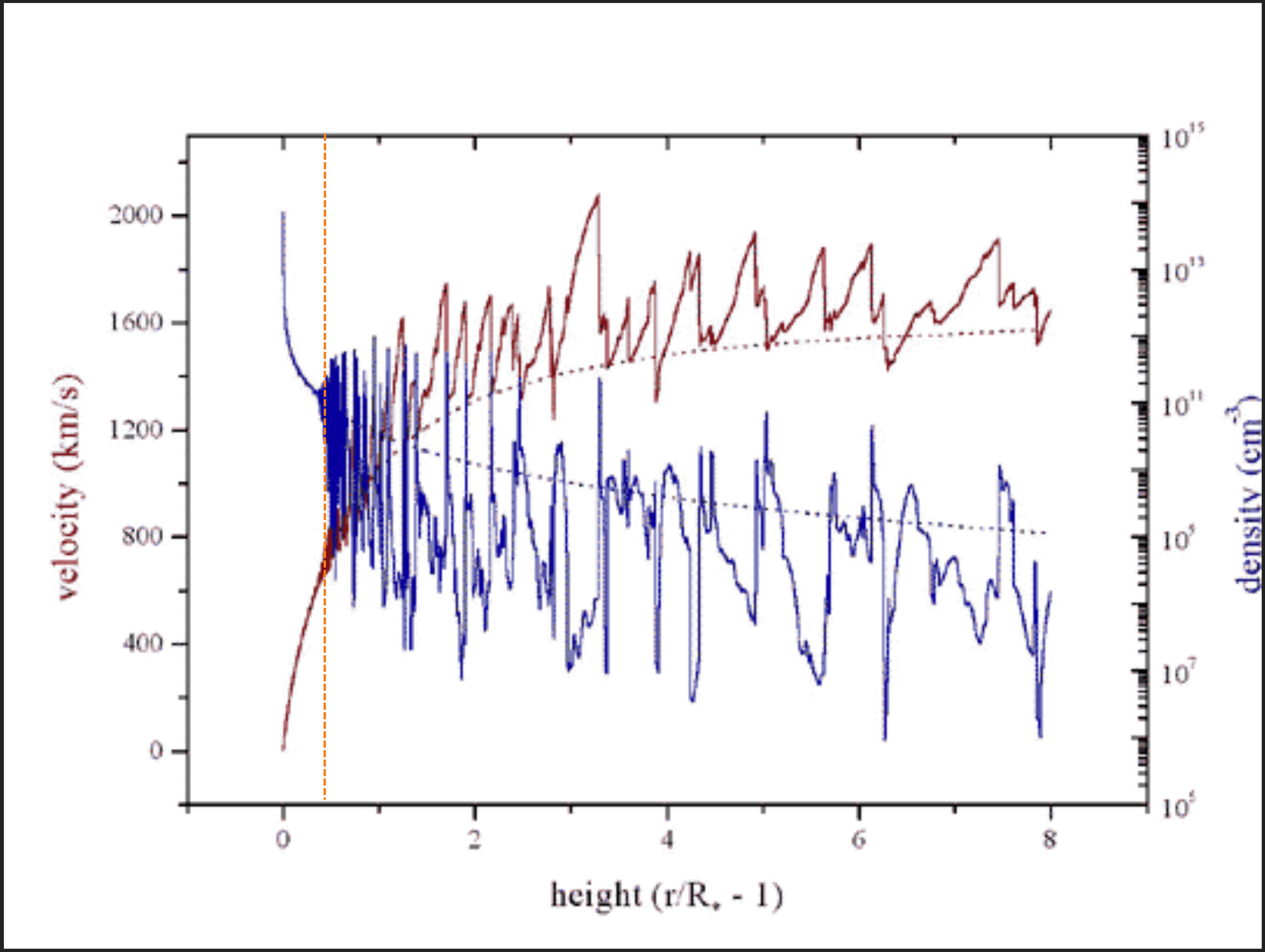

X-RAYS ARE PRODUCED BY EMBEDDED WIND SHOCKS (EWS)

Less than 1% of the wind is emitting X-rays

>99% of the wind is cold and X-ray *absorbing*

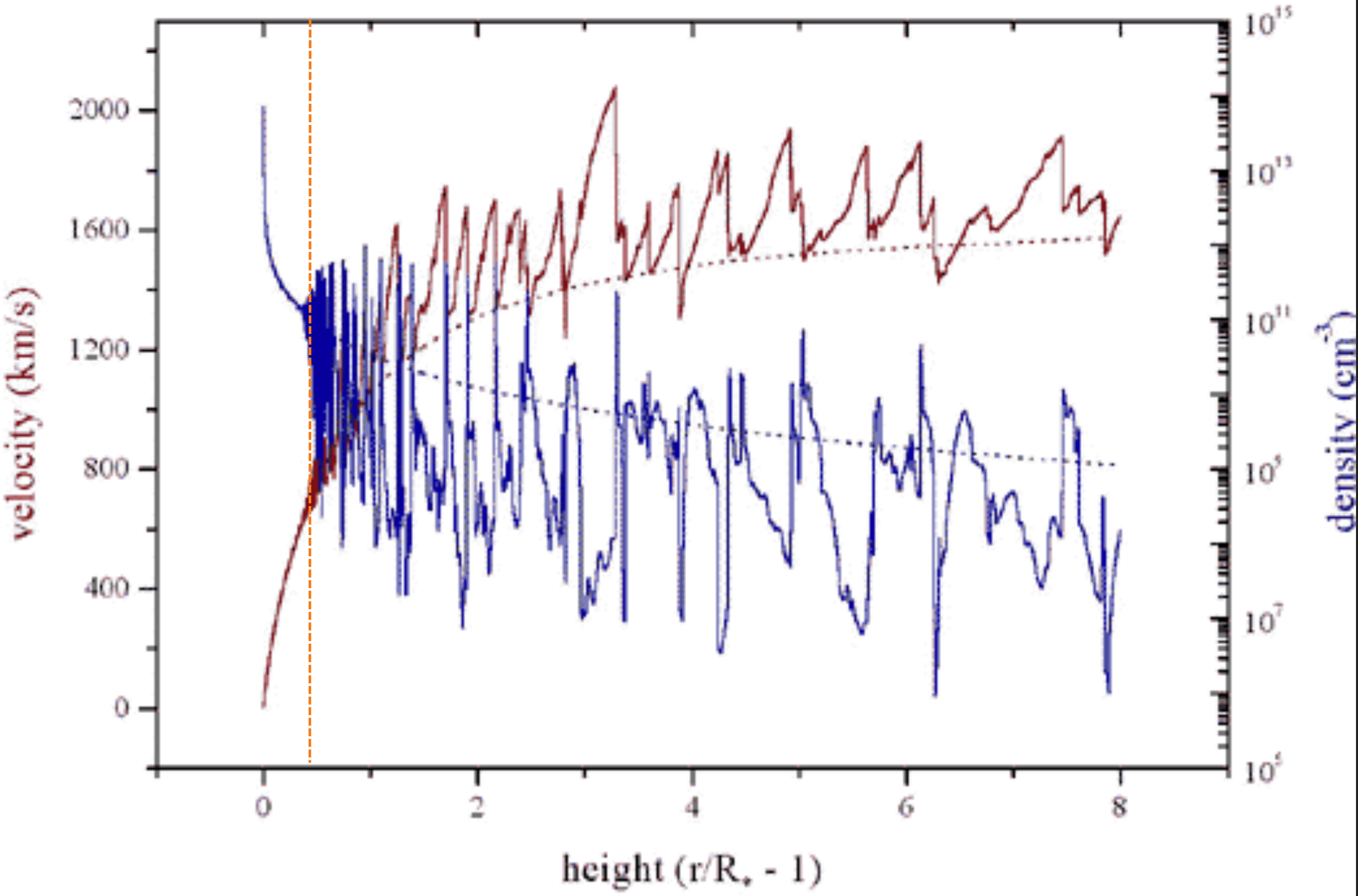

X-RAYS ARE PRODUCED BY EMBEDDED WIND SHOCKS (EWS)

>99% of the wind is cold and X-ray *absorbing*

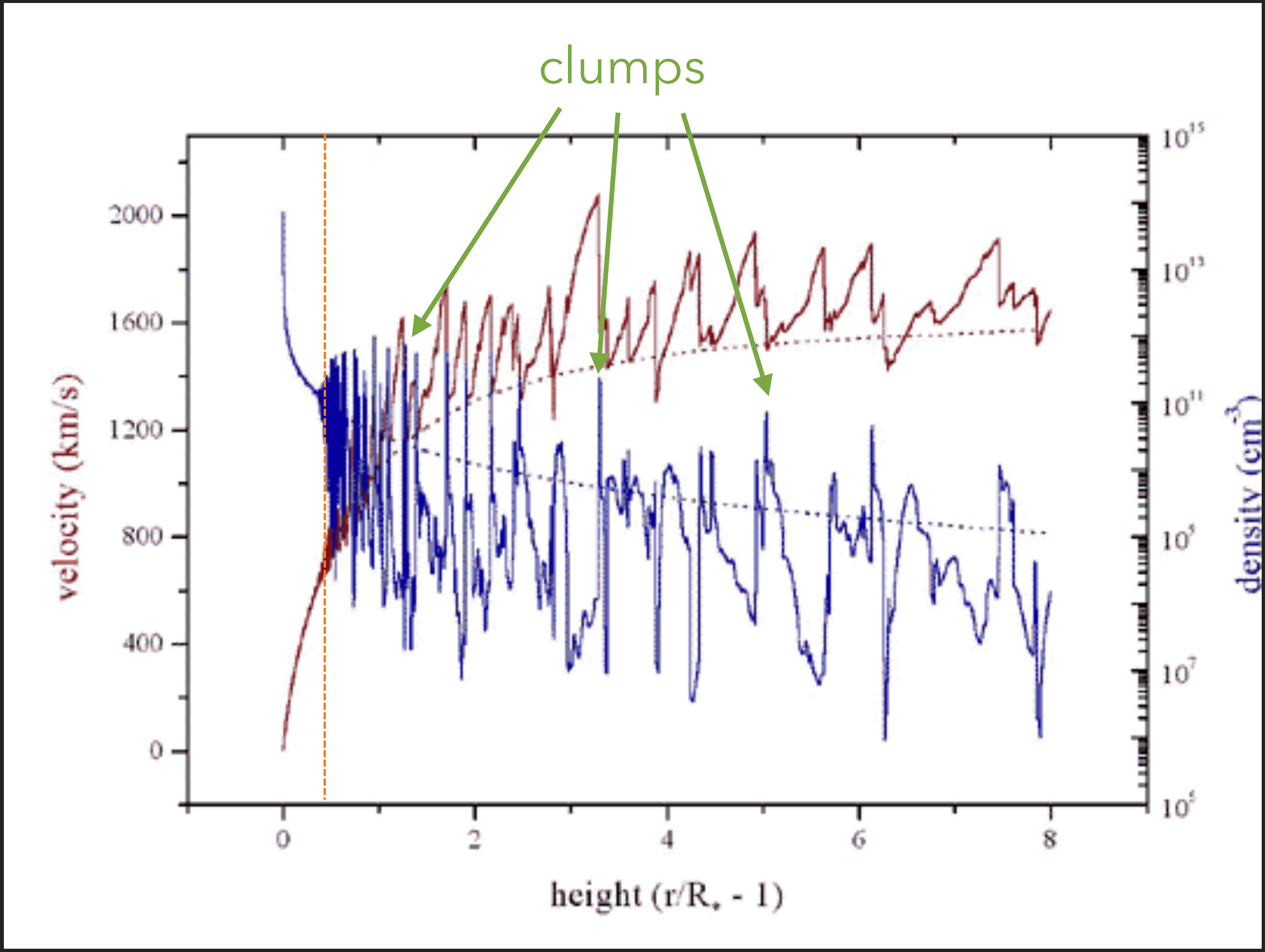

1-D NATURE OF HYDRO SIMULATIONS IS A SEVERE LIMITATION

Lack of observed time variability suggests numerous (>100) individual post-shock cooling volumes in the wind

2-D LDI SIMULATIONS

Clumps are small-scale and numerous

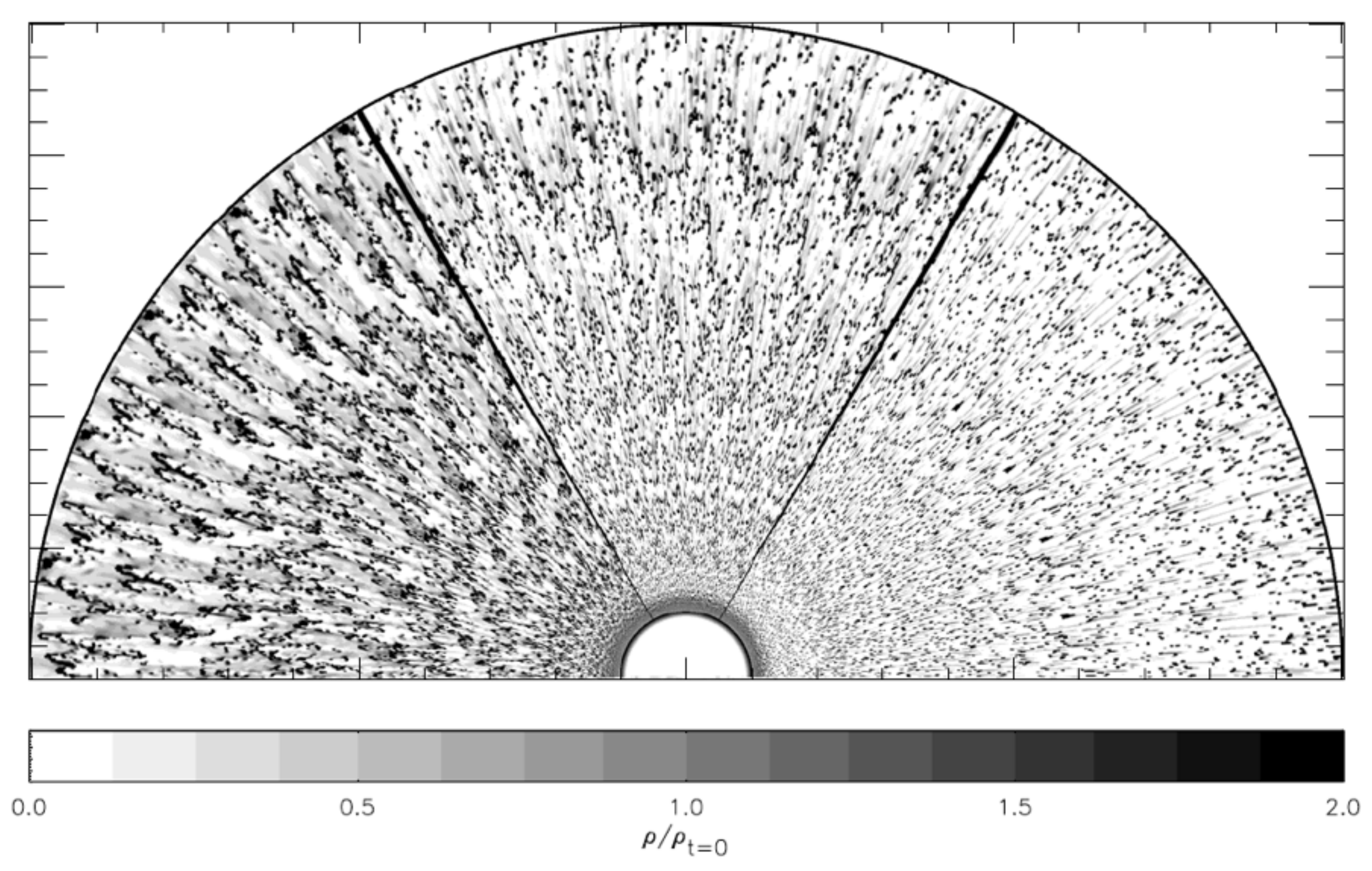

Dessart & Owocki 2003

X-RAY OBSERVABLES

Thermal X-ray emission from the shock-heated wind plasma

Photoelectric (continuum) absorption by the clumpy, cool wind

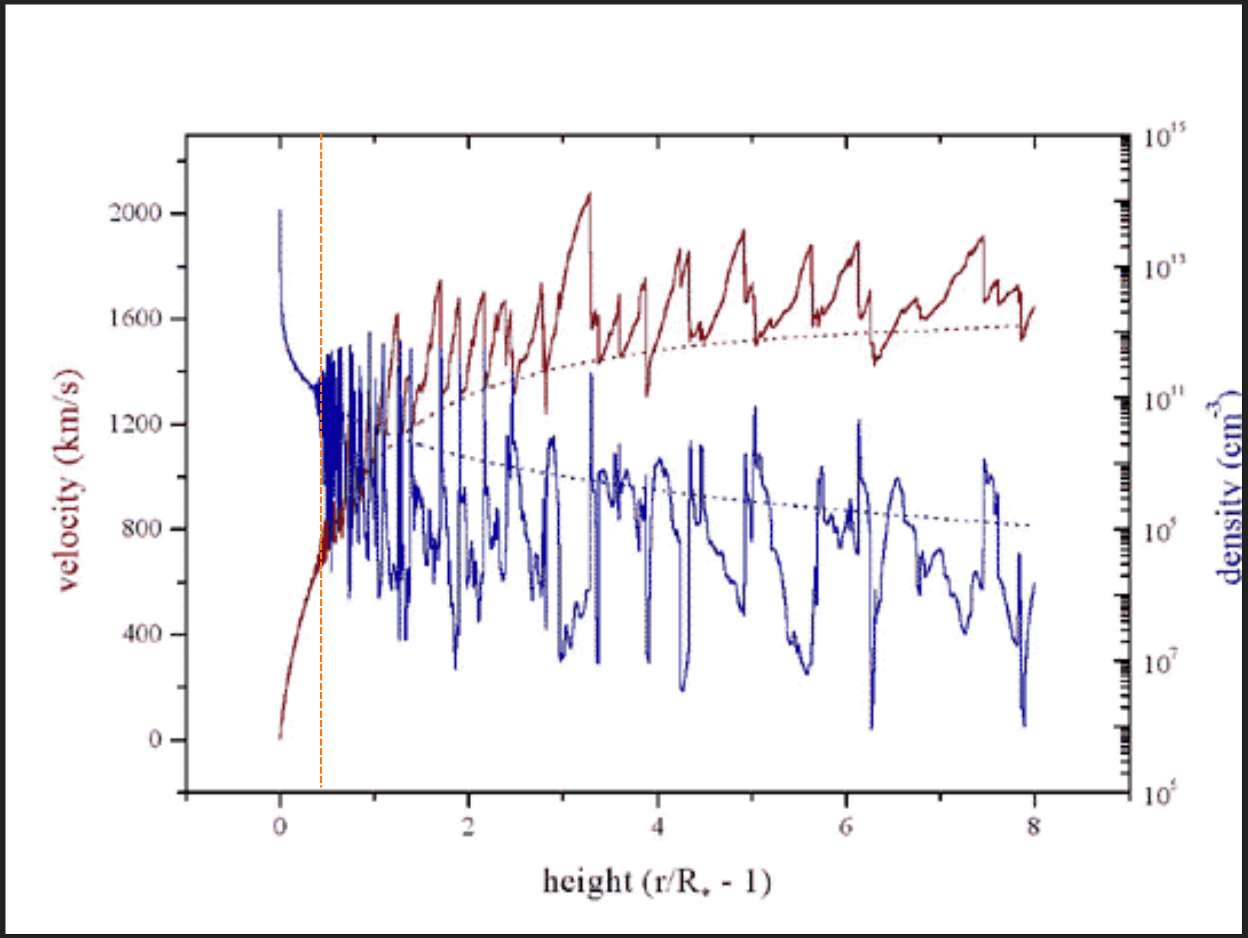

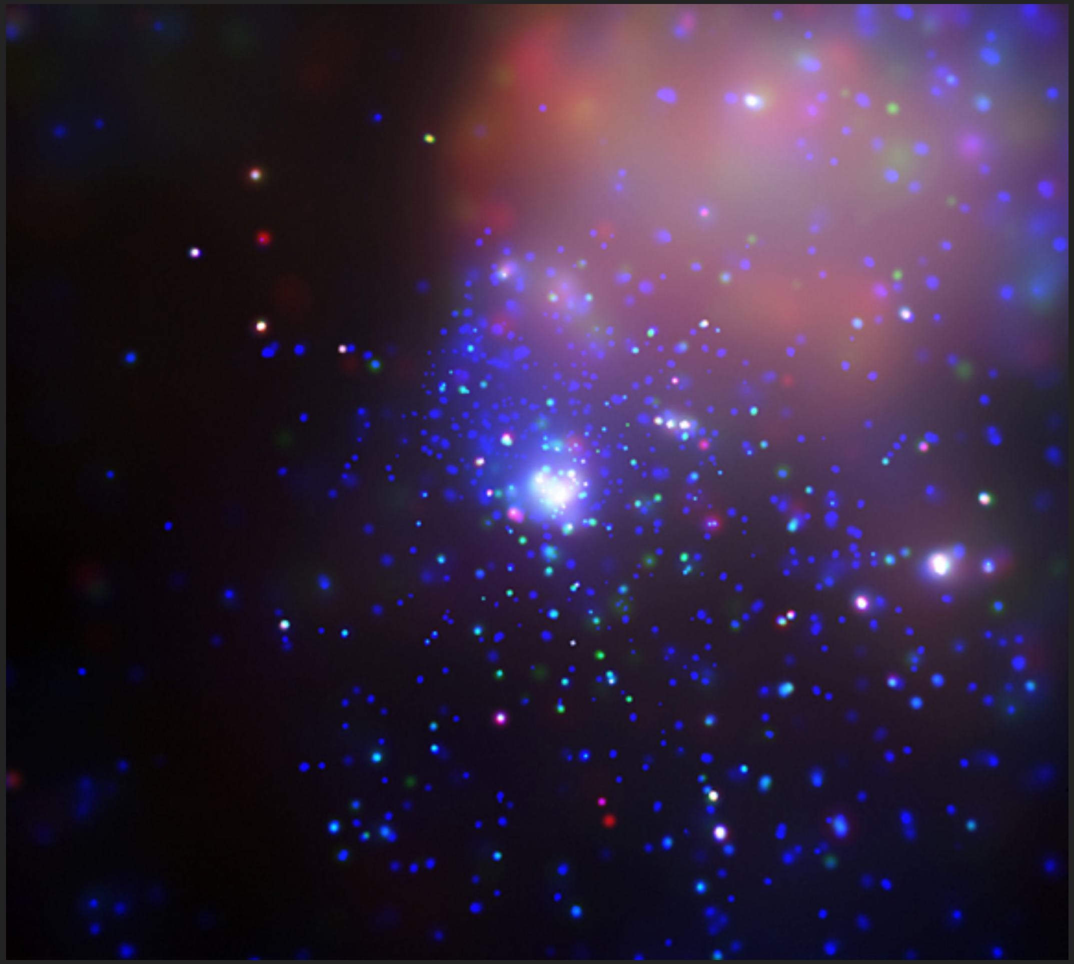

Chandra: Carina

CHANDRA LAUNCHED IN 1999

first high-resolution X-ray spectrograph

response to photons with hν ~ 0.5 keV up to a few keV (corresp. ~5Å to 24Å)

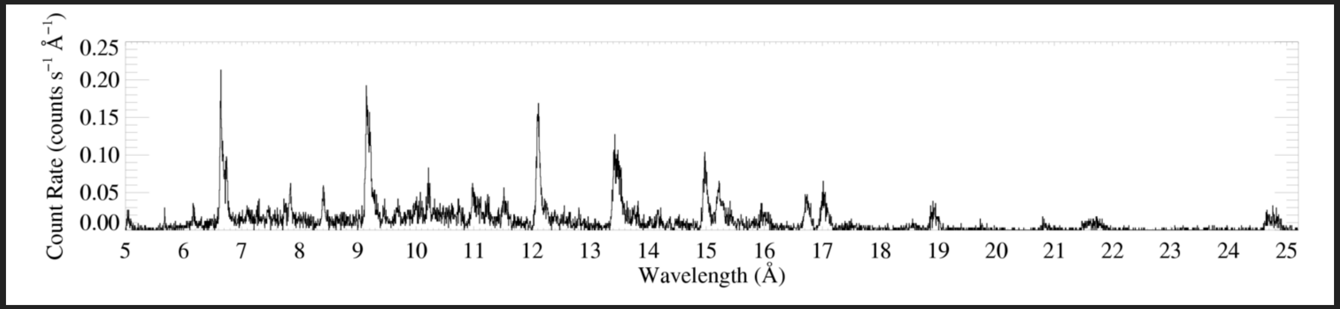

X-ray imaging? > 0.5 arc sec, at best (100s of AU)

spectroscopy (λ/Δλ < 1000 corresp. v > 300 km/s)

X-RAY SPECTRAL FORMATION

Emission lines:

from hot,

transparent gas

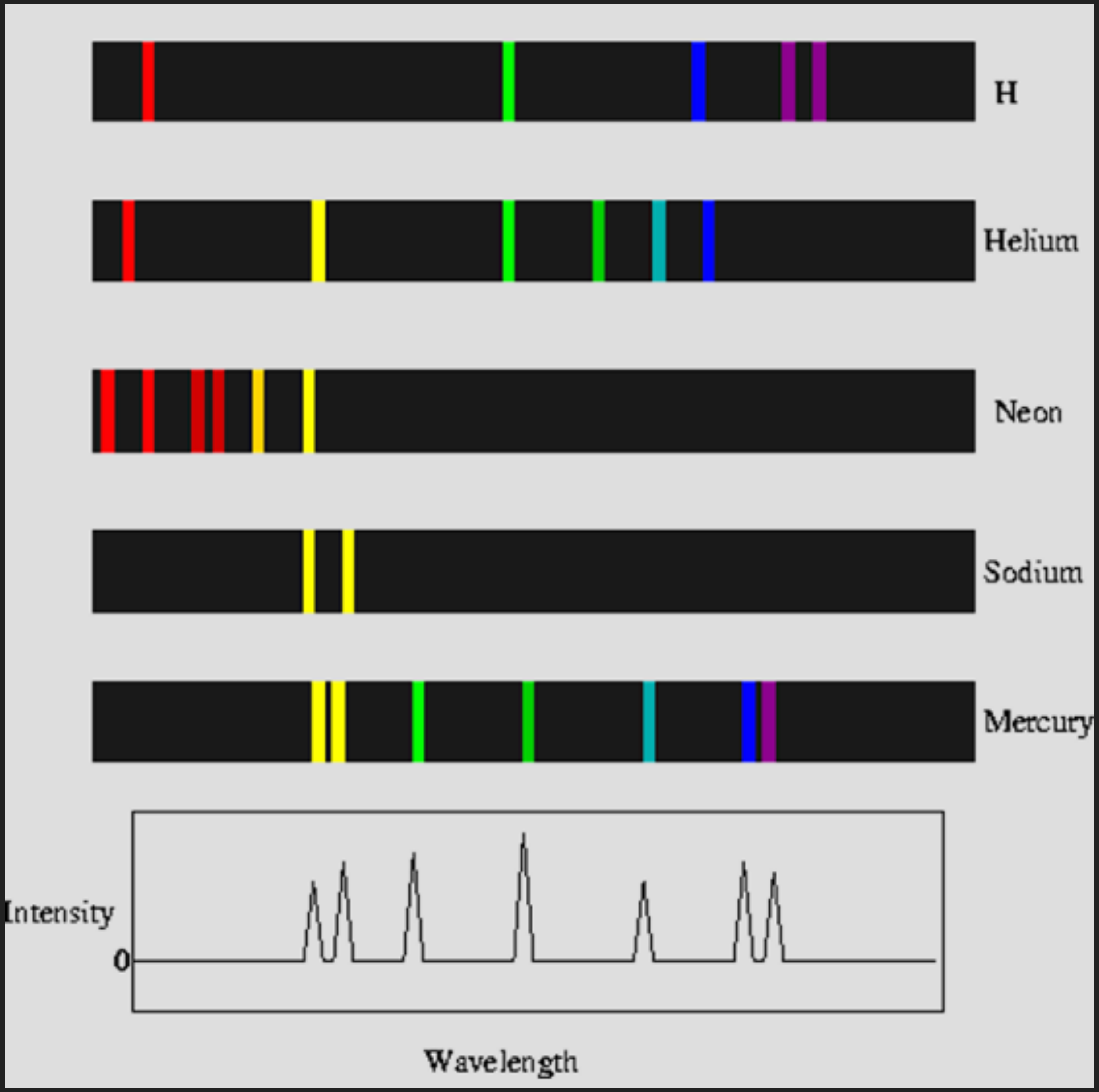

X-RAY SPECTRAL FORMATION

Thermal emission

Equilibrium

Optically thin

X-RAY SPECTRAL FORMATION

like the solar corona

low density

Thermal emission

collisions up, spontaneous down;
nearly all bound electrons in the ground state;
"coronal approximation"
⇒ emission line dominated

Equilibrium

Optically thin

X-RAY SPECTRAL FORMATION

like the solar corona

low density

Thermal emission

Equilibrium

Optically thin

steady-state; Maxwellian, $T_i = T_e$; ionization: collisional from ground state = recombination

X-RAY SPECTRAL FORMATION

like the solar corona

low density

Thermal emission

Equilibrium

Optically thin

Some strong lines may show optical depth effects (2nd order effect on spectra);

But, cold wind component can be optically thick to X-rays produced in the hot component

X-RAY SPECTRAL FORMATION

plasma with $T > 10^6$ K radiates X-rays ($h\nu > 100$ eV)

shocks heat plasma to $T \sim 10^6$ K
if $\Delta V_{shock} \sim 300$ km/s
and $T \sim (\Delta V_{shock})^2$

CHANDRA GRATING SPECTROSCOPY

ζ Pup (O4 If)

in front of the Gum Nebula

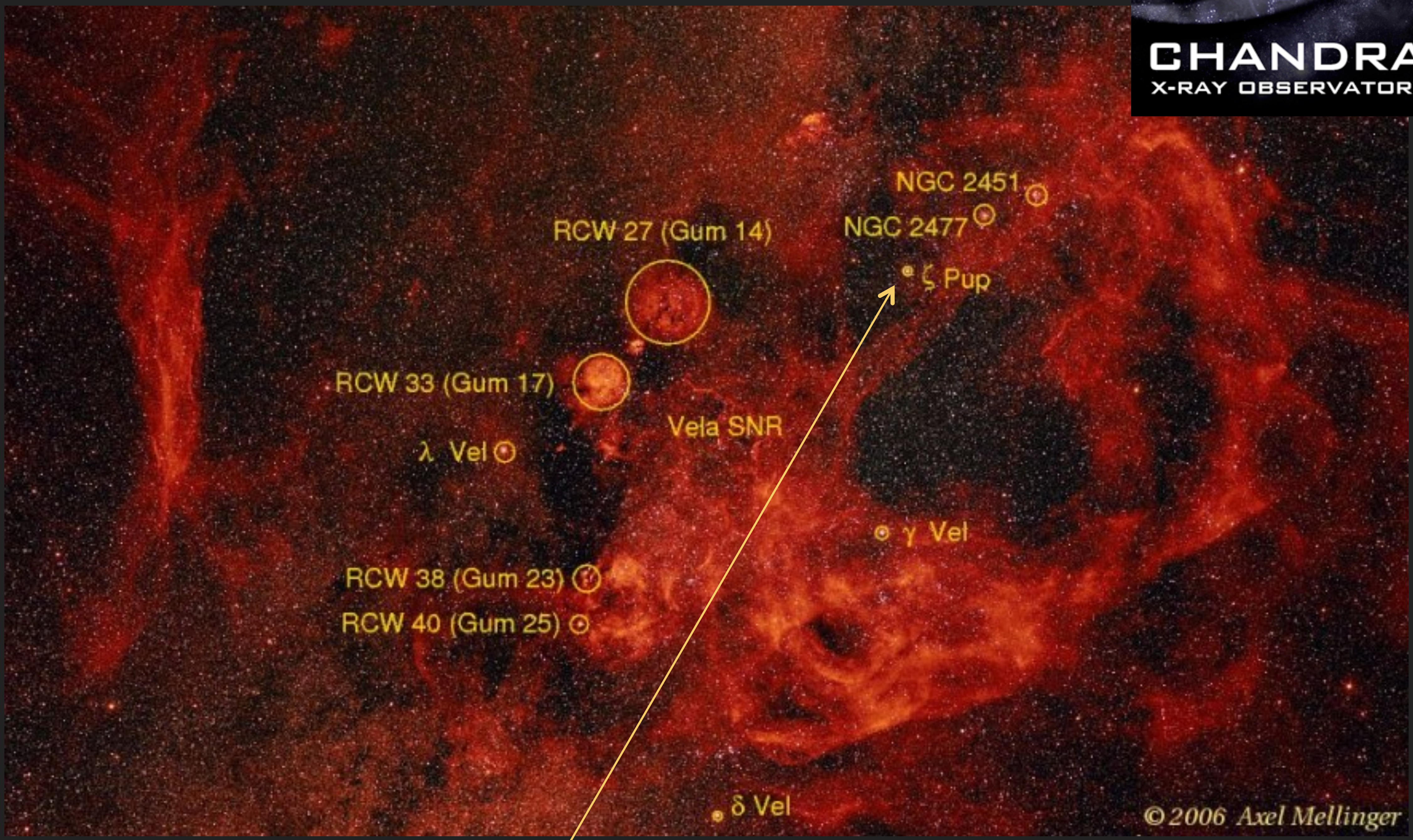

CHANDRA GRATING (HETGS/MEG) SPECTRA

ζ Pup (O4 If)

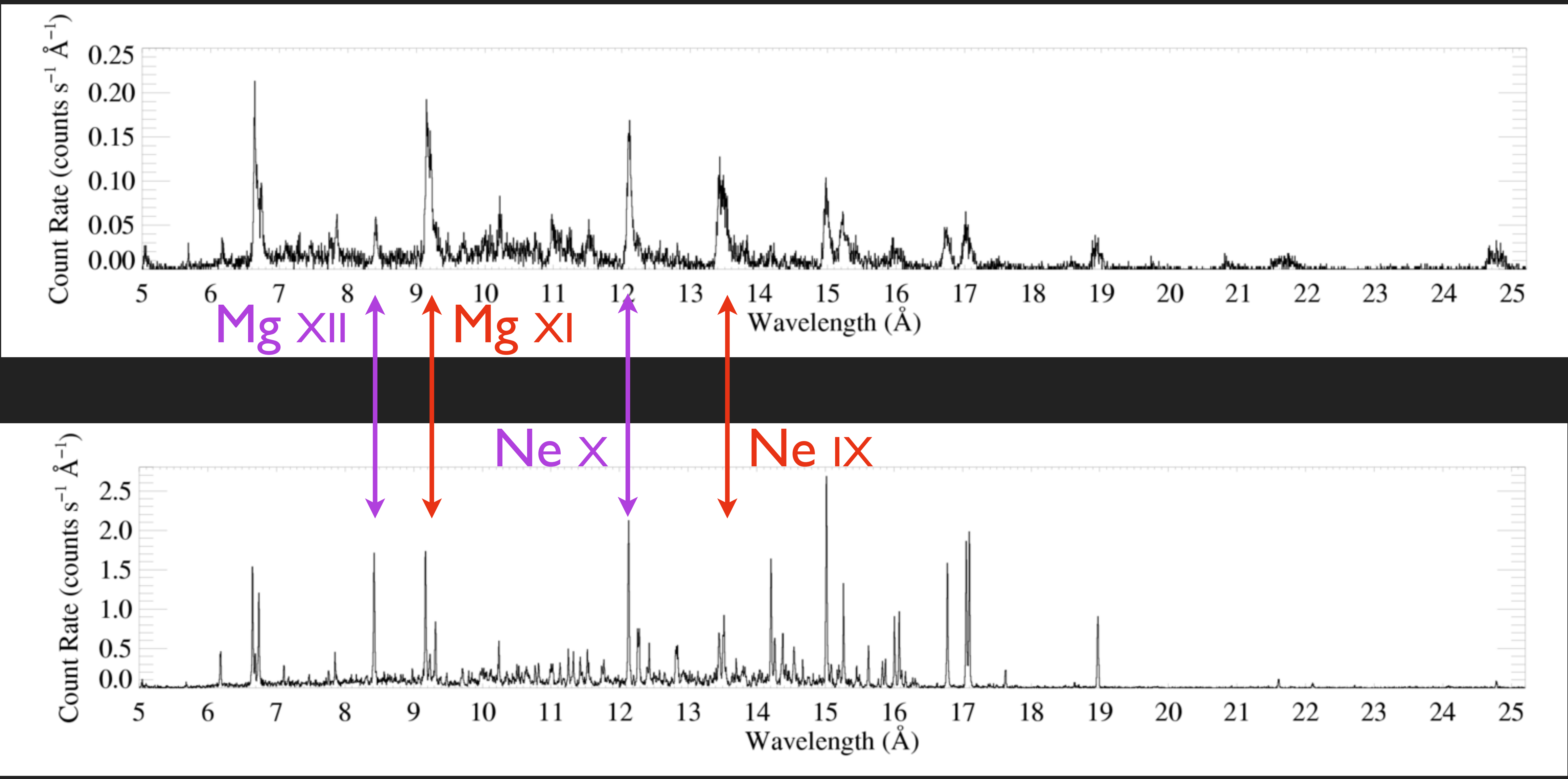

Capella (G5 III)

CHANDRA GRATING (HETGS/MEG) SPECTRA

T ~ few 10^6 K (late-type stars's coronae are hotter)

ζ Pup (O4 If)

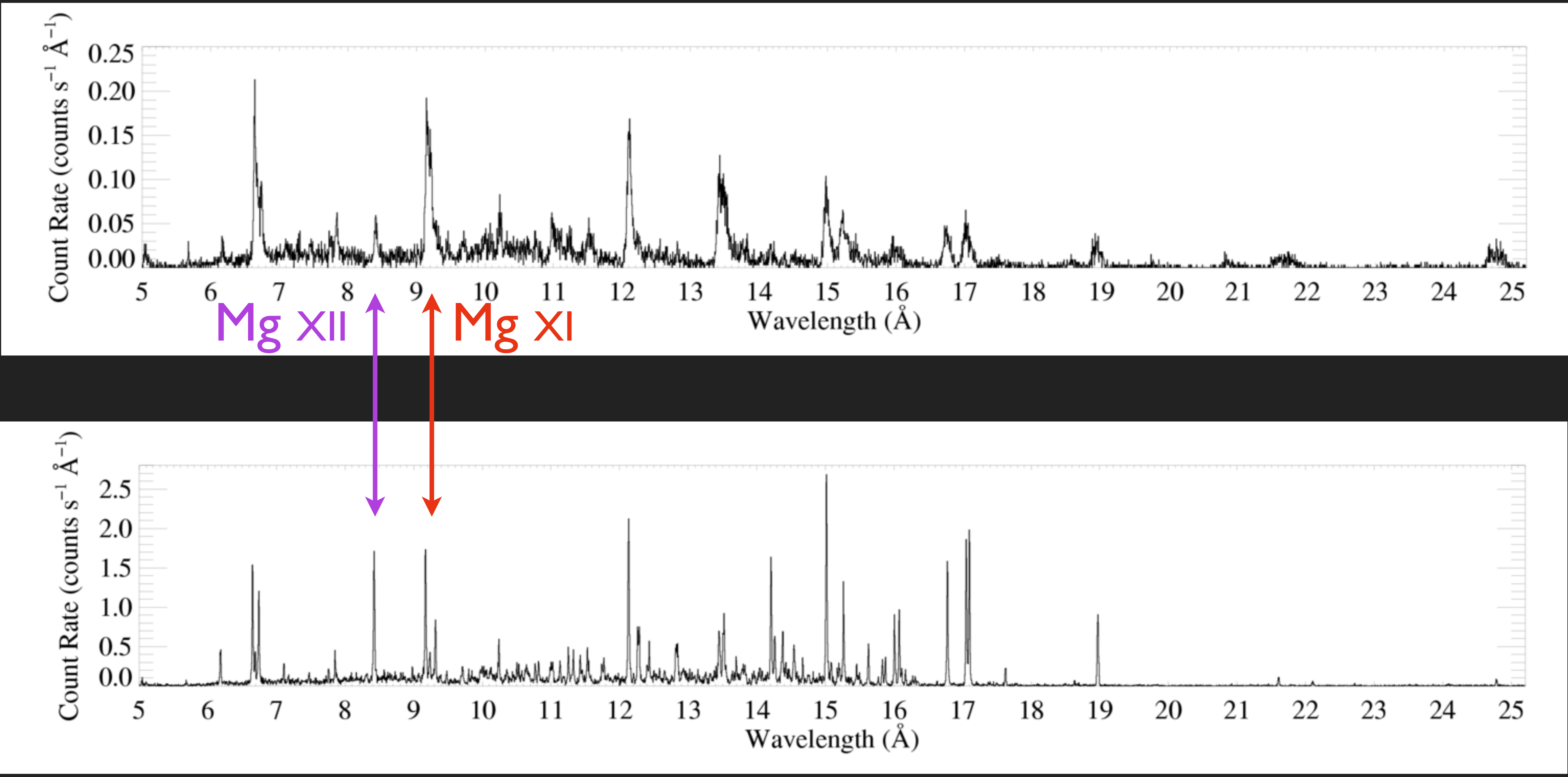

Capella (G5 III)

CHANDRA GRATING (HETGS/MEG) SPECTRA

Zoom in

ζ Pup (O4 If)

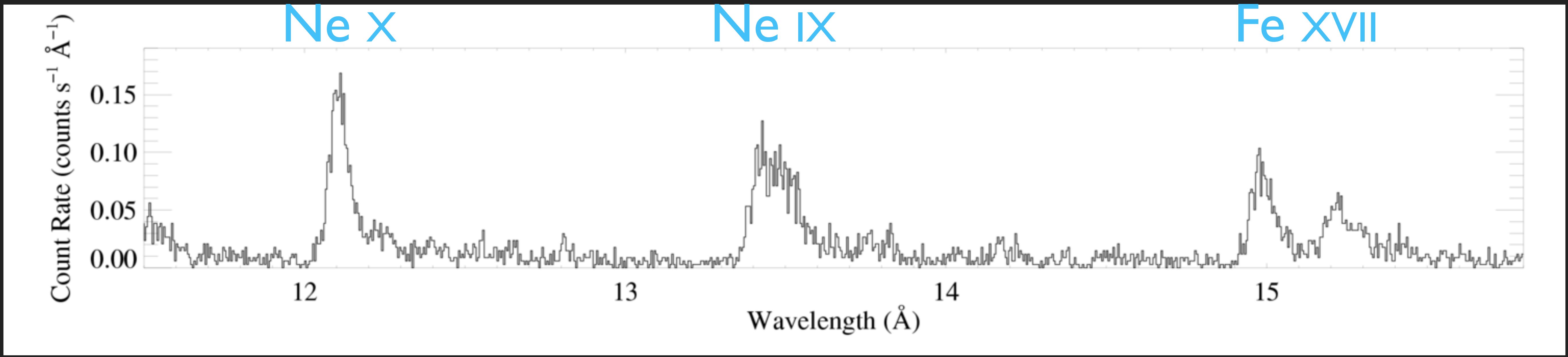

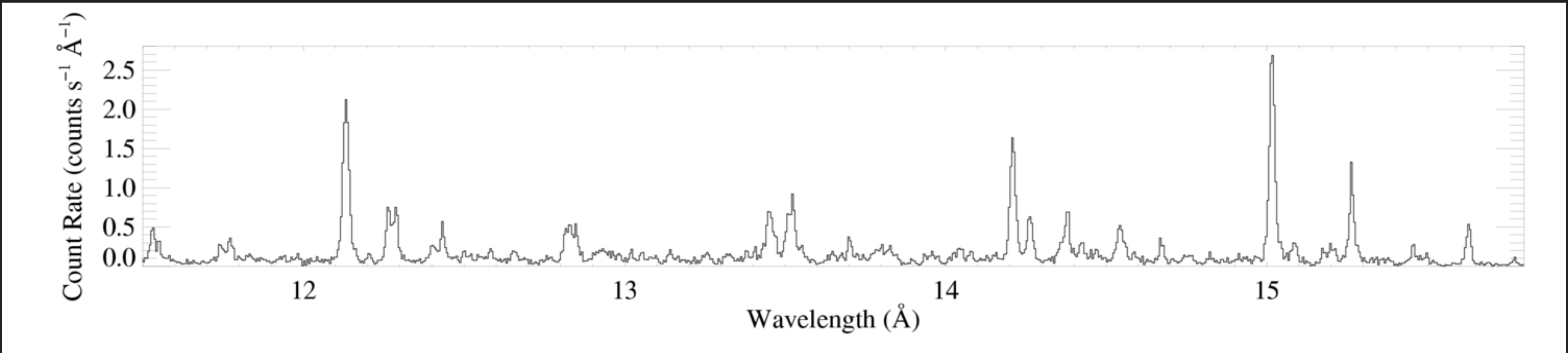

Capella (G5 III)

CHANDRA GRATING (HETGS/MEG) SPECTRA

Zoom in

ζ Pup (O4 If)

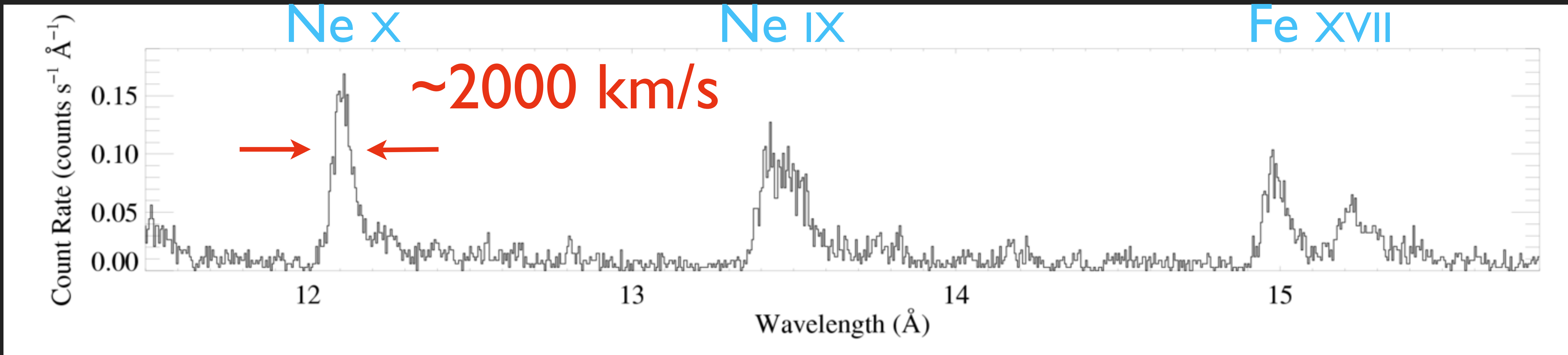

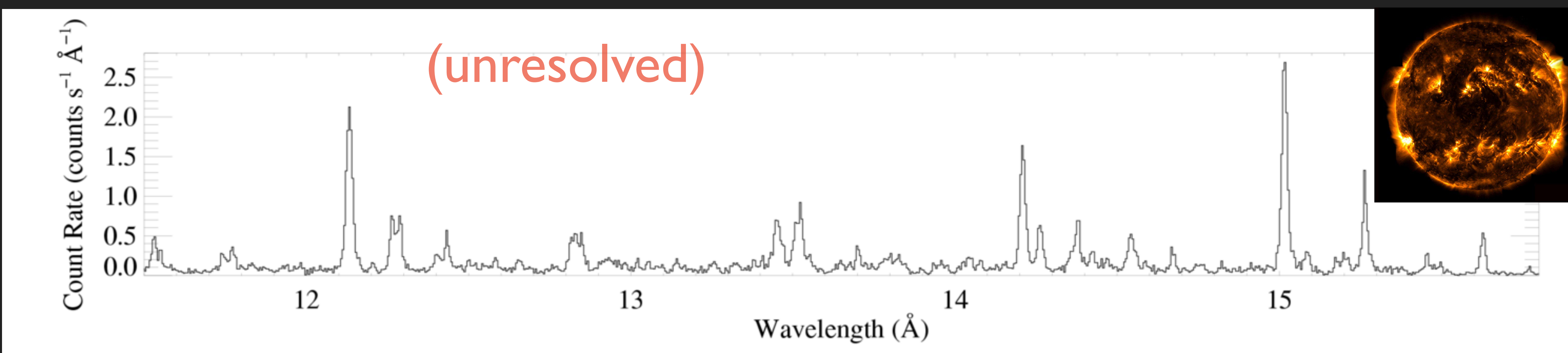

Capella (G5 III)

CONCLUSIVE EVIDENCE THE X-RAYS ARISE IN THE WIND

Zoom in

ζ Pup (O4 If)

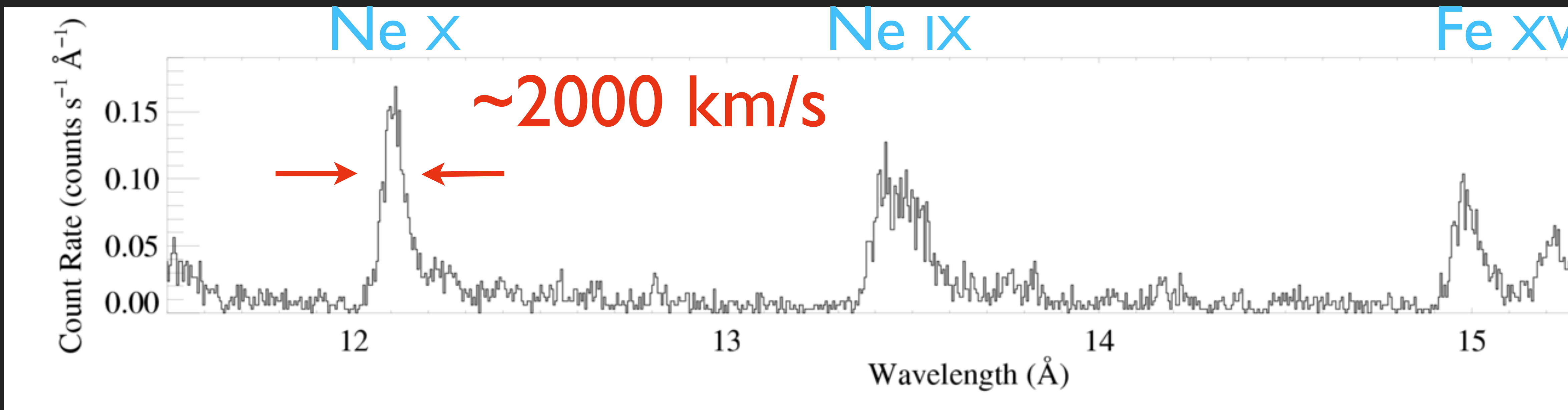

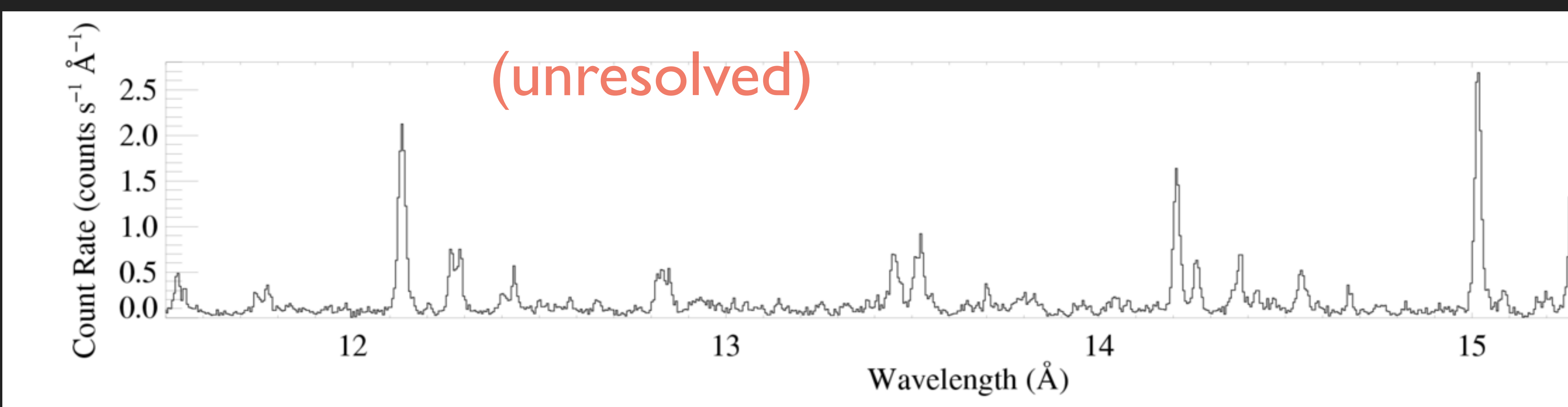

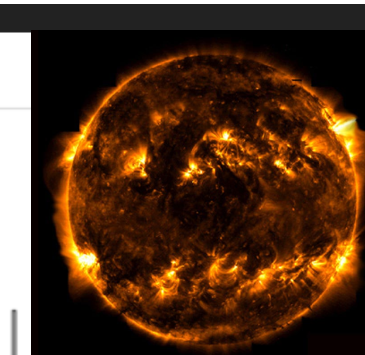

Capella (G5 III)

CHANDRA GRATING (HETGS/MEG) SPECTRA

Zoom in even more

the lines are asymmetric!

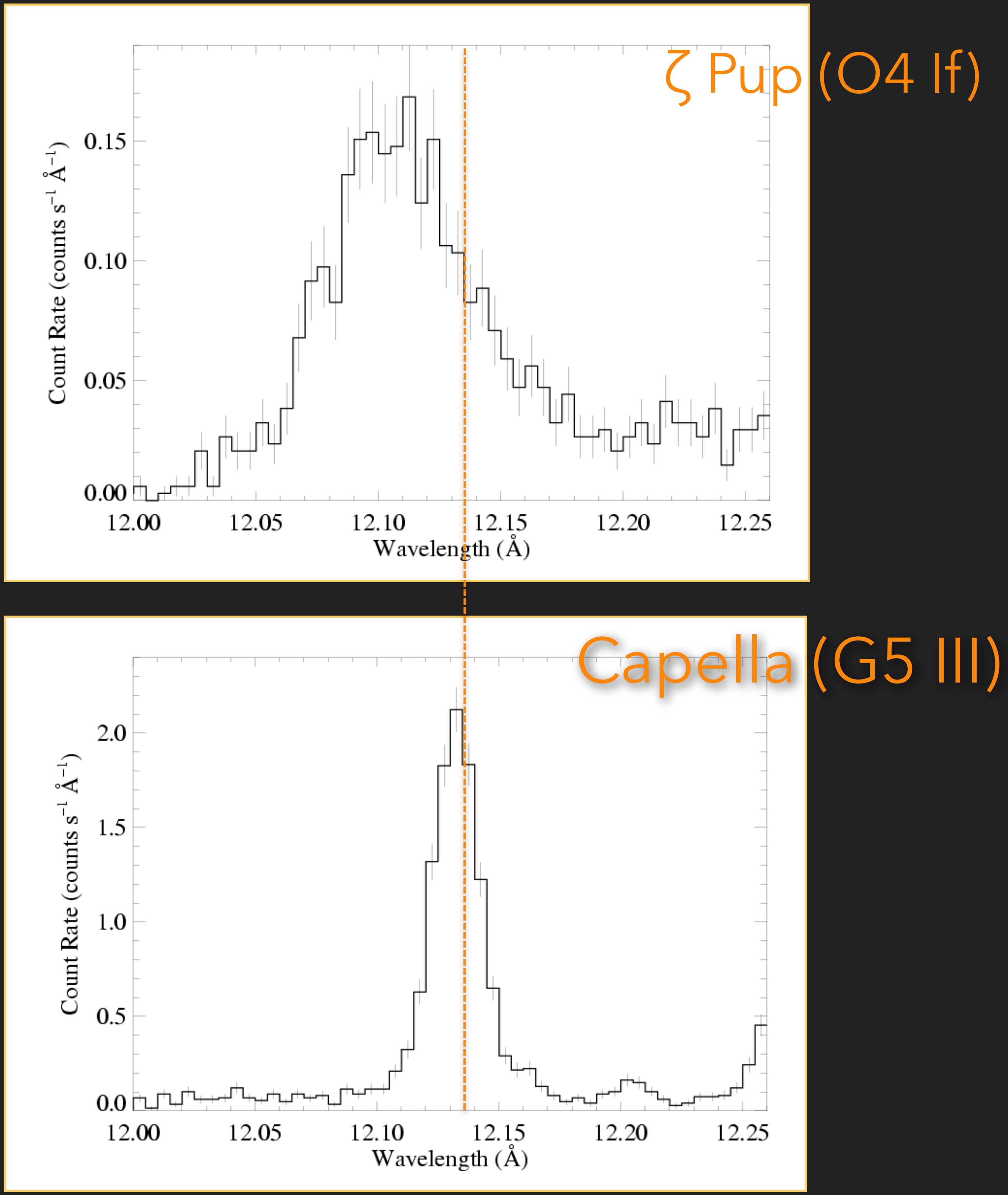

DATA MODELING APPROACH

Quantitative modeling of the X-ray spectrum *based on* the LDI numerical hydro simulations

DATA MODELING APPROACH

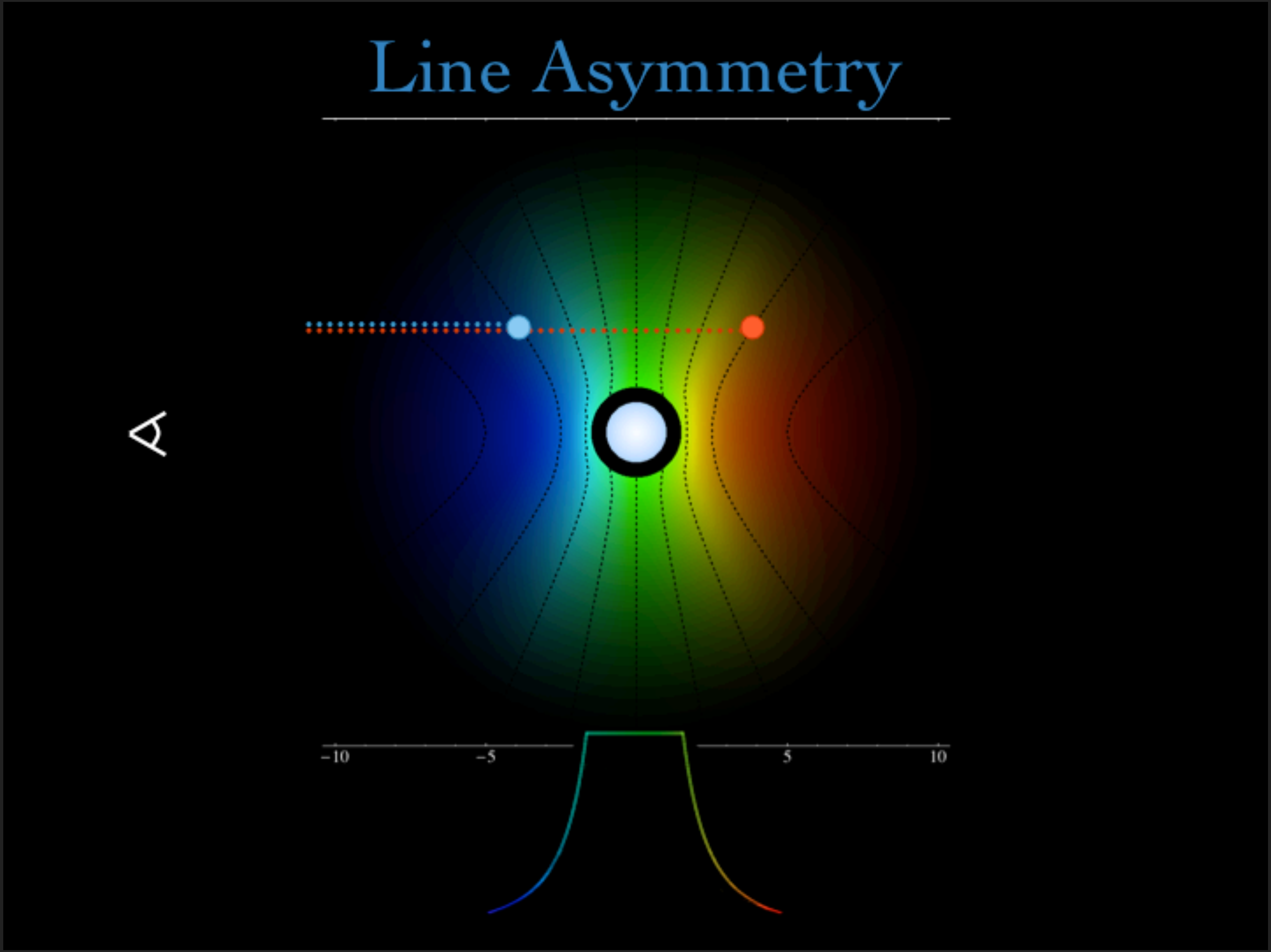

DATA MODELING APPROACH

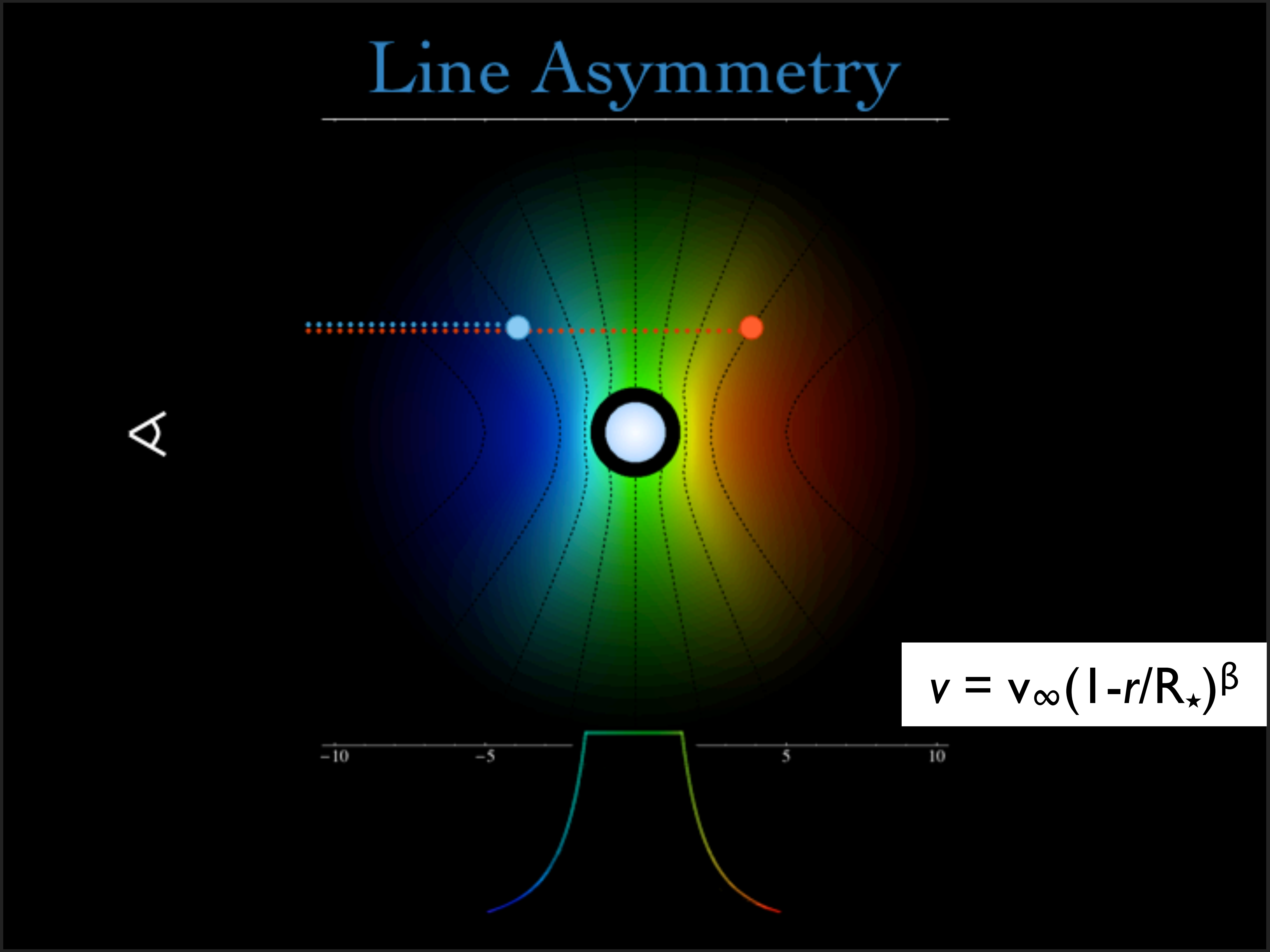

$$v = v_\infty(1 - r/R_\star)^\beta$$

DATA MODELING APPROACH

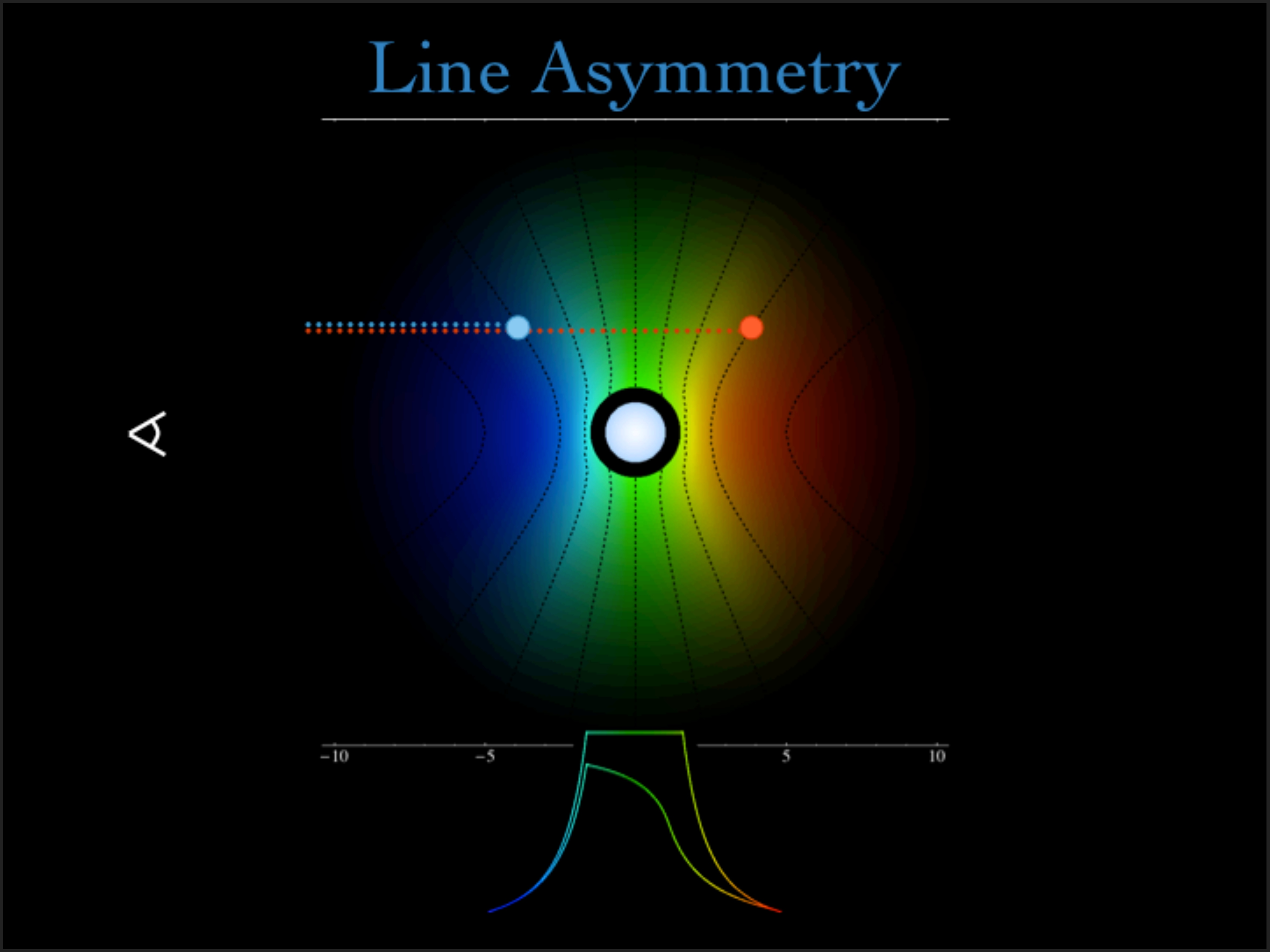

DATA MODELING APPROACH

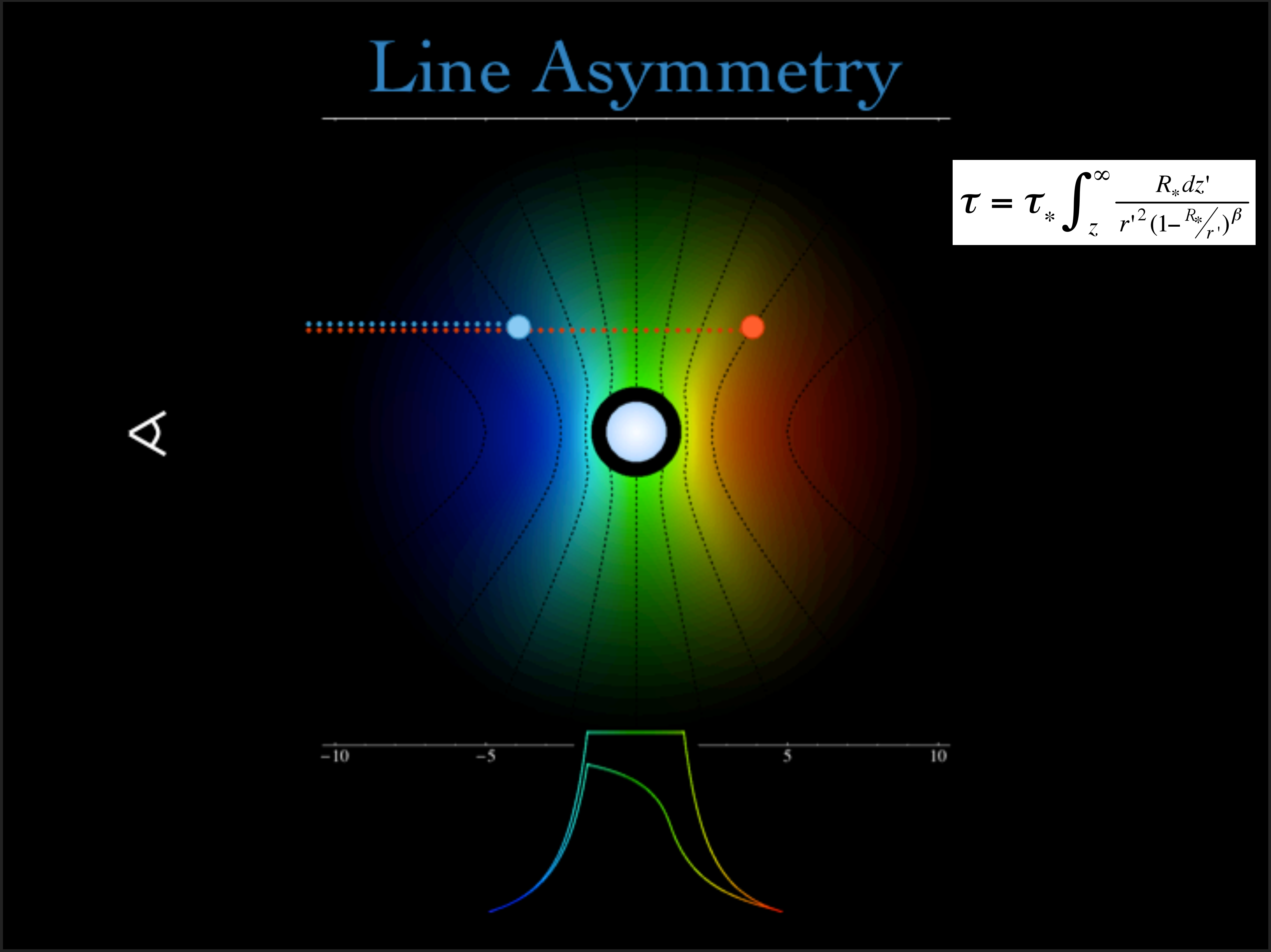

$$\tau = \tau_* \int_z^\infty \frac{R_* dz'}{r'^2 (1 - {R_*}/{r'})^\beta}$$

DATA MODELING APPROACH

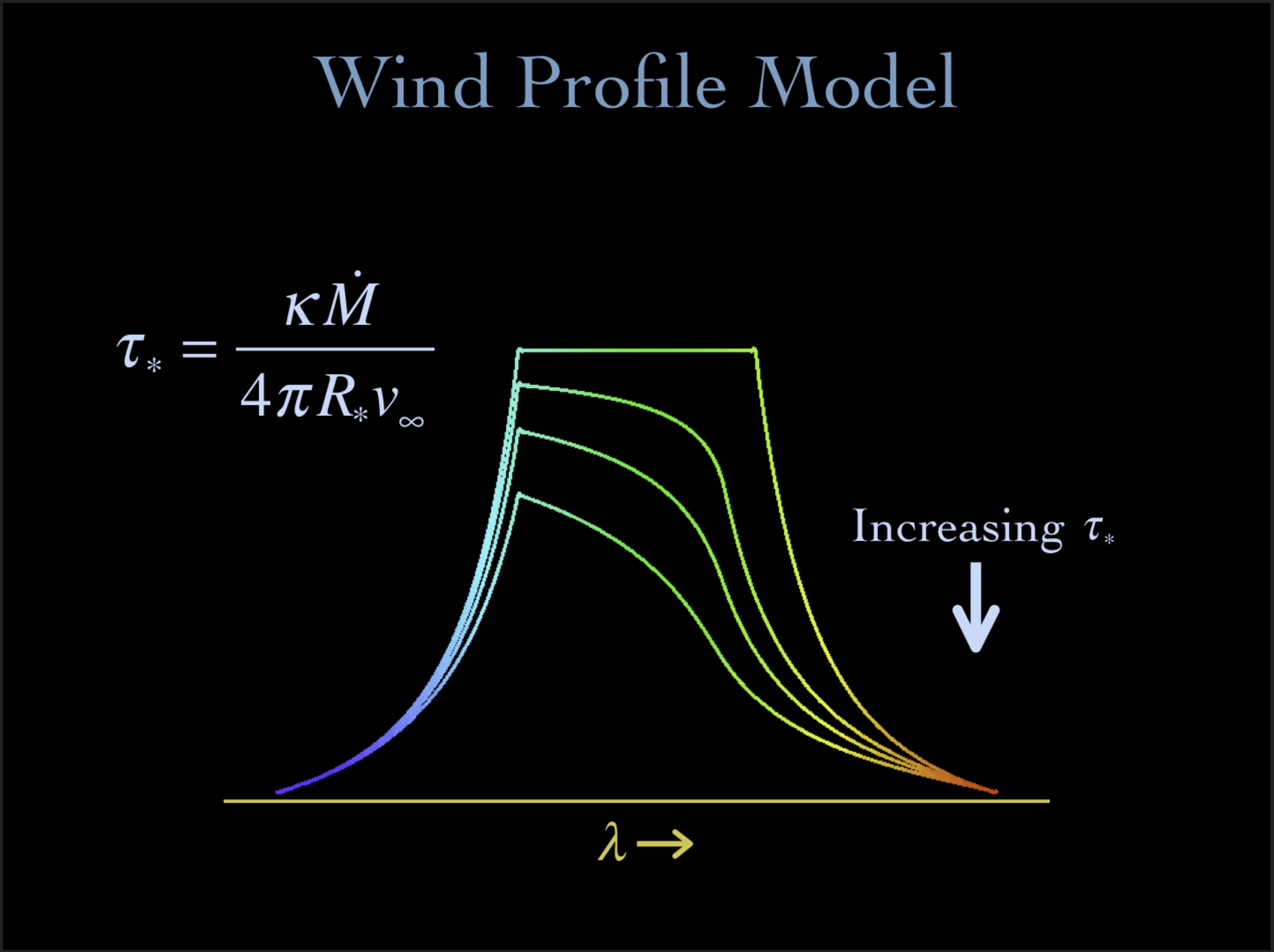

LINE PROFILES SHAPES

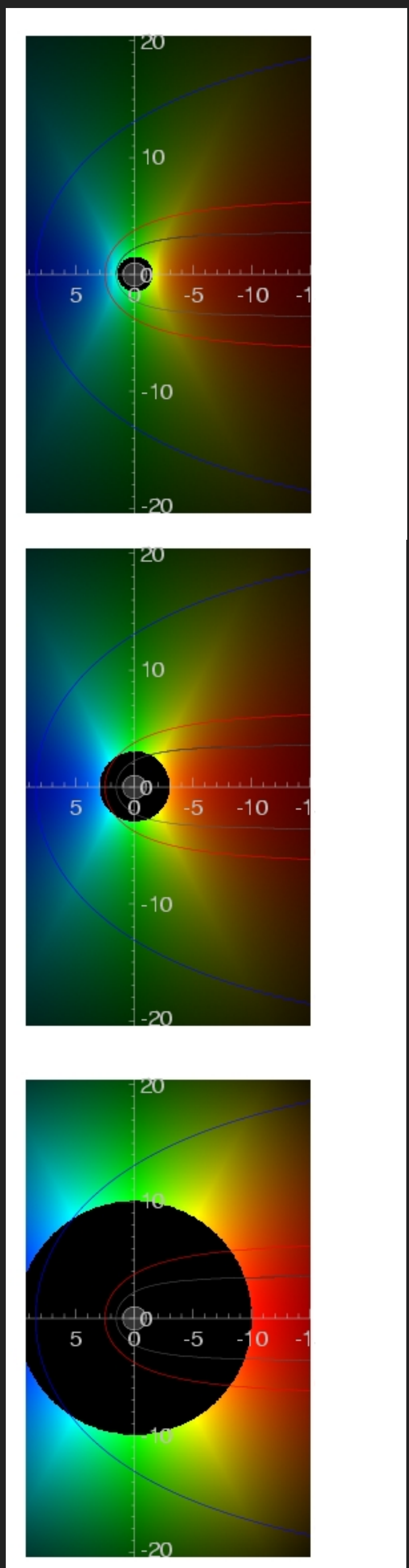

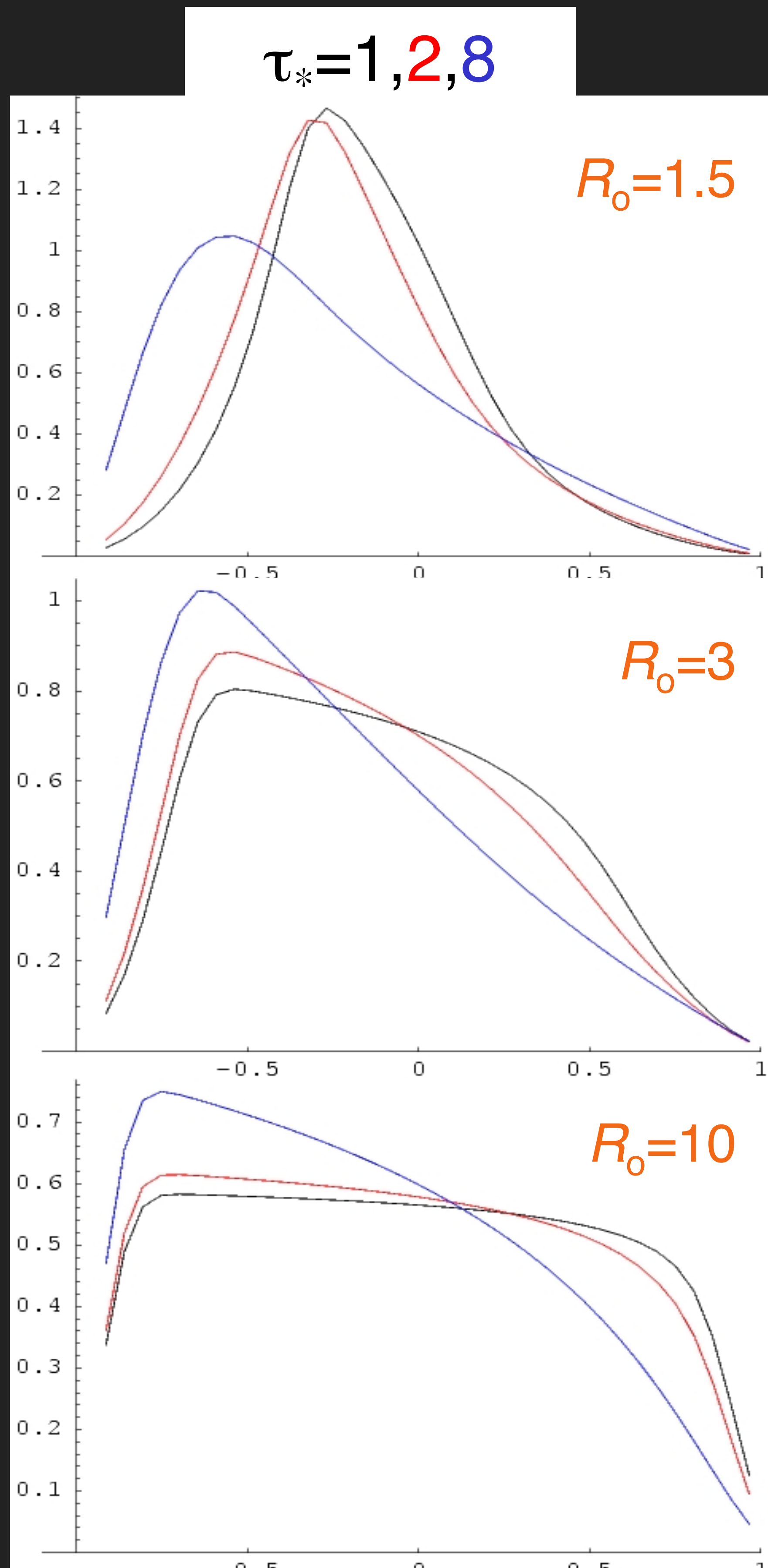

key parameters: R_o & $\tau_\star$

$$v = v_\infty(1 - r/R_\star)^\beta$$

$j \sim \rho^2$ for $r/R_* > R_o$,

$= 0$ otherwise

$$\tau = \tau_* \int_z^\infty \frac{R_* dz'}{r'^2 (1 - {R_*}/{r'})^\beta}$$

$$\tau_* \equiv \frac{\kappa \dot{M}}{4\pi R_* v_\infty}$$

HOT PLASMA KINEMATICS AND LOCATION

R_o controls the line width via v(r)

$R_o = 1.5\ R_\star$

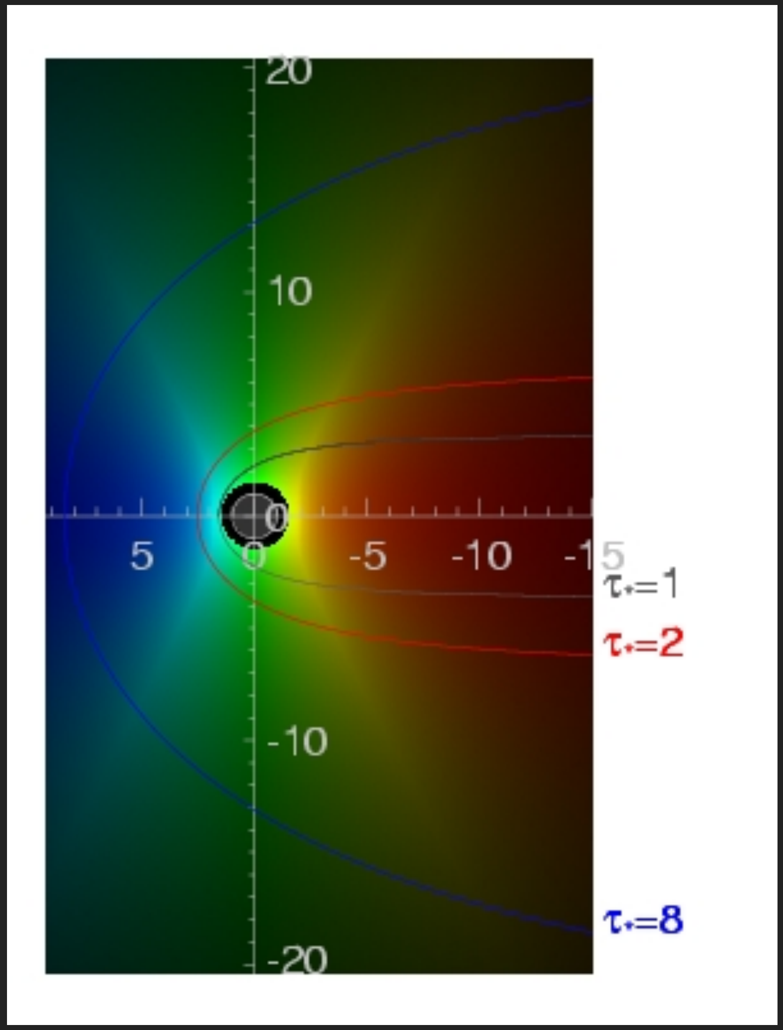

$R_o = 3\ R_\star$

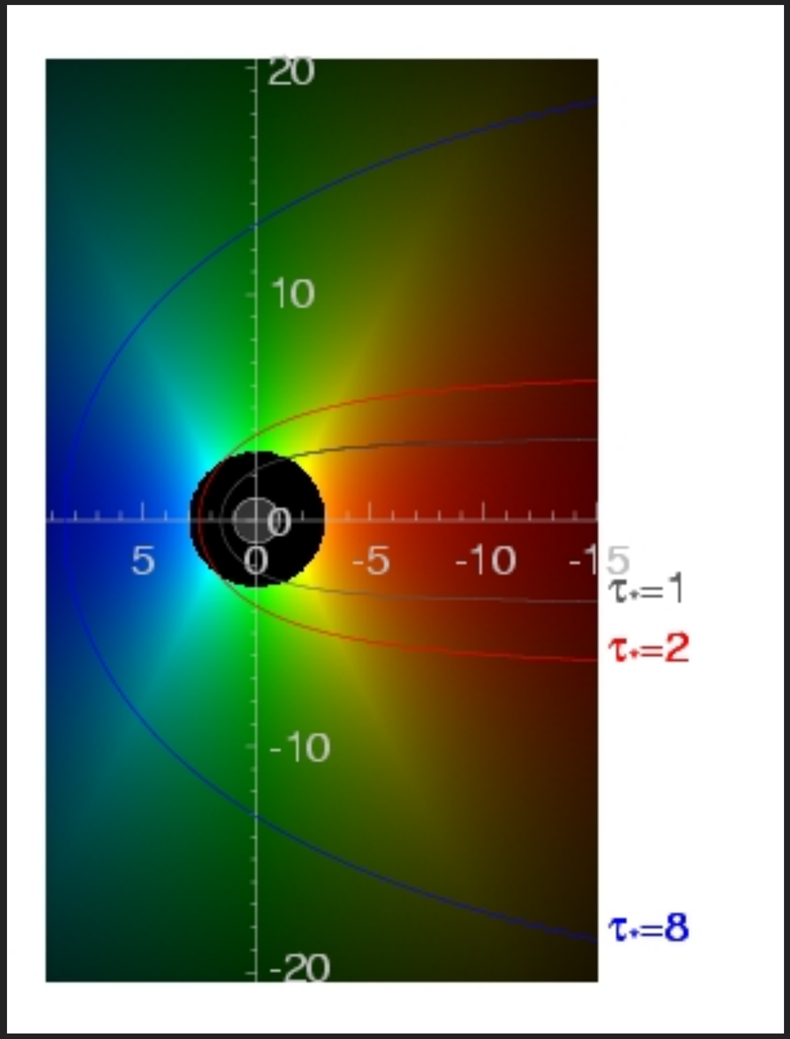

$R_o = 10\ R_\star$

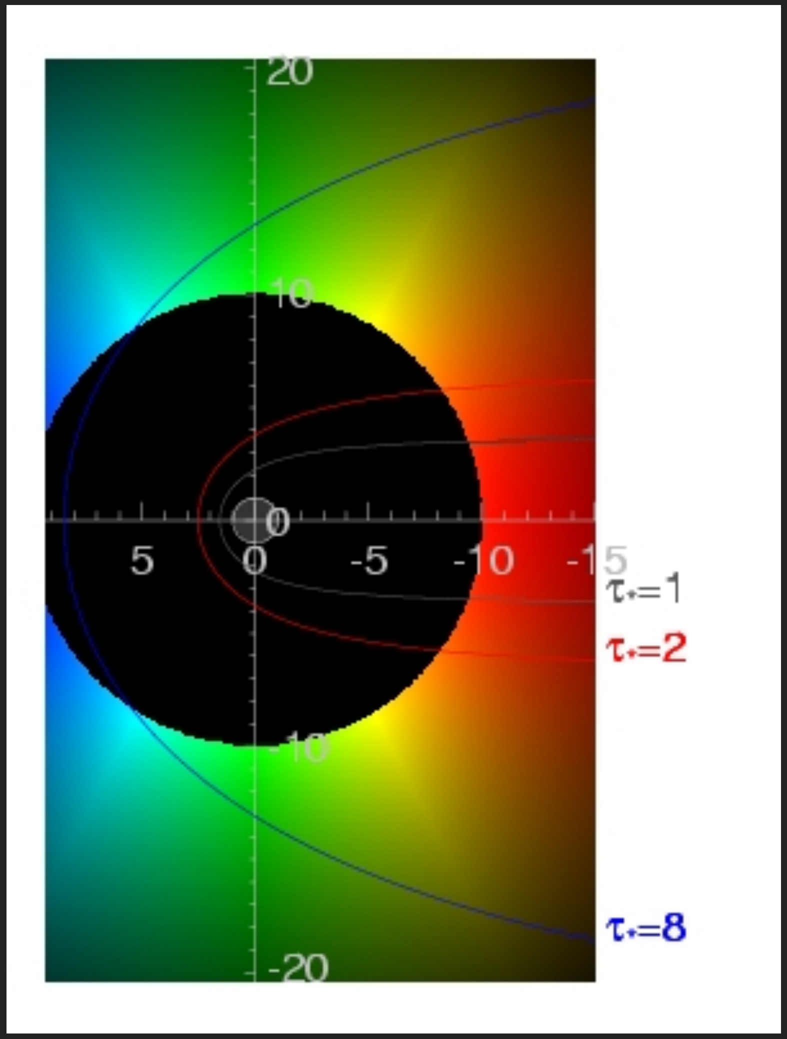

FITTING THIS MODEL TO AN EMISSION LINE

Fe XVII in the *Chandra* MEG spectrum of ζ Pup

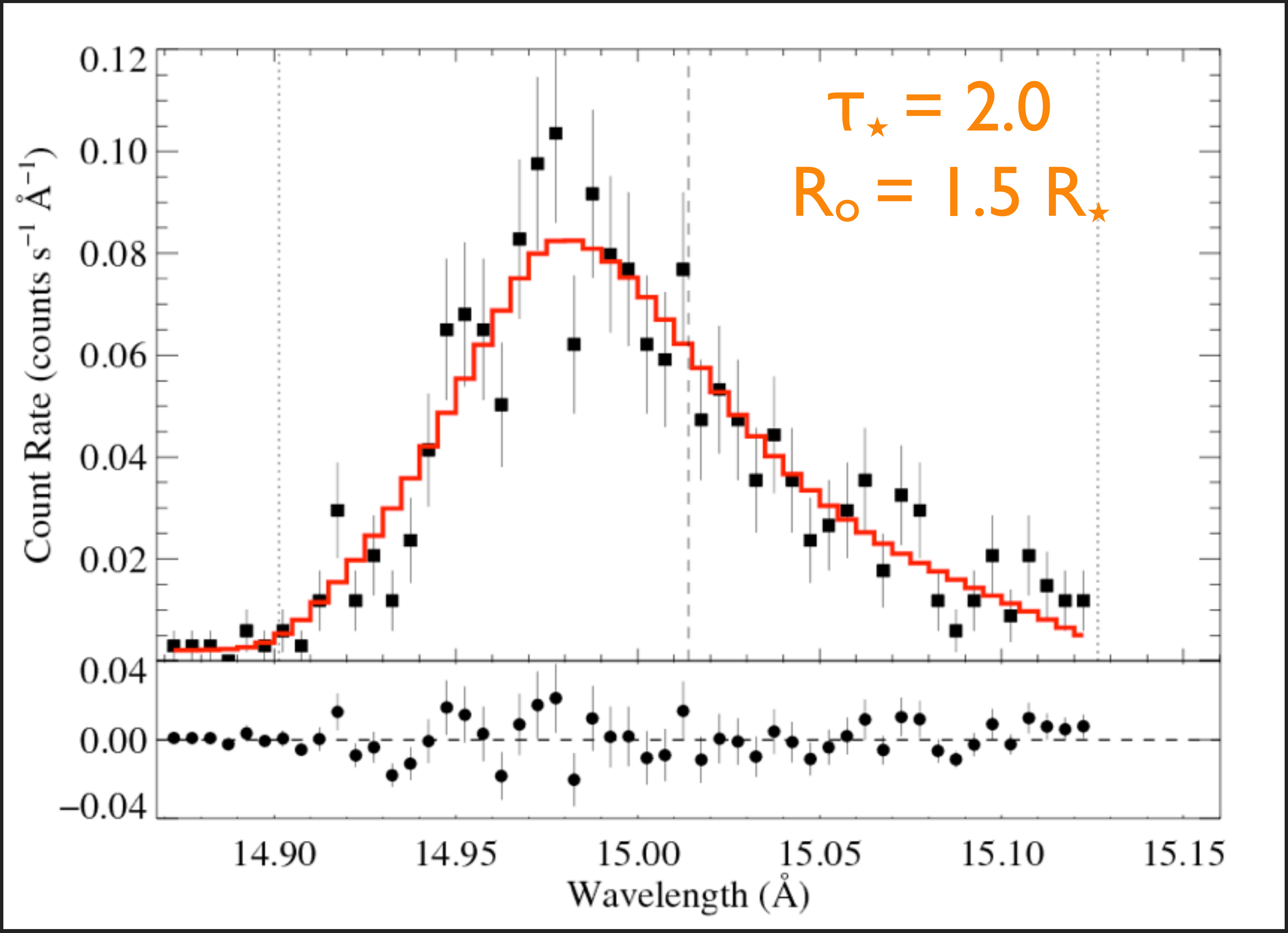

DISTRIBUTION OF R_0 VALUES FOR ZETA PUP

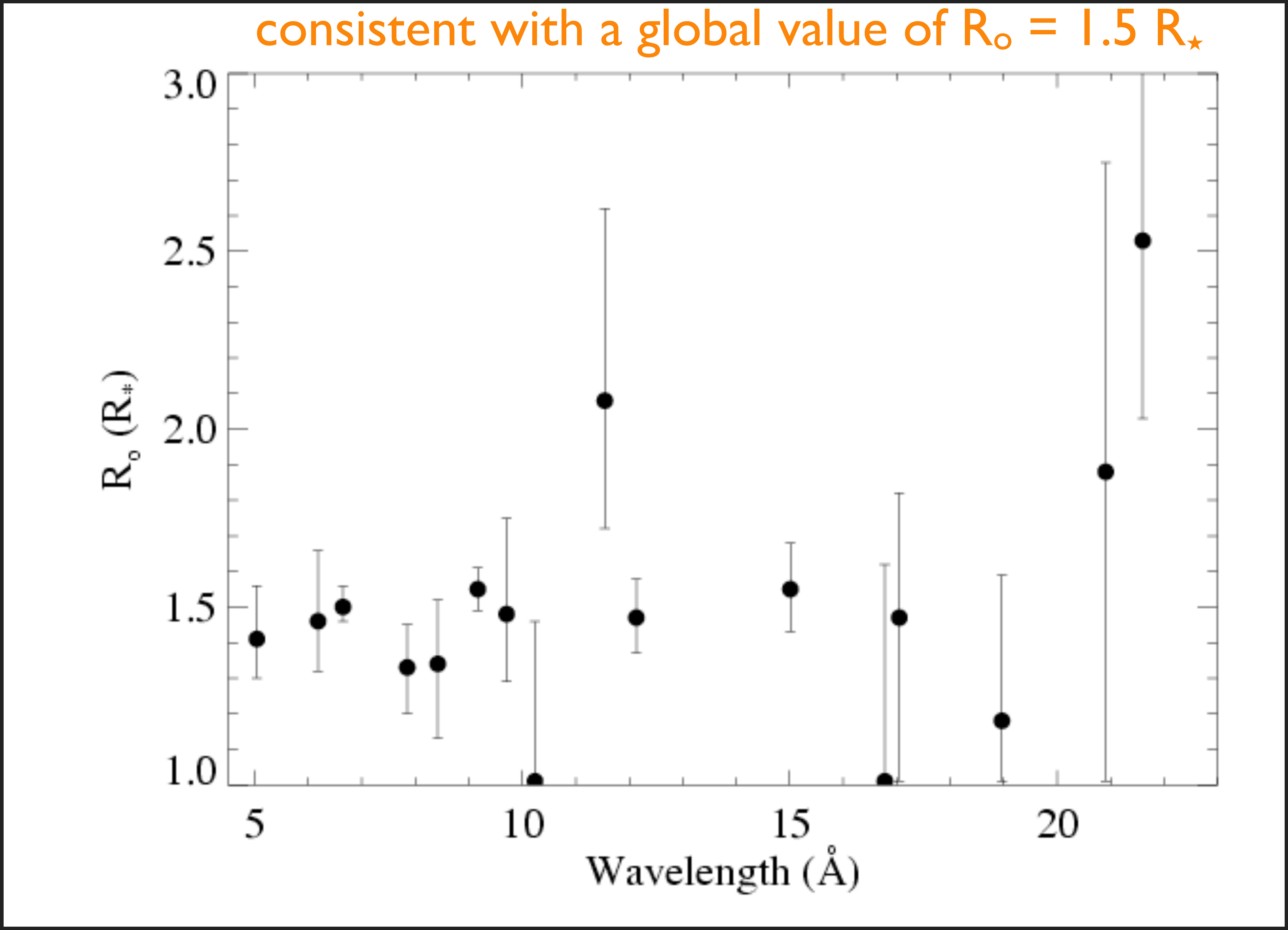

NUMEROUS SHOCKS ABOVE 1.5 $R_\star$

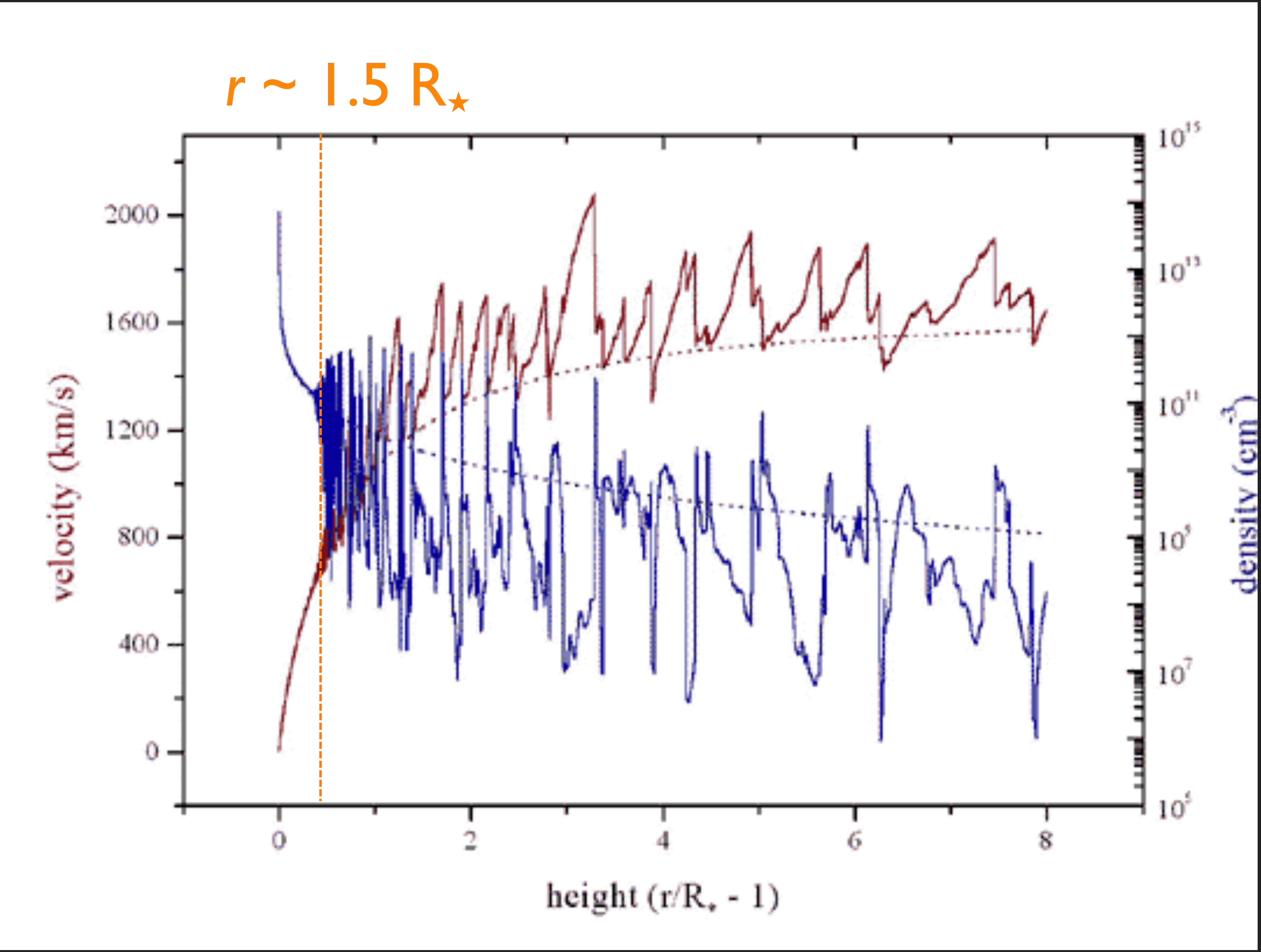

HIGH-RESOLUTION X-RAY SPECTROSCOPY OF O STAR WINDS

The profiles also tell us about the level of **wind absorption**

Wind Profile Model

$$\tau_* = \frac{\kappa \dot{M}}{4\pi R_* v_\infty}$$

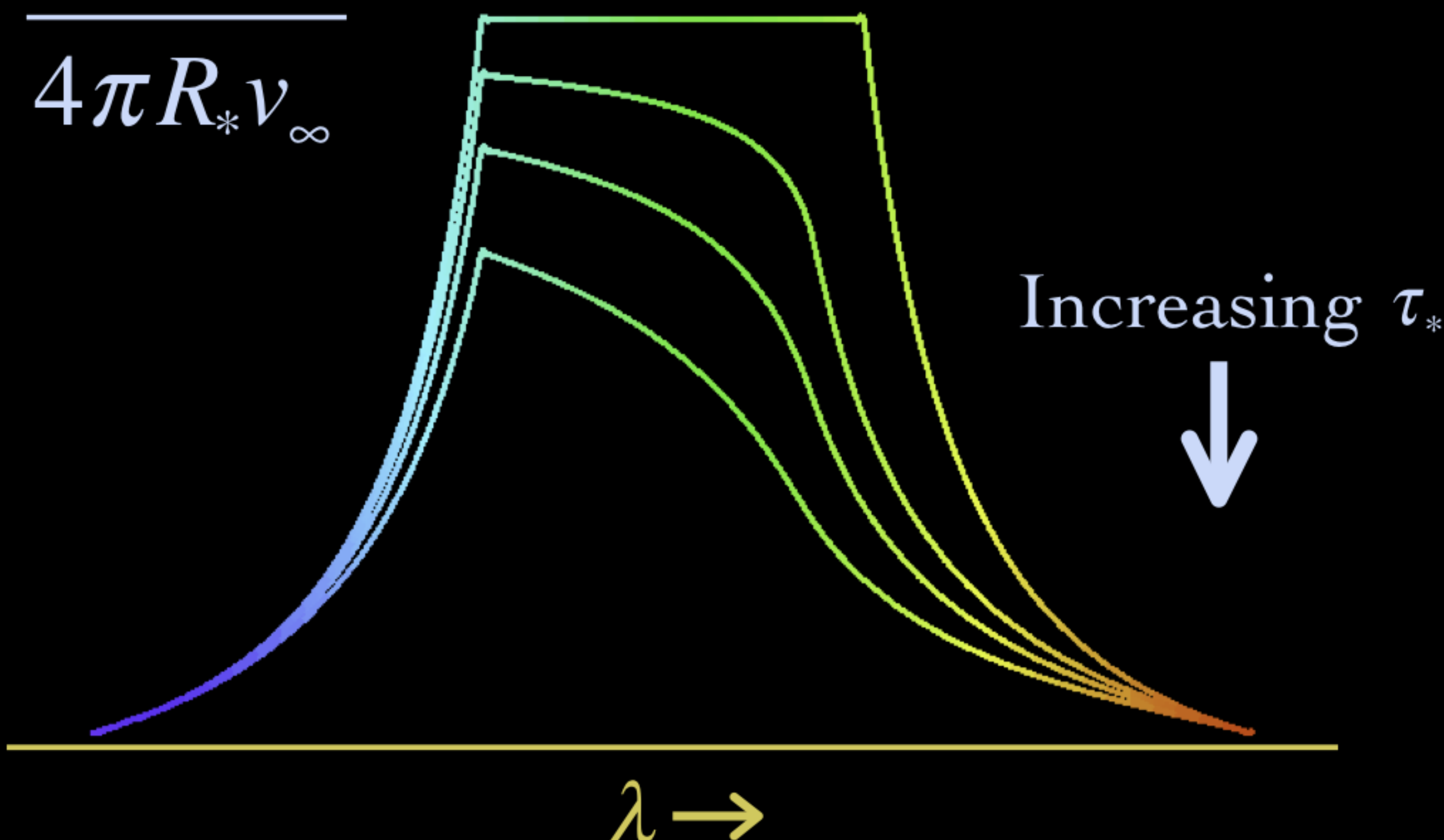

FITTING THIS MODEL TO AN EMISSION LINE

Fe XVII in the *Chandra* MEG spectrum of ζ Pup

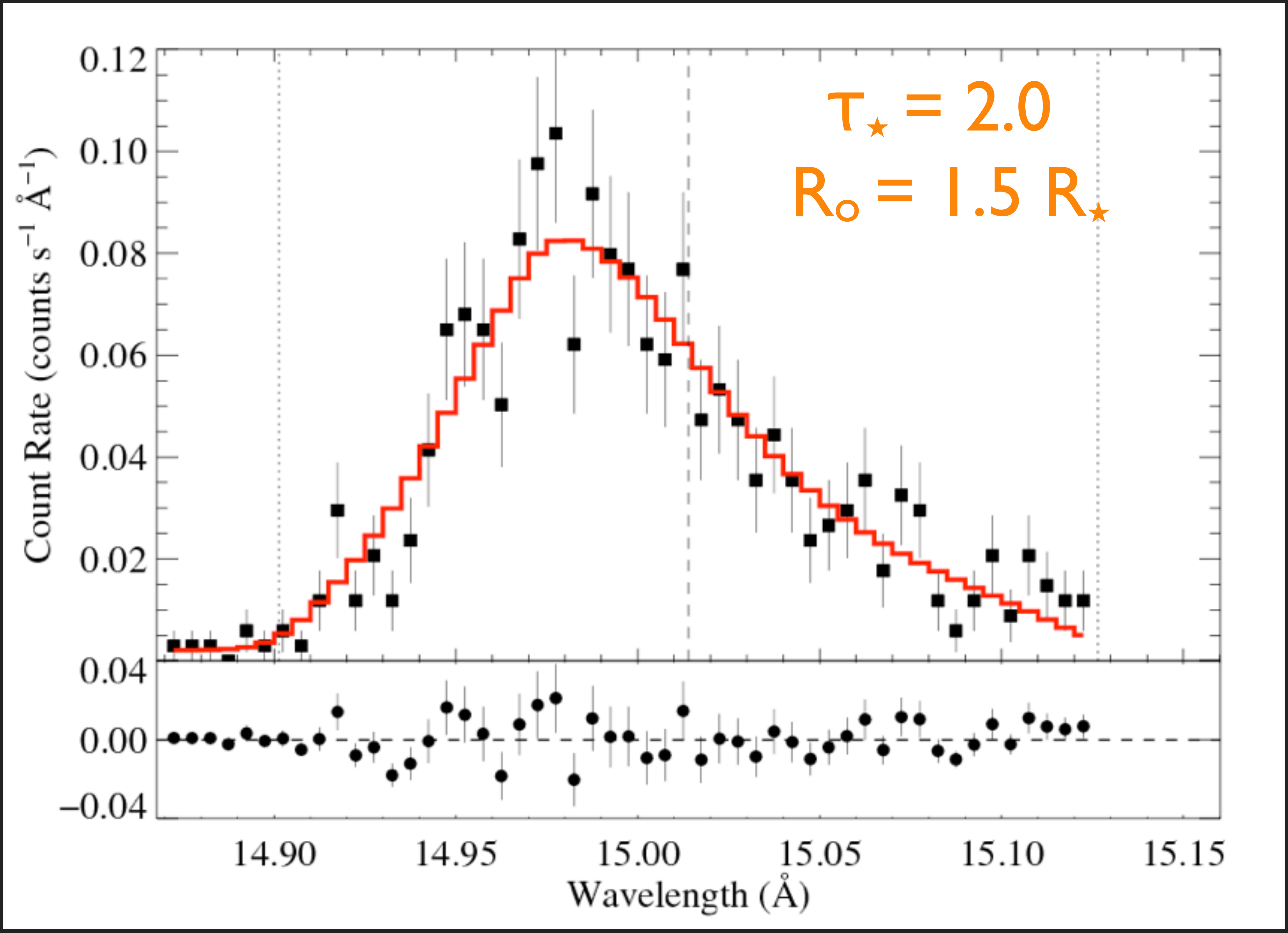

QUANTIFYING THE WIND OPTICAL DEPTH

opacity of the cold wind component (due to bound-free transitions in C, N, O, Ne, Fe)

wind mass-loss rate

$$\dot{M} = 4\pi r^2 v \rho$$

$$\tau_* \equiv \frac{\kappa \dot{M}}{4\pi R_* v_\infty}$$

stellar radius

wind terminal velocity

SOFT X-RAY WIND OPACITY

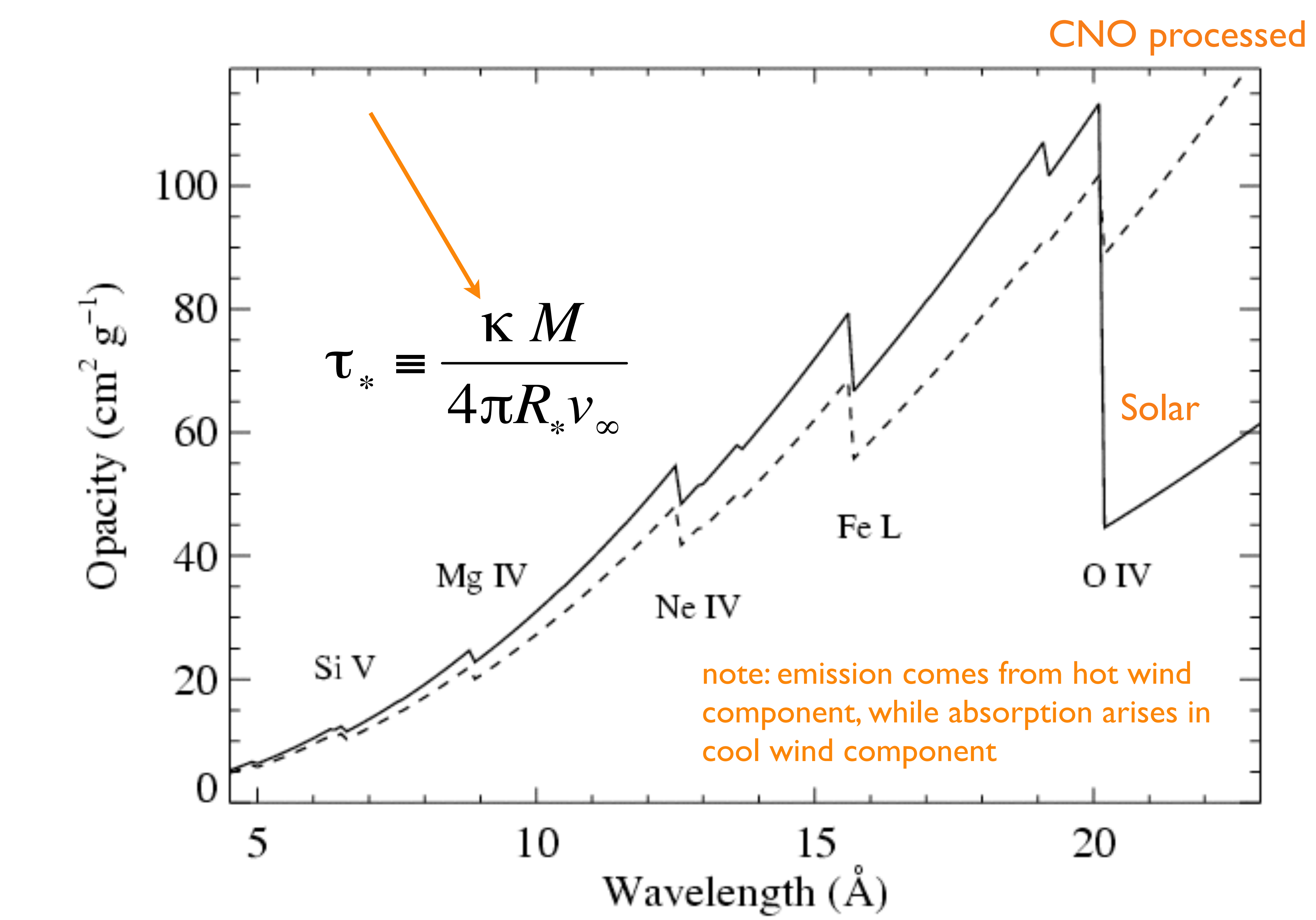

ZETA PUP CHANDRA: THREE EMISSION LINES

Mg Lya: 8.42 Å

Ne Lya: 12.13 Å

O Lya: 18.97 Å

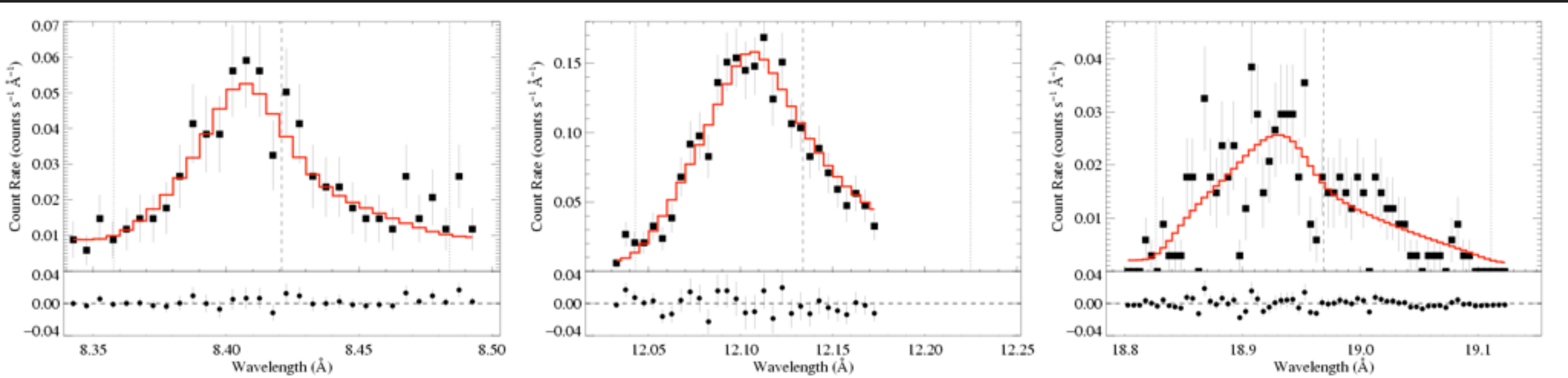

$\tau_* \sim 1$

$\tau_* \sim 2$

$\tau_* \sim 3$

Recall:

$$\tau_* \equiv \frac{\kappa \dot{M}}{4\pi R_* v_\infty}$$

ZETA PUP CHANDRA: THREE EMISSION LINES

Results from the 3 line fits shown previously

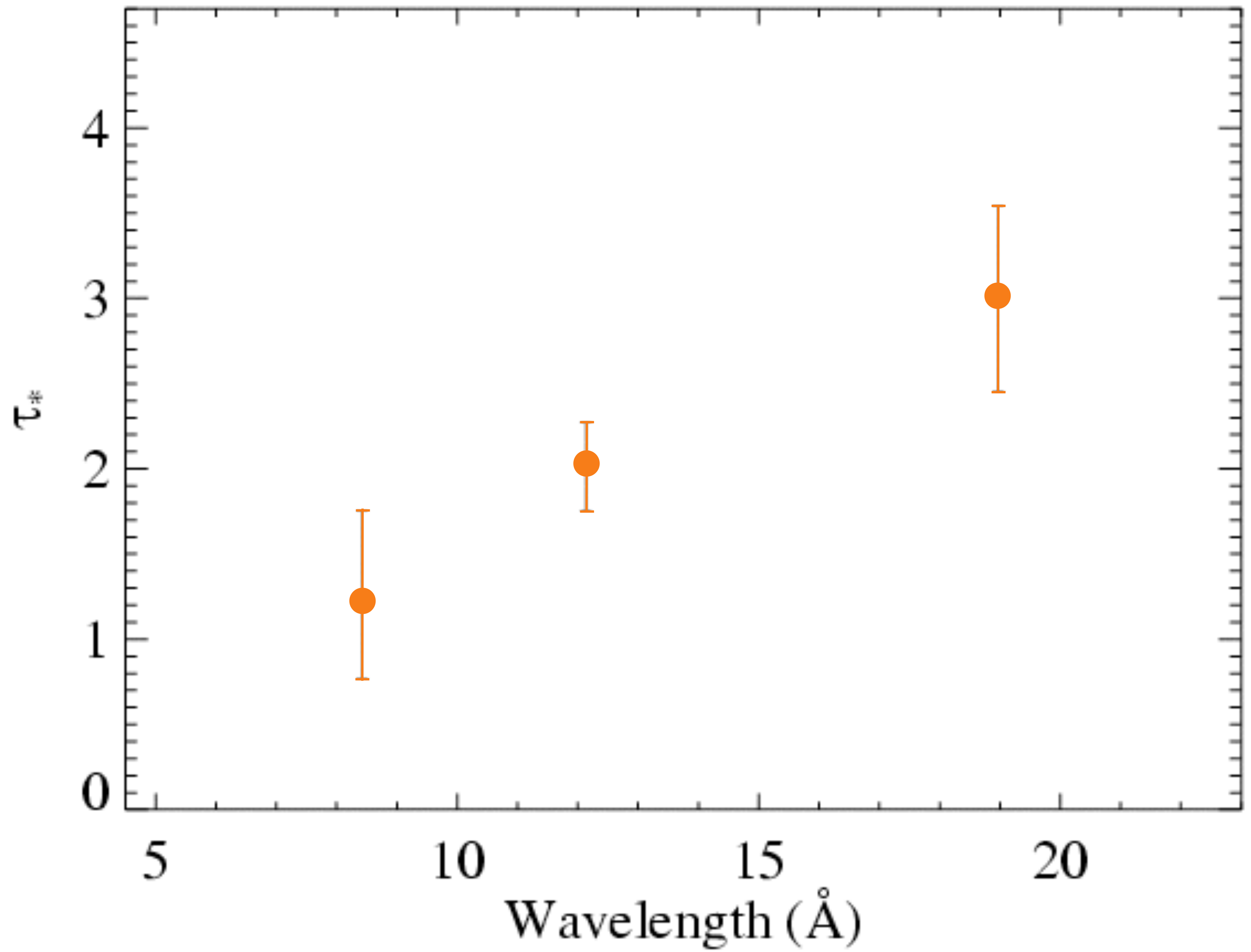

ZETA PUP CHANDRA: ALL 16 EMISSION LINES

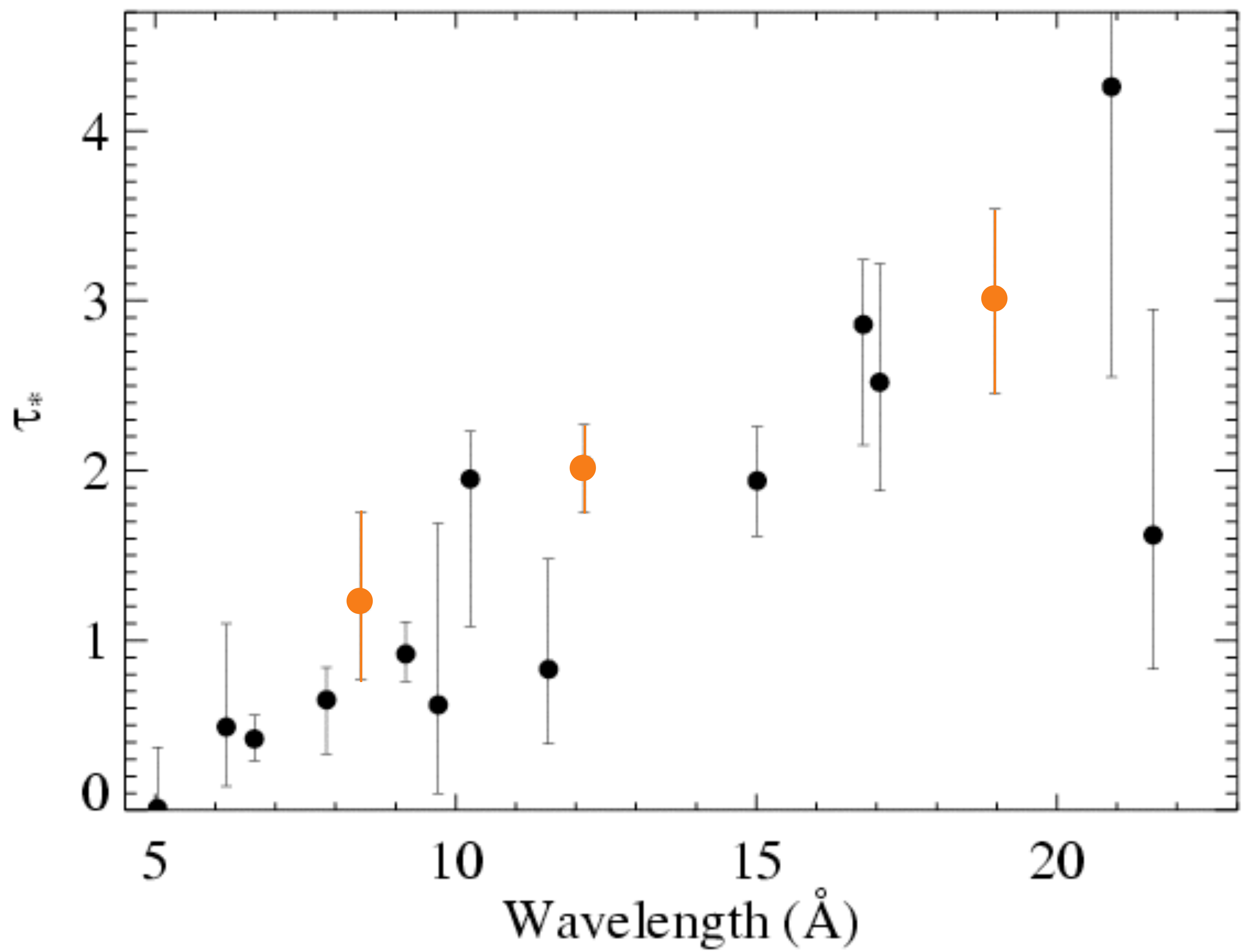

ZETA PUP CHANDRA: ALL 16 EMISSION LINES

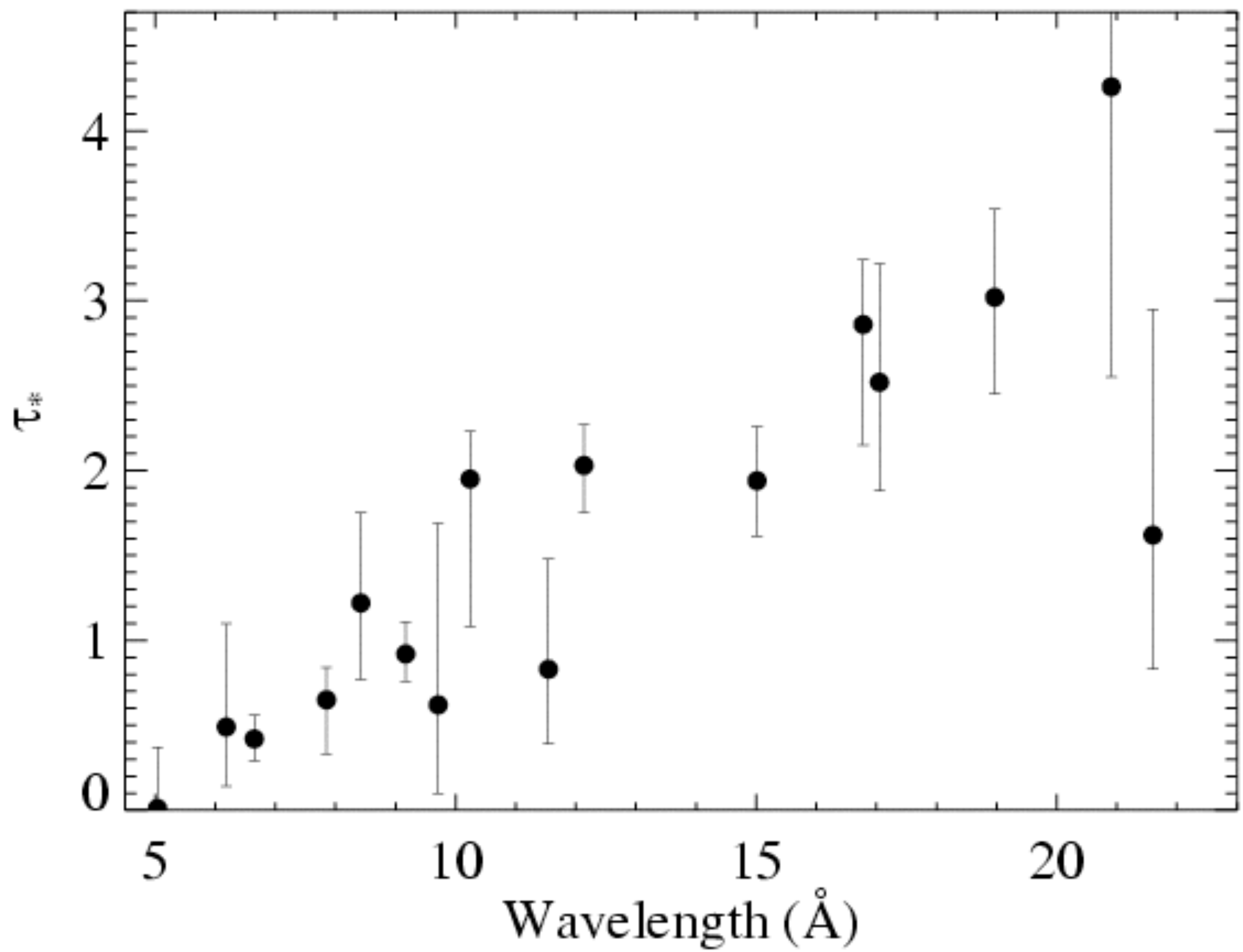

ZETA PUP CHANDRA: ALL 16 EMISSION LINES

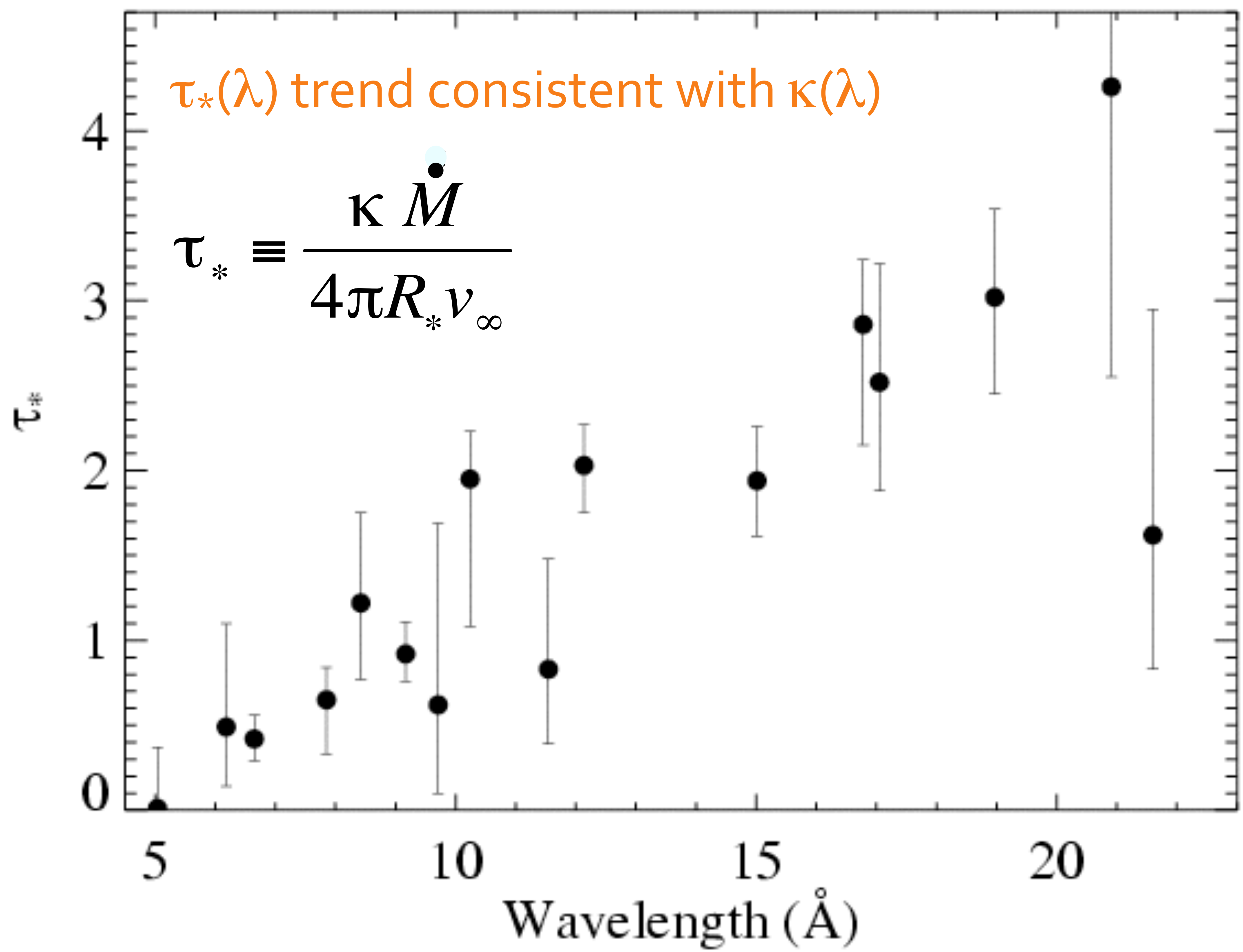

SOFT X-RAY WIND OPACITY

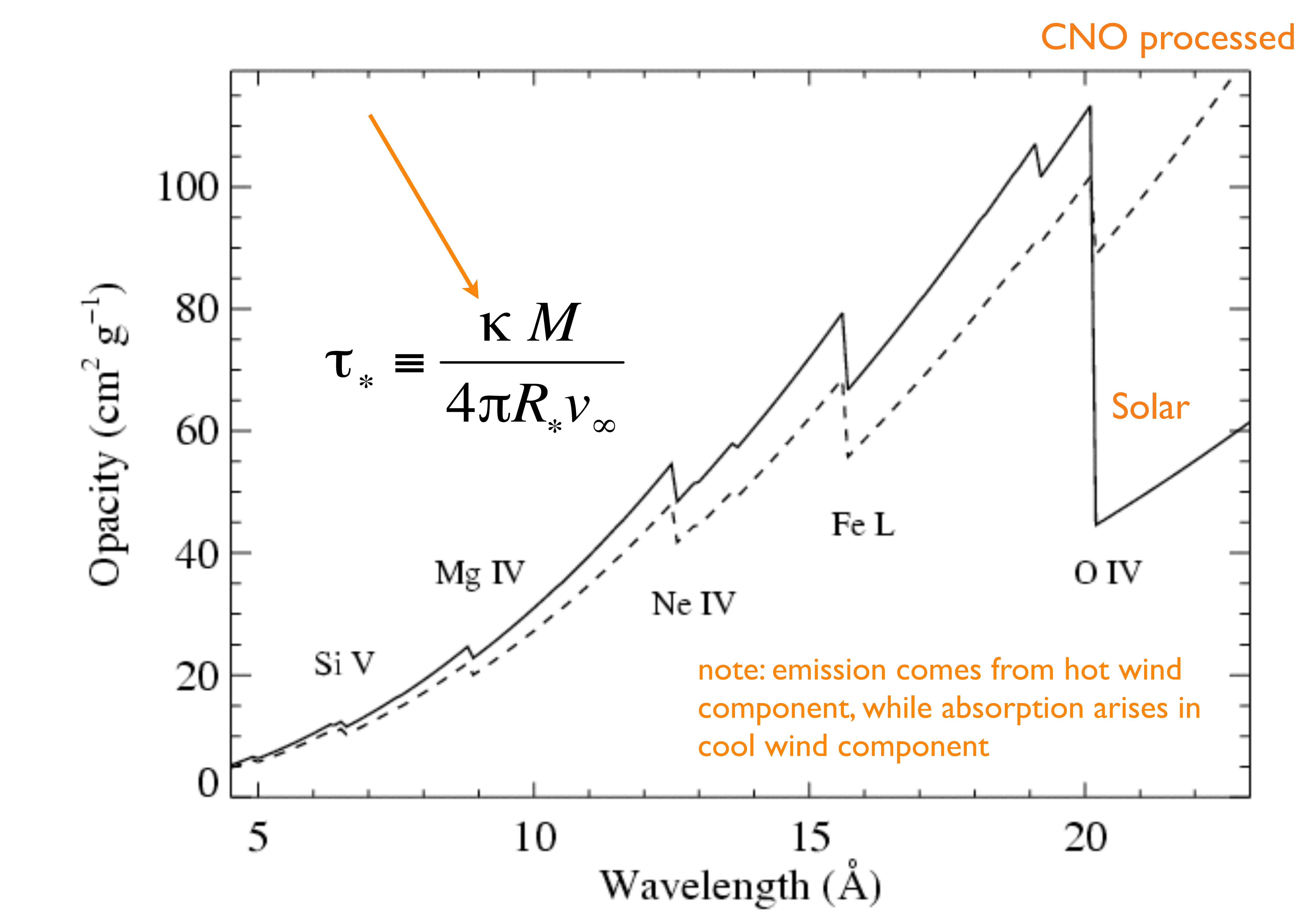

FITTING THE ENSEMBLE OF OPTICAL DEPTH VALUES

- $\dot{M}$ becomes the free parameter of the fit to the $\tau_*(\lambda)$ trend

$$\tau_* \equiv \frac{\kappa \dot{M}}{4\pi R_* v_\infty}$$

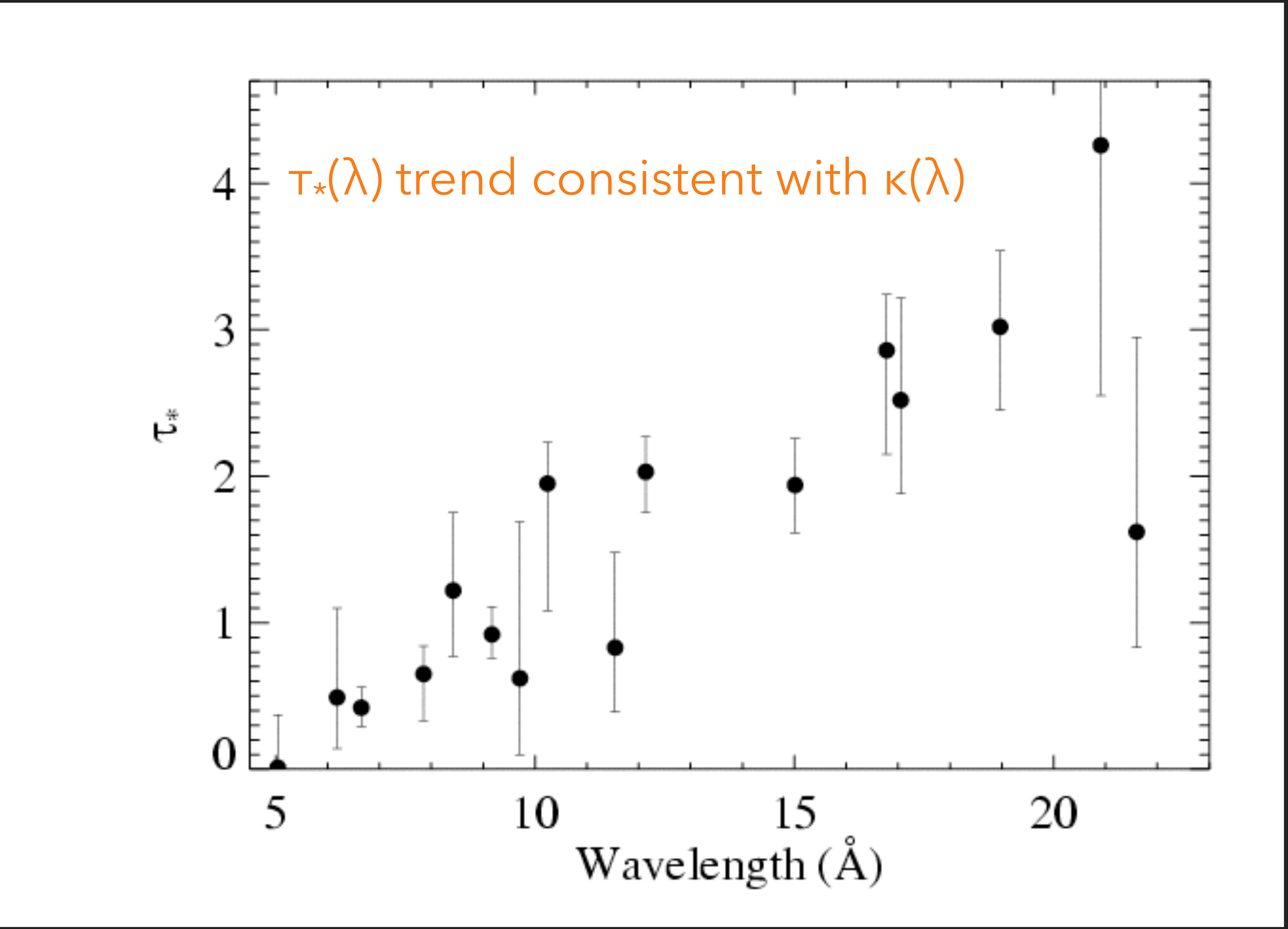

FITTING THE ENSEMBLE OF OPTICAL DEPTH VALUES

- $\dot{M}$ becomes the free parameter of the fit to the $\tau_*(\lambda)$ trend

$$\tau_* \equiv \frac{\kappa \dot{M}}{4\pi R_* v_\infty}$$

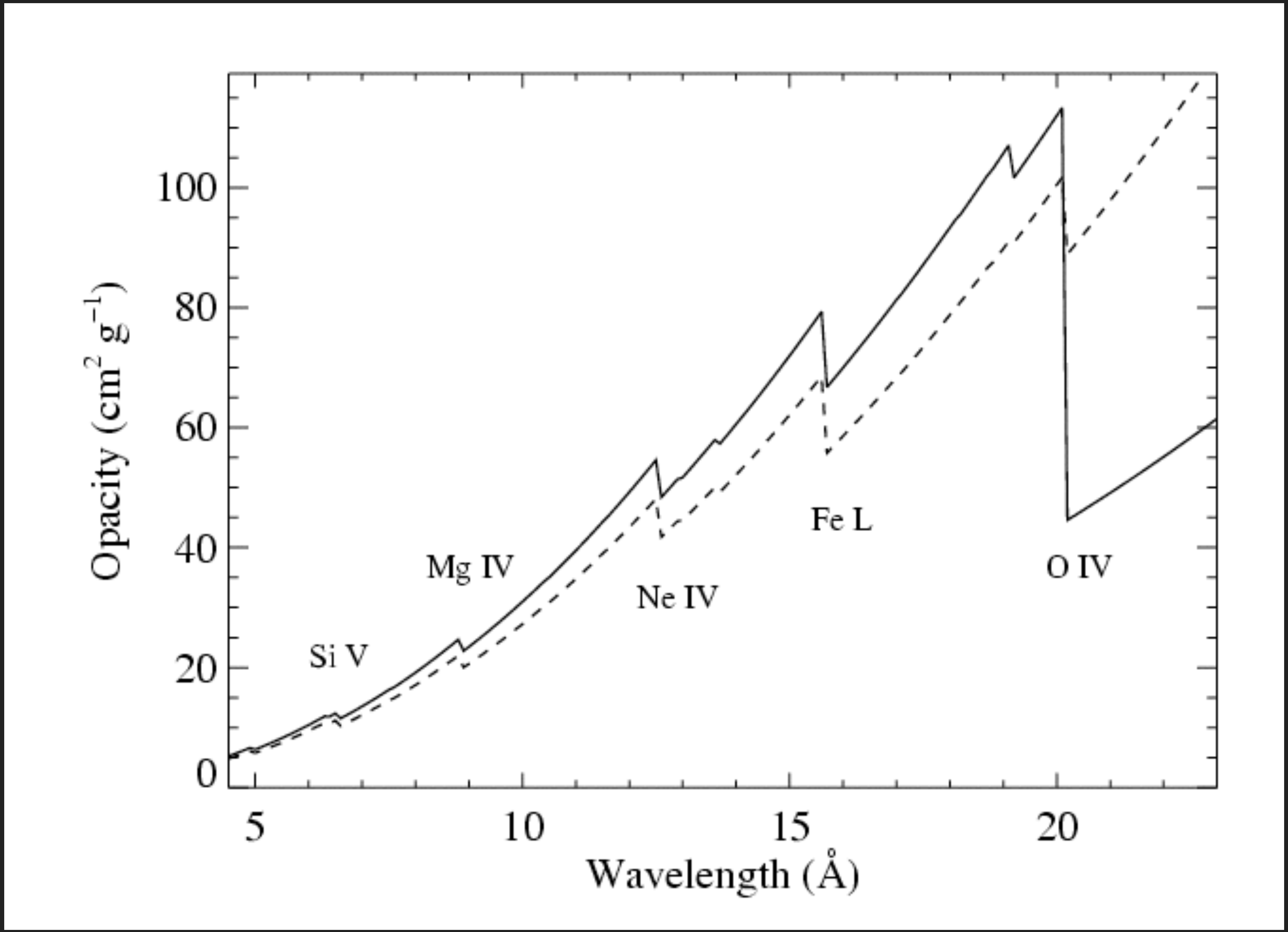

TO FIND THE MASS-LOSS RATE

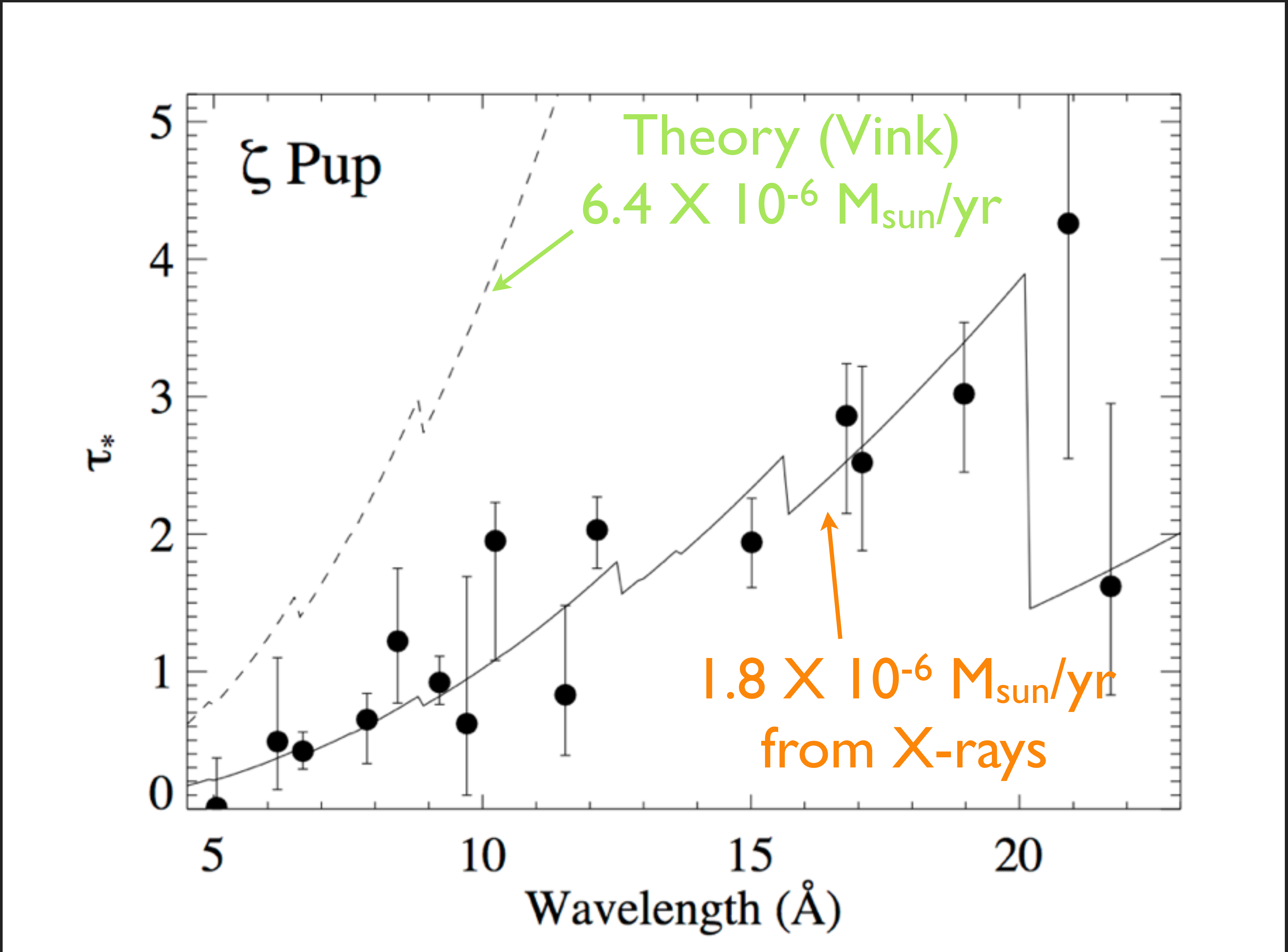

THEORETICAL MASS-LOSS RATE IS CLEARLY TOO HIGH

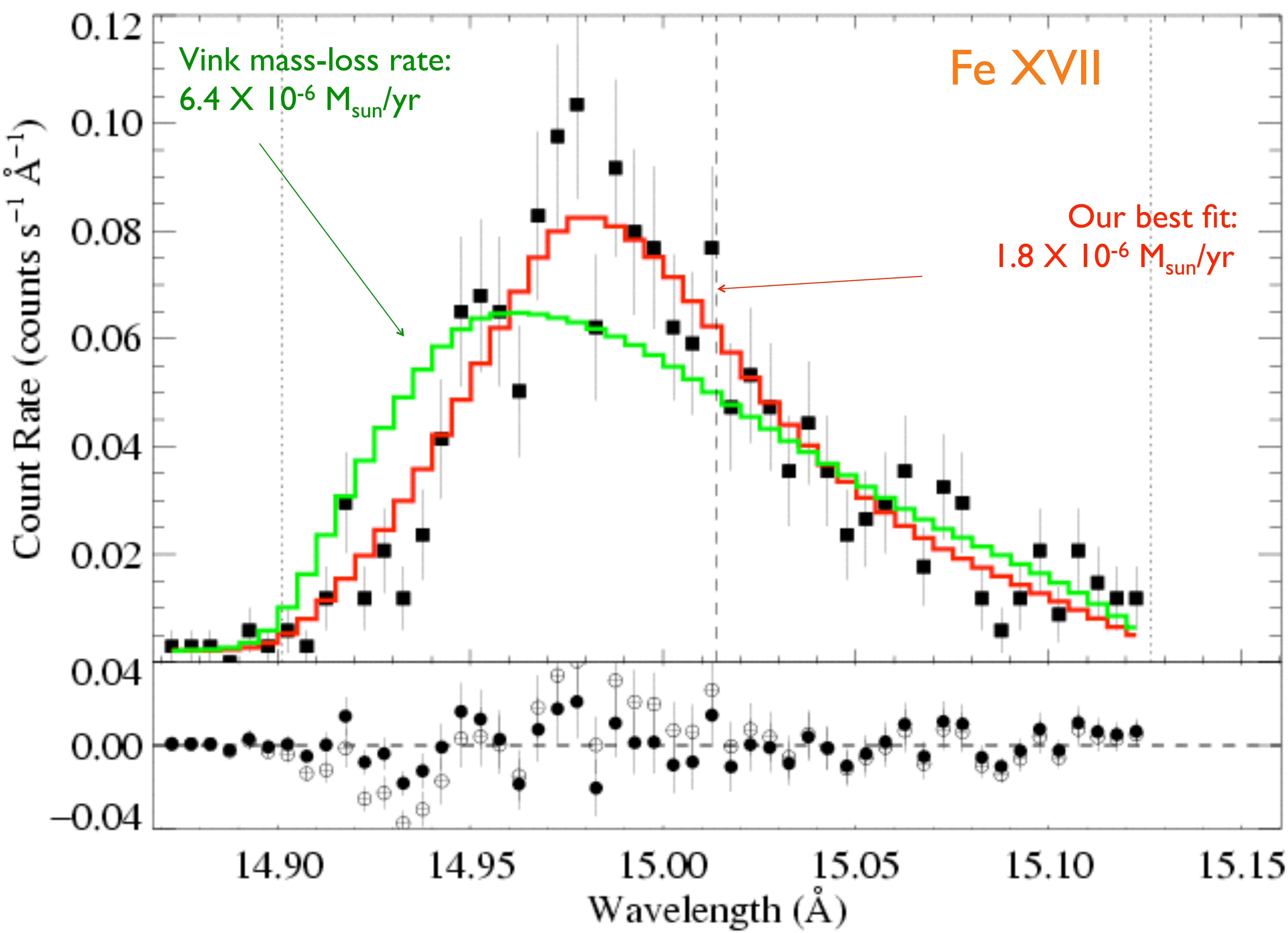

AND HISTORICAL MASS-LOSS RATE DETERMINATION, TOO

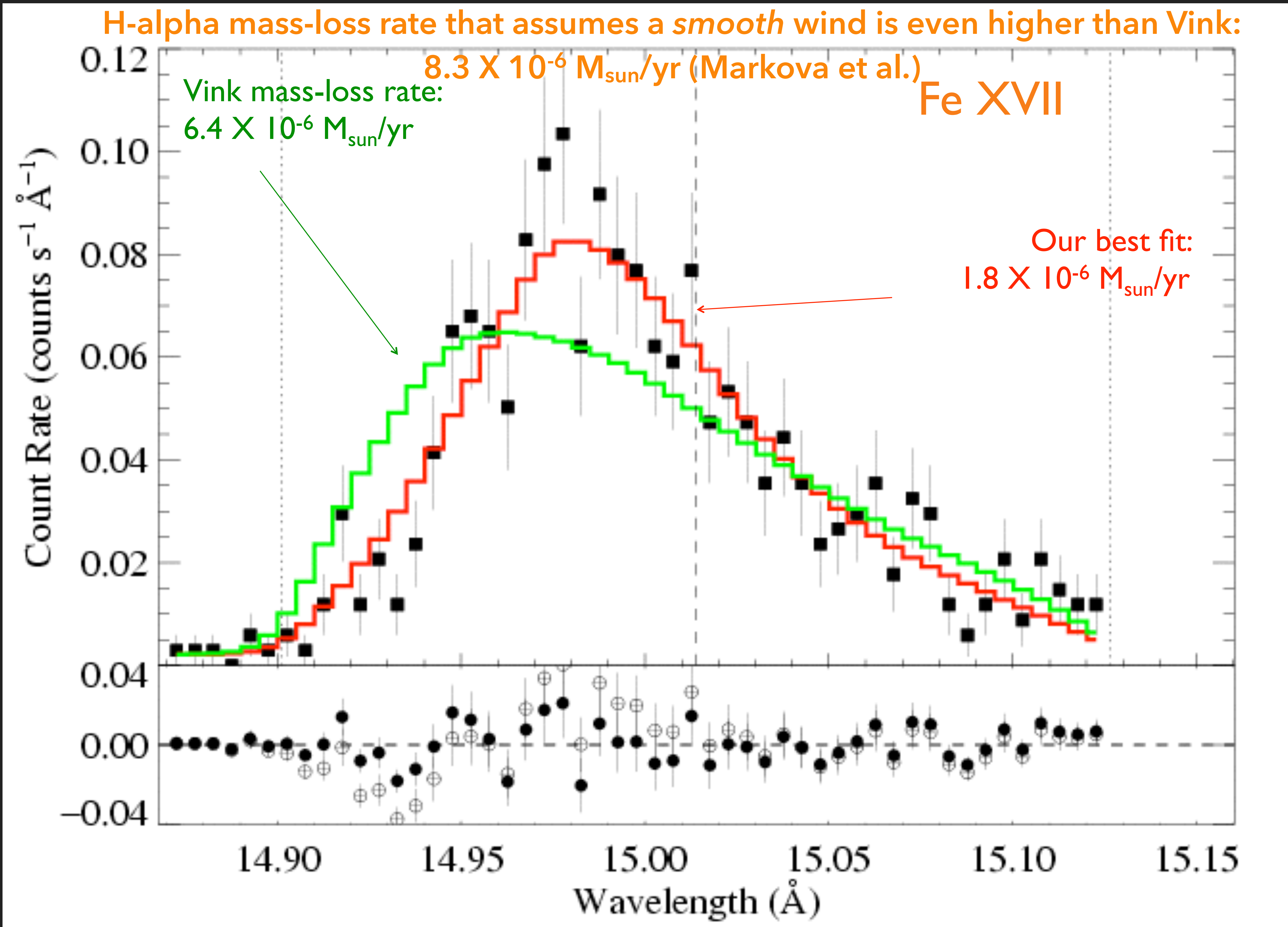

X-RAY LINE PROFILE BASED MASS-LOSS RATE

implications for clumping

basic definition: $f_{cl} \equiv \langle\rho^2\rangle/\langle\rho\rangle^2$

clumping factor

X-RAY LINE PROFILE BASED MASS-LOSS RATE

implications for clumping

basic definition: $f_{cl} \equiv \langle\rho^2\rangle / \langle\rho\rangle^2$

from density-squared diagnostics like Hα, IR & radio free-free

from (column) density diagnostic like $\tau_\star$ from X-ray profiles

ZETA PUP: RADIALLY VARYING CLUMPING

for $\dot{M} = 1.8 \times 10^{-6}$ M_{sun}/yr

$$f_{cl} \equiv \langle\rho^2\rangle / \langle\rho\rangle^2$$

$$\dot{M}_{cl} \equiv \dot{M}_{smooth} / f_{cl}^{0.5}$$

$f_{cl} = 5.4$ @ $r < 1.12\ R_*$	Hα
$f_{cl} = 22.6$ @ $1.12 < r < 1.5\ R_*$	Hα
$f_{cl} = 13.9$ @ $1.5 < r < 2\ R_*$	Hα
$f_{cl} = 9.8$ @ $2 < r < 15\ R_*$	IR
$f_{cl} = 5.4$ @ $r > 15\ R_*$	radio

Hα

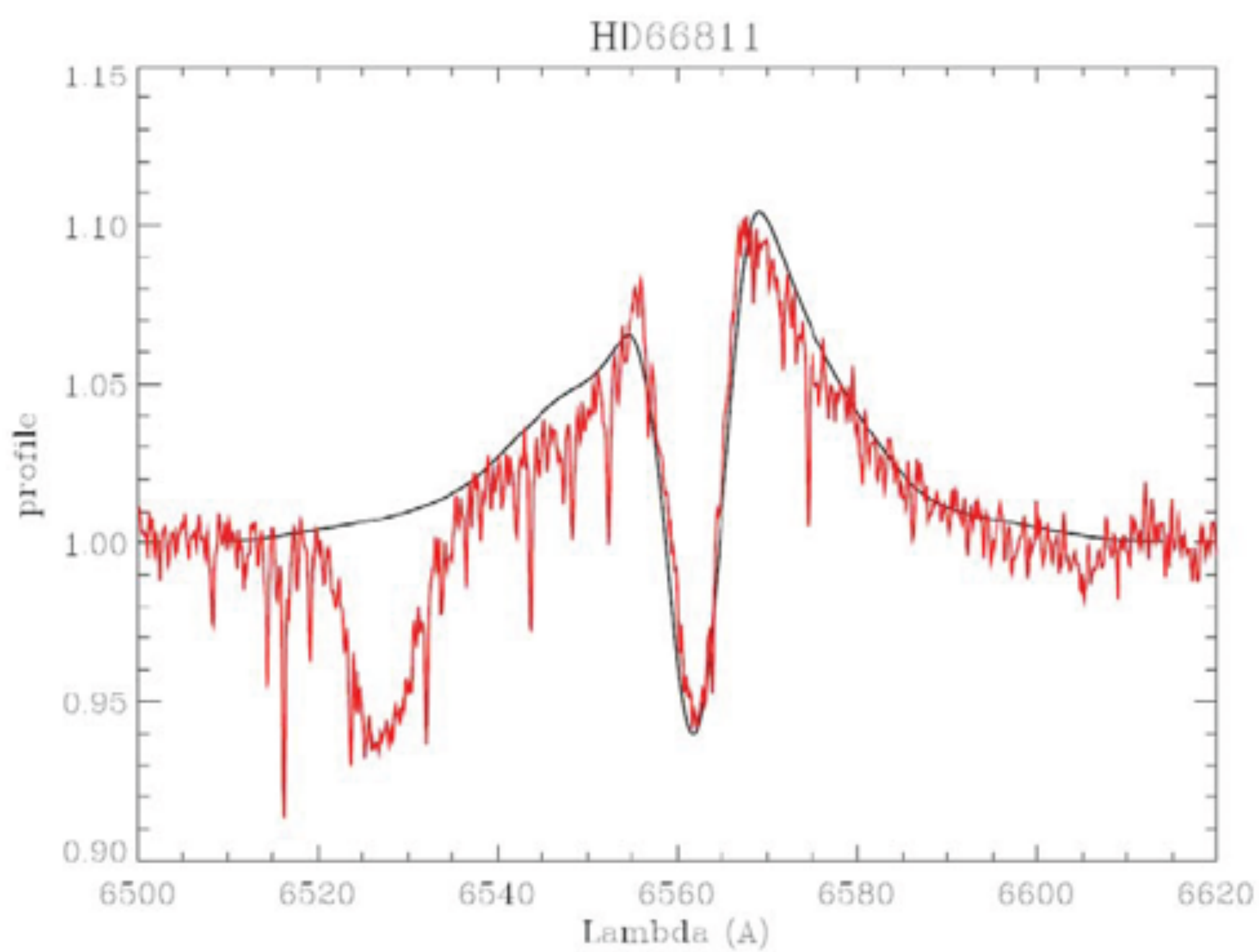

IR radio

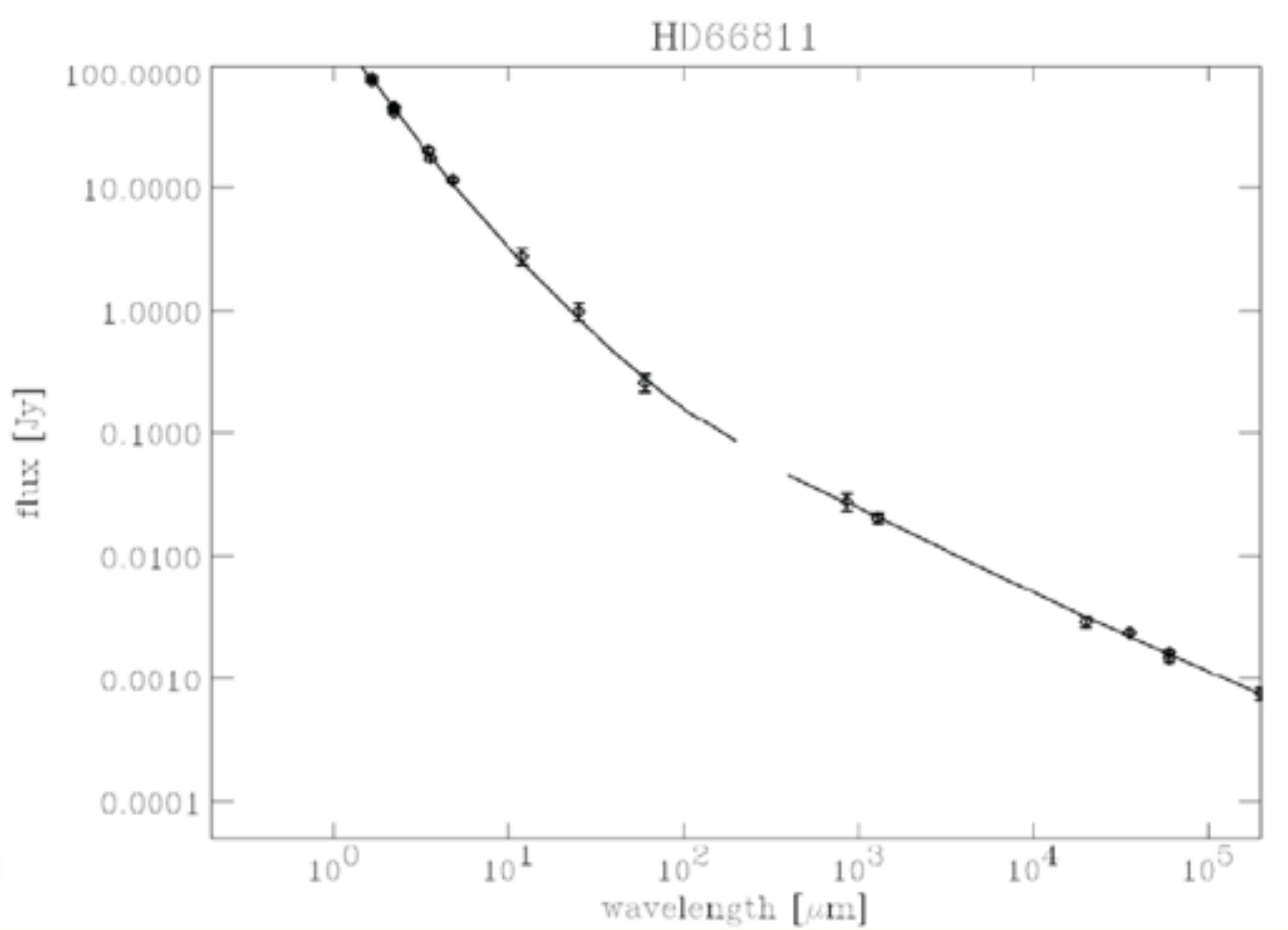

ZETA PUP: RADIALLY VARYING CLUMPING

base of the wind ($r < 1.5\ R_\star$)

is clumped

...but...

$f_{cl} = 5.4$ @ $r < 1.12\ R_*$ — Hα

$f_{cl} = 22.6$ @ $1.12 < r < 1.5\ R_*$ — Hα

$f_{cl} = 13.9$ @ $1.5 < r < 2\ R_*$ — Hα

$f_{cl} = 9.8$ @ $2 < r < 15\ R_*$ — IR

$f_{cl} = 5.4$ @ $r > 15\ R_*$ — radio

recall: X-ray $R_o = 1.5\ R_\star$

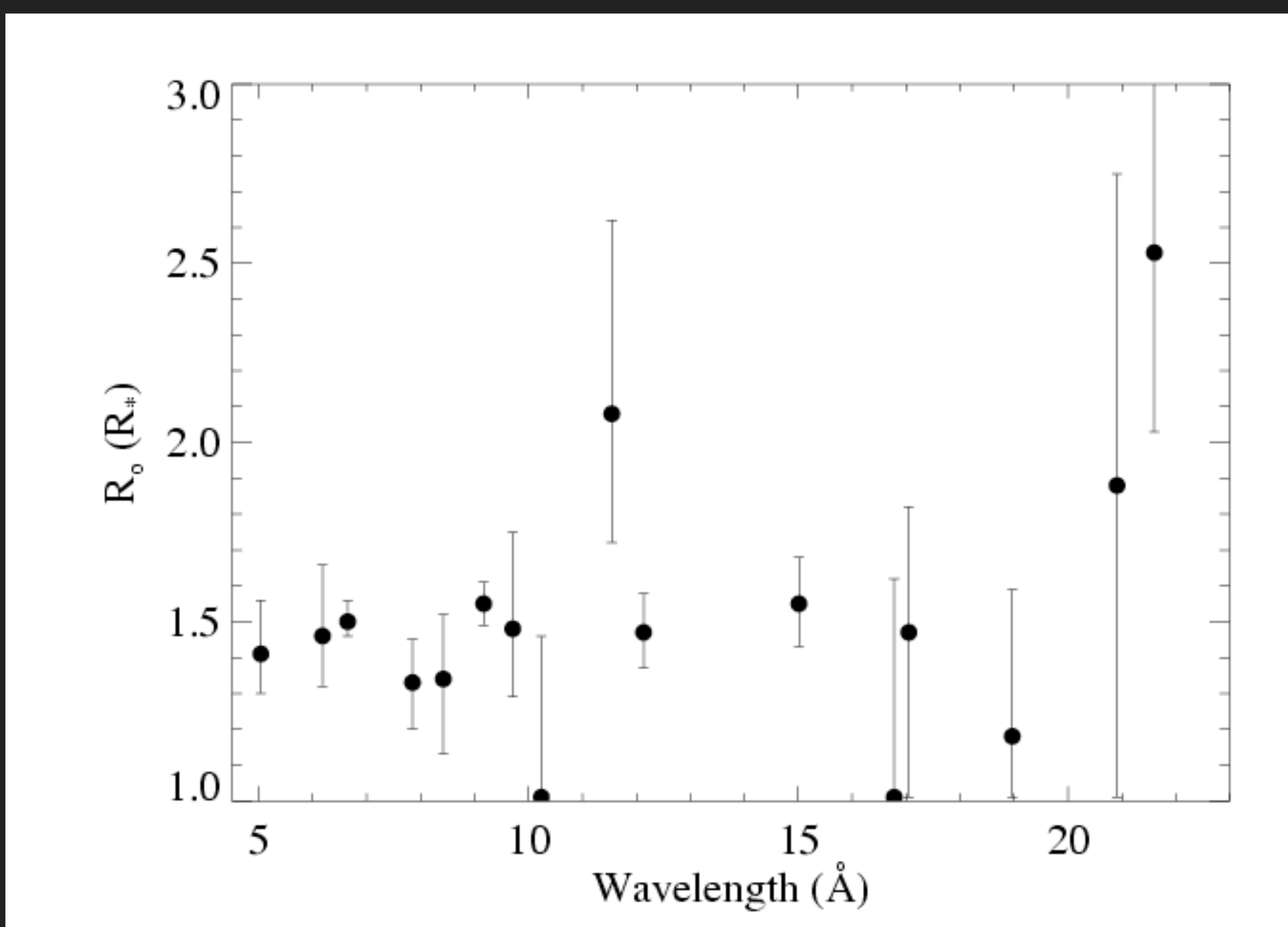

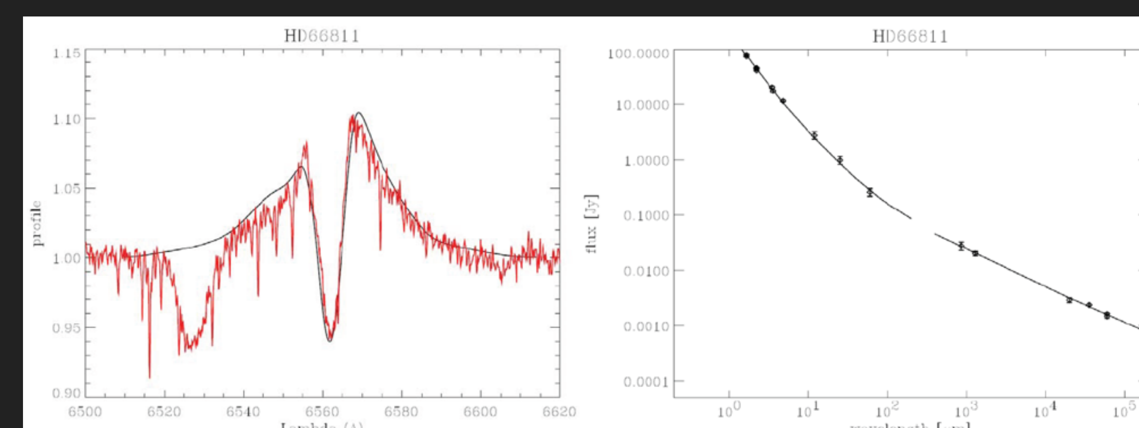

EXTENSION OF X-RAY PROFILE MASS-LOSS RATE DIAGNOSTIC TO OTHER STARS

lower mass-loss rates than theory predicts
with clumping factors typically of ~ 20

Cohen et al., 2014, *MNRAS*, 439, 908

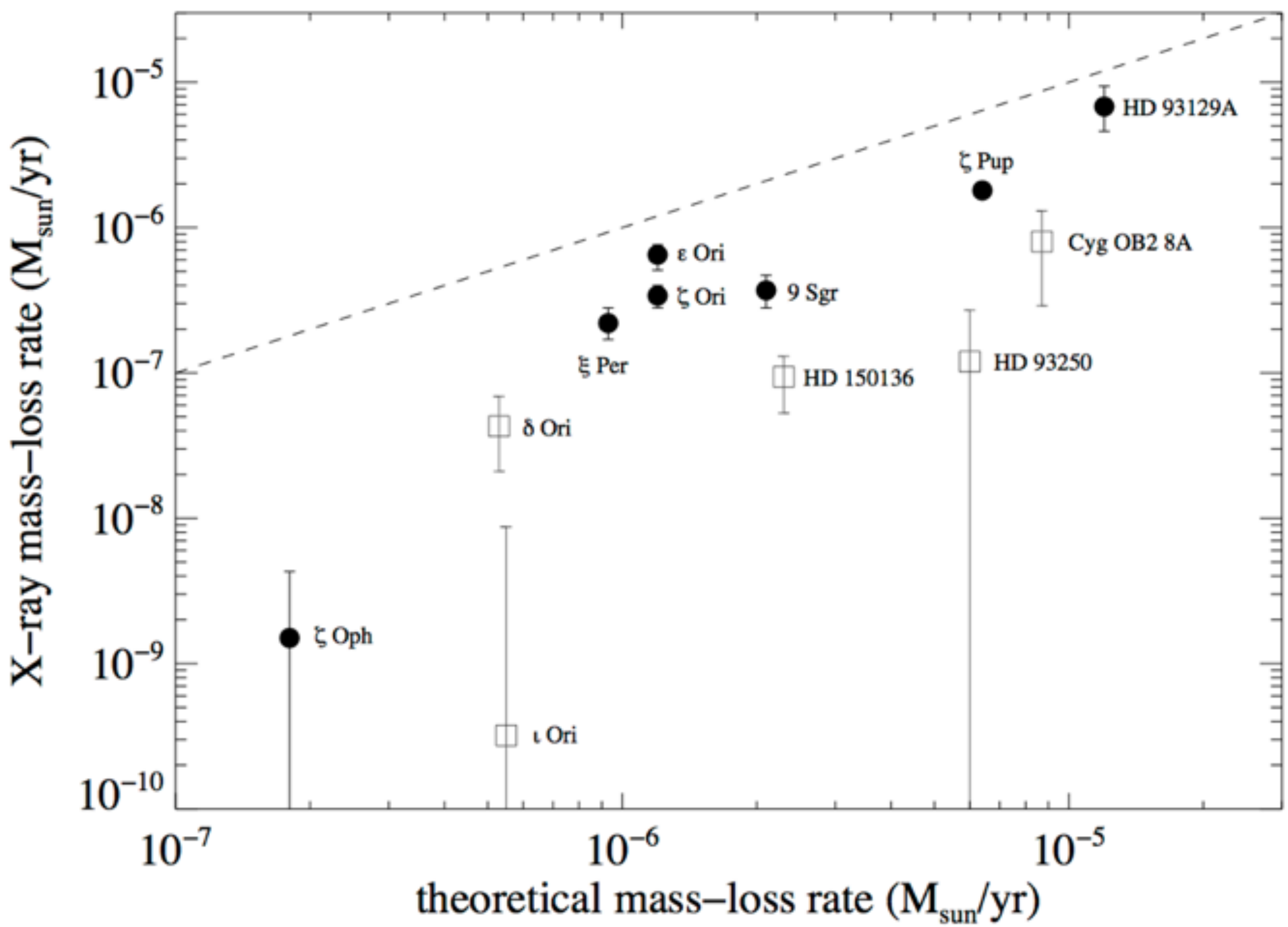

X-ray mass-loss rates: a few times less than theoretical predictions

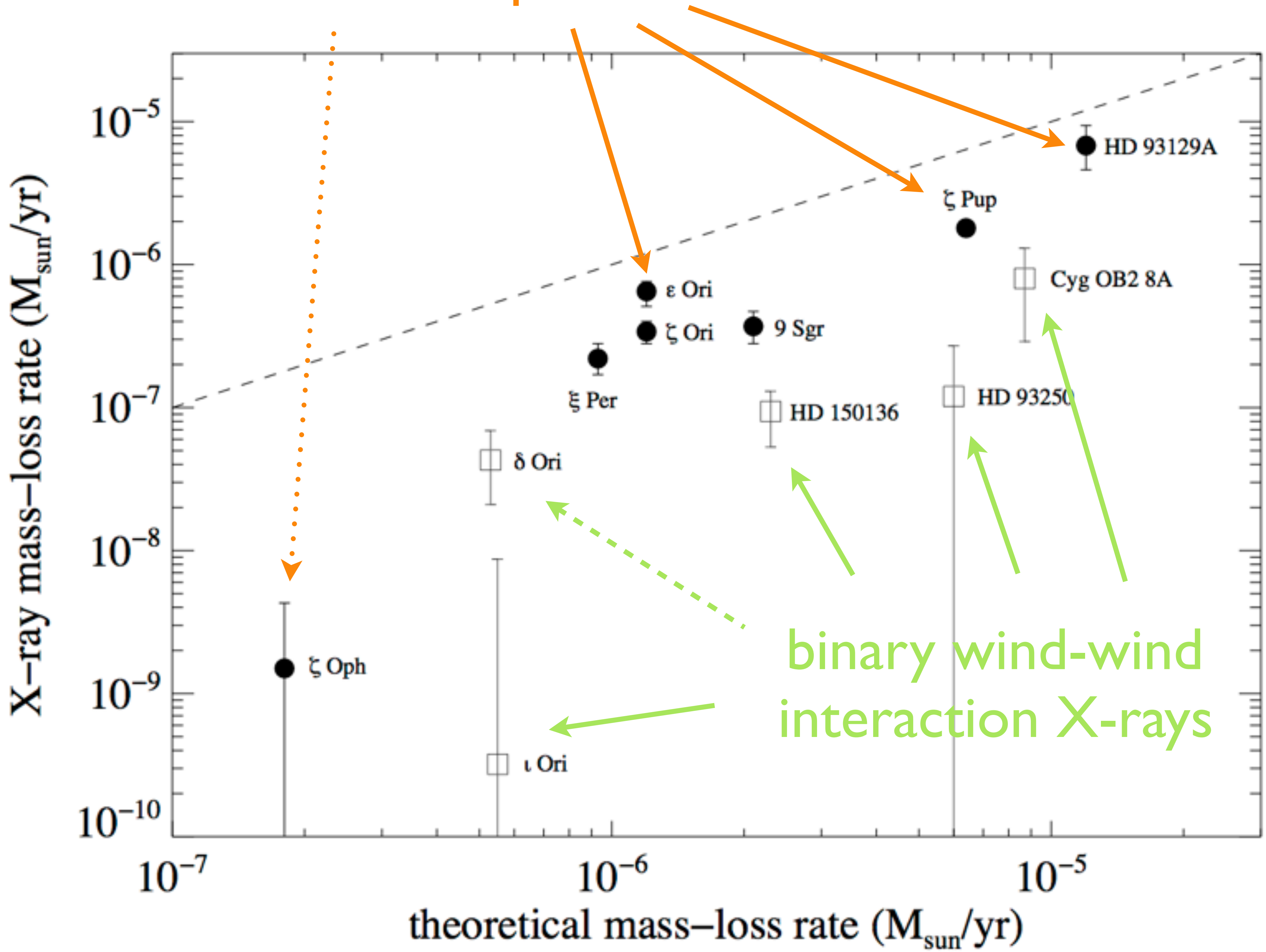

MASSIVE STAR WINDS VIA X-RAY SPECTROSCOPY

embedded wind shocks above $R_o = 1.5\ R_{star}$

lower wind mass-loss rates

clumping with $f_{cl} \sim 10$ to 20, down to wind base

Spectroscopy + modeling : information about spatial structure

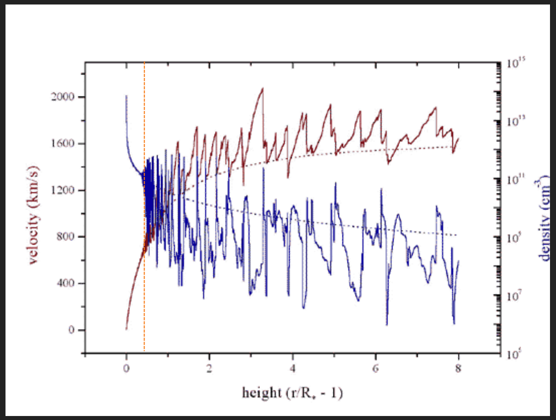

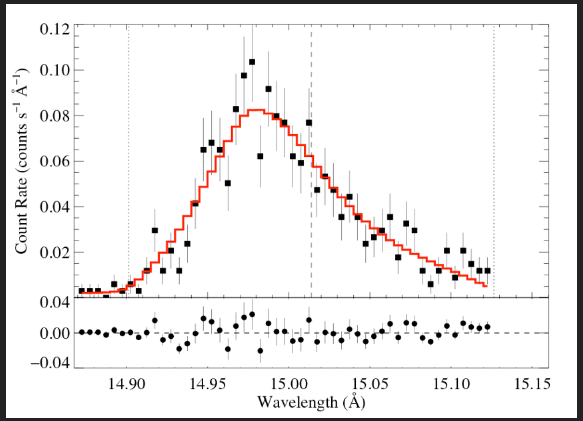

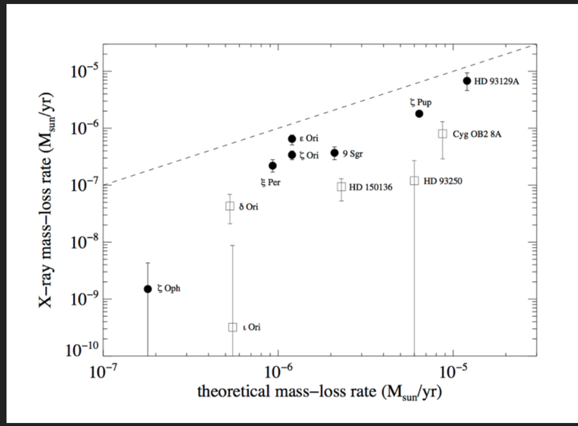

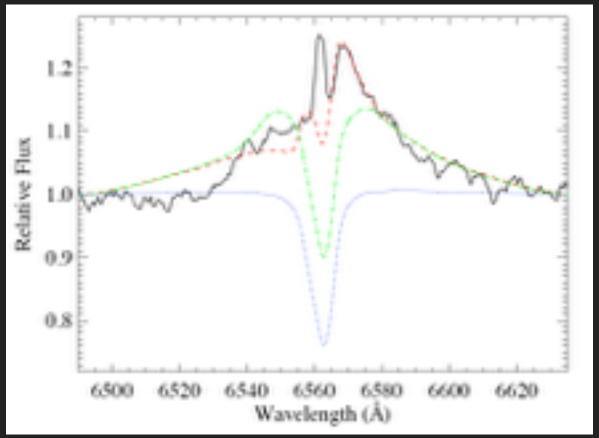

A SUBSET OF MASSIVE STARS HAVE LARGE-SCALE MAGNETIC FIELDS

theta-1 Ori C is the prototype magnetic O star

Hubble Space Telescope, Orion Nebula

A SUBSET OF MASSIVE STARS HAVE LARGE-SCALE MAGNETIC FIELDS

theta-1 Ori C is the prototype magnetic O star

Chandra X-ray image of the core of Orion

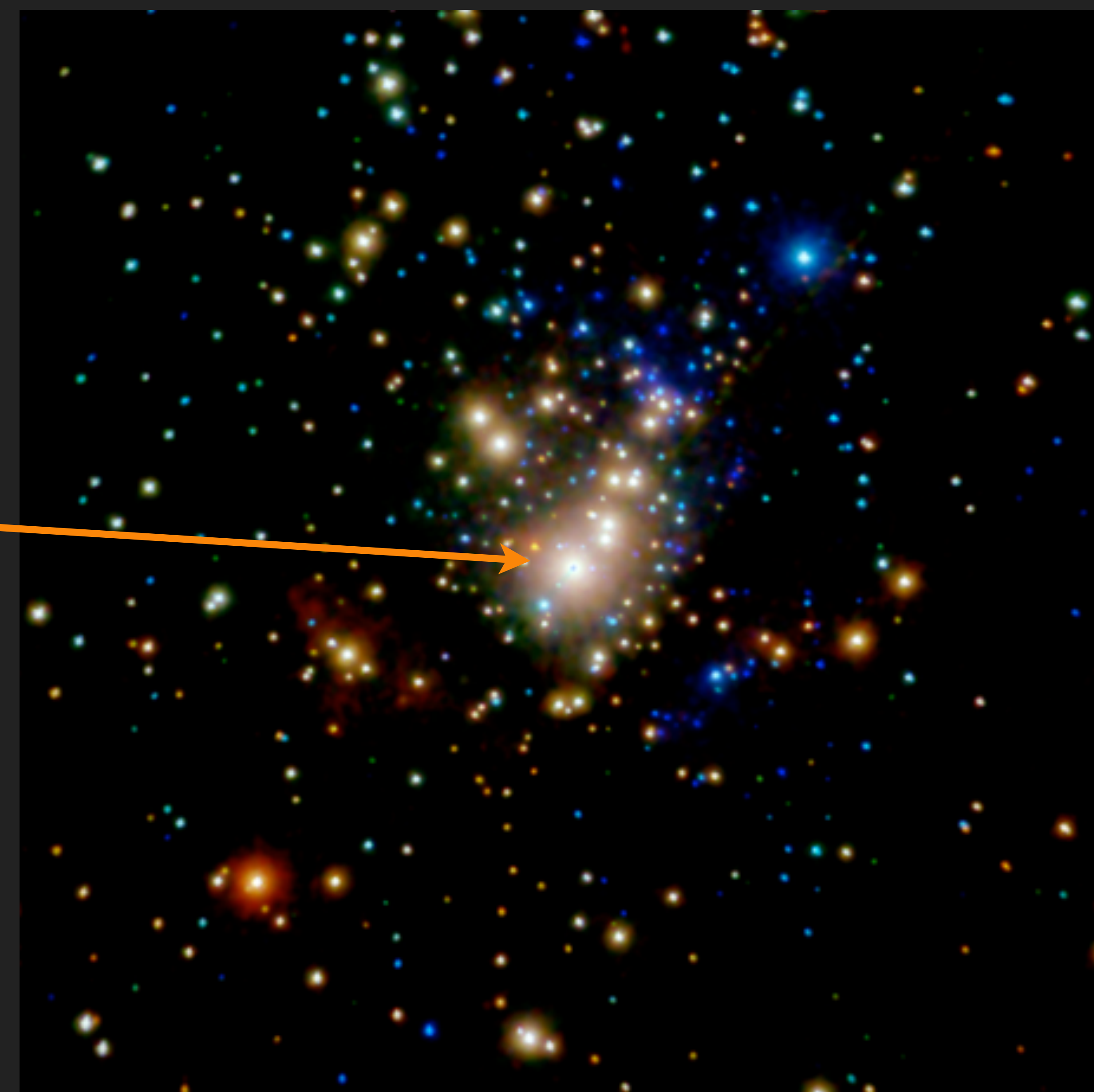

FIELDS ARE OFTEN TILTED DIPOLES

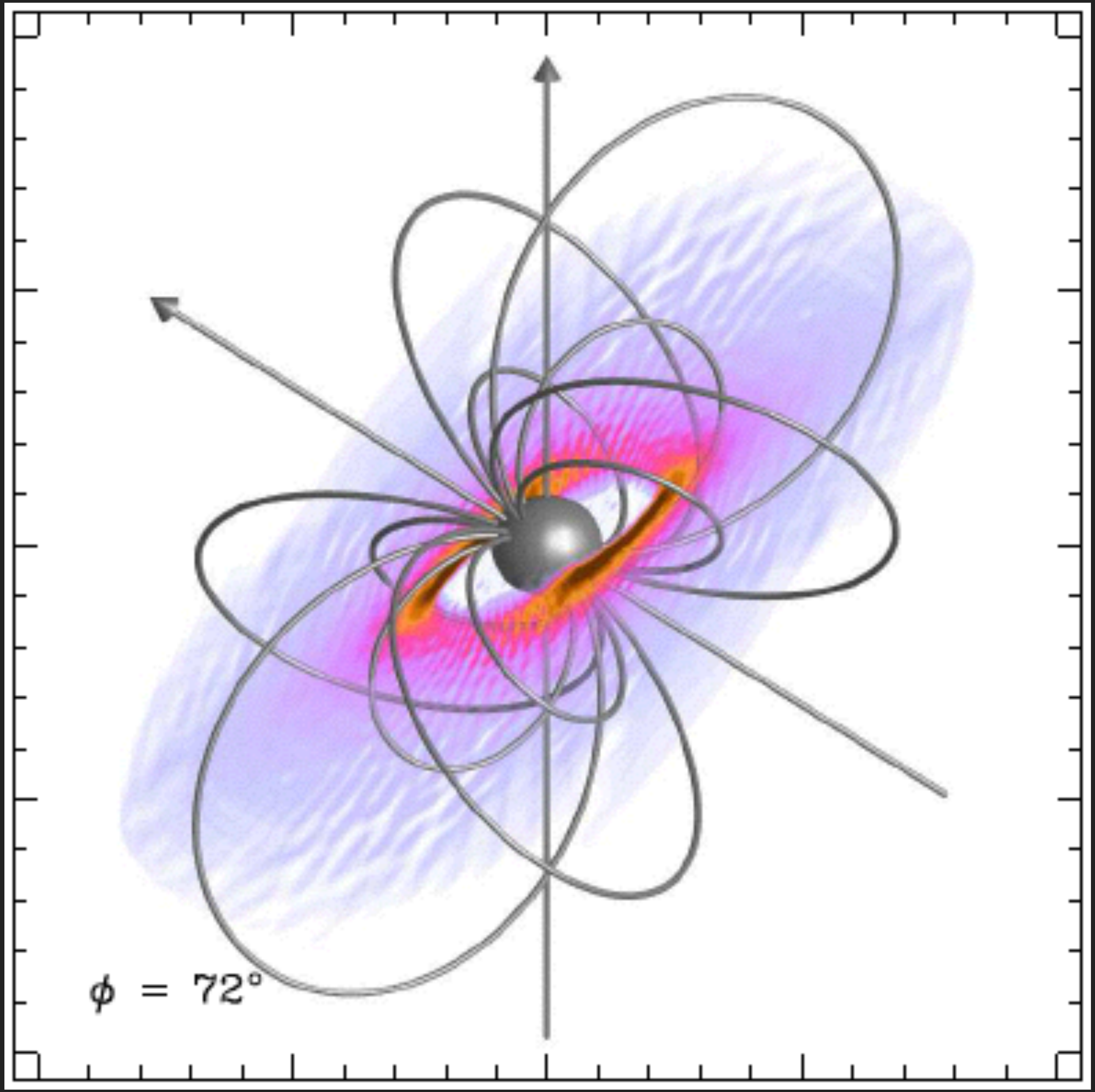

RRM model, Richard Townsend

A SUBSET OF MASSIVE STARS HAVE LARGE-SCALE MAGNETIC FIELDS

about 10% and the fields appear to be "fossil" fields

– no active dynamo

MHD simulation, Asif ud-Doula

http://astro.swarthmore.edu/~cohen/presentations/t1oc-lowvinf-logd_new.m4v

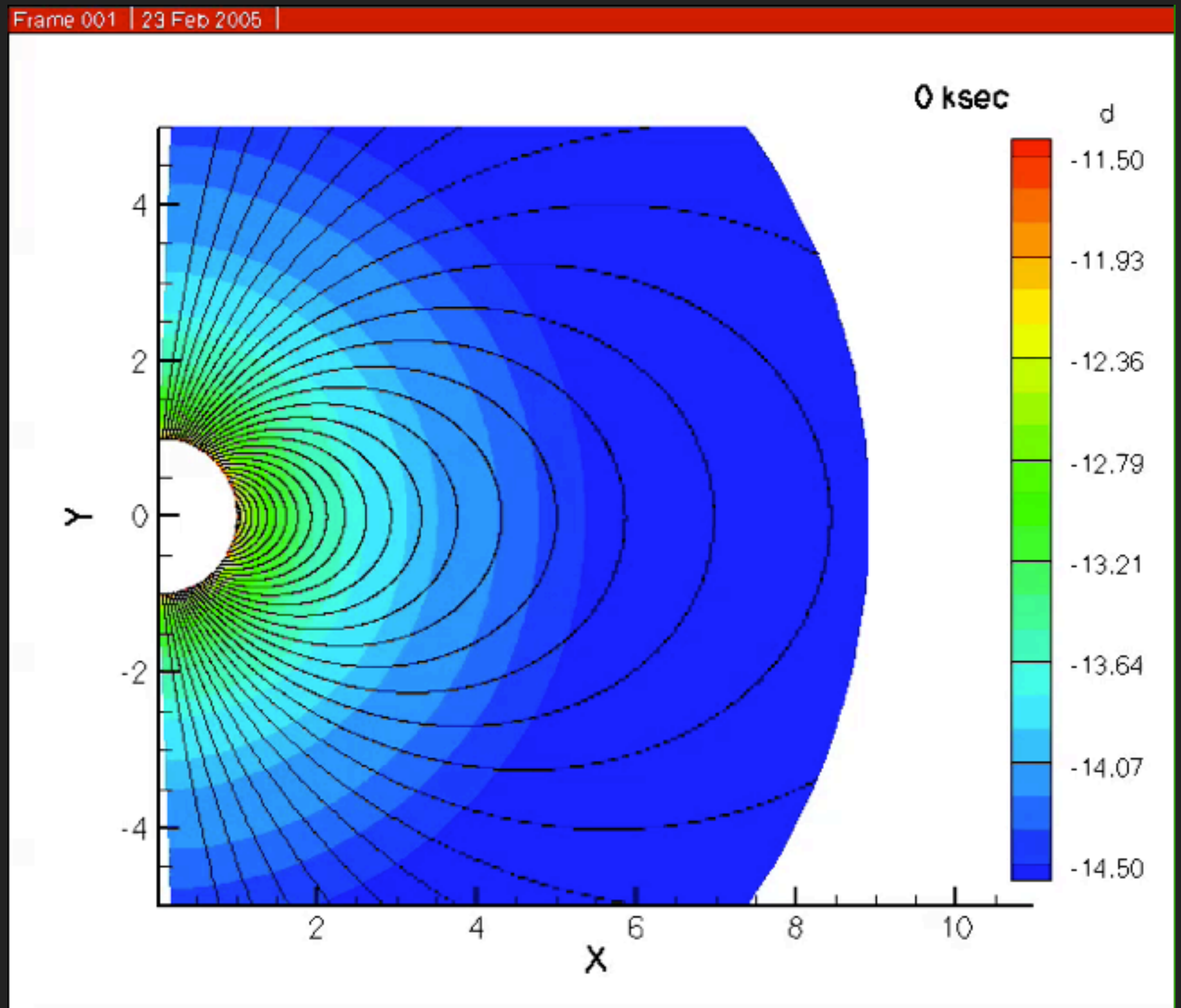

A SUBSET OF MASSIVE STARS HAVE LARGE-SCALE MAGNETIC FIELDS

Wind flows from two hemispheres collide:

shock heating to > 10^7 K

MHD simulation, Asif ud-Doula

http://astro.swarthmore.edu/~cohen/presentations/t1oc-lowvinf-logT_new.m4v

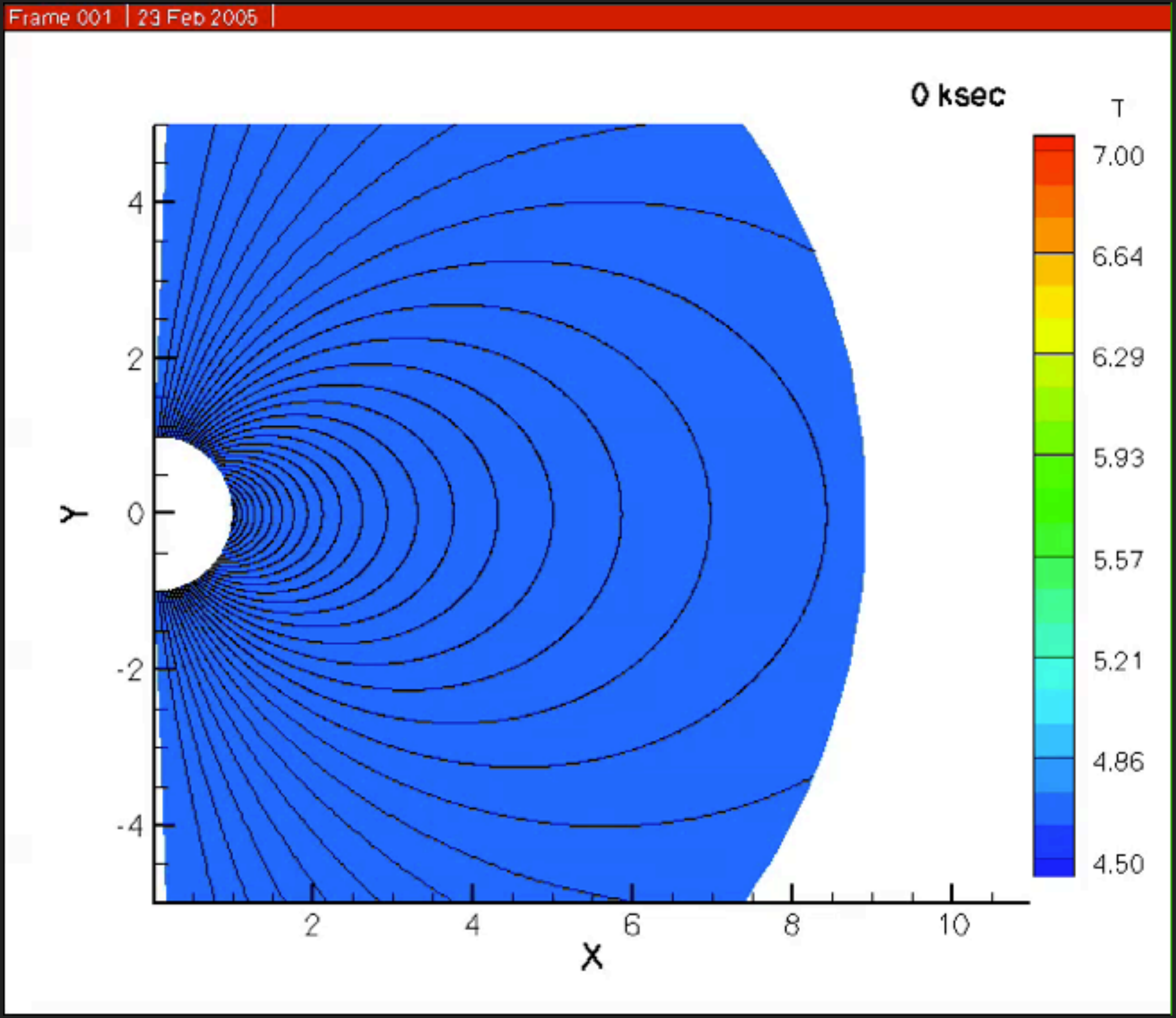

A SUBSET OF MASSIVE STARS HAVE LARGE-SCALE MAGNETIC FIELDS

Wind flows from two hemispheres collide:
shock heating to > 10^7 K

MHD simulation, Asif ud-Doula

hotter than seen in EWS

temperature

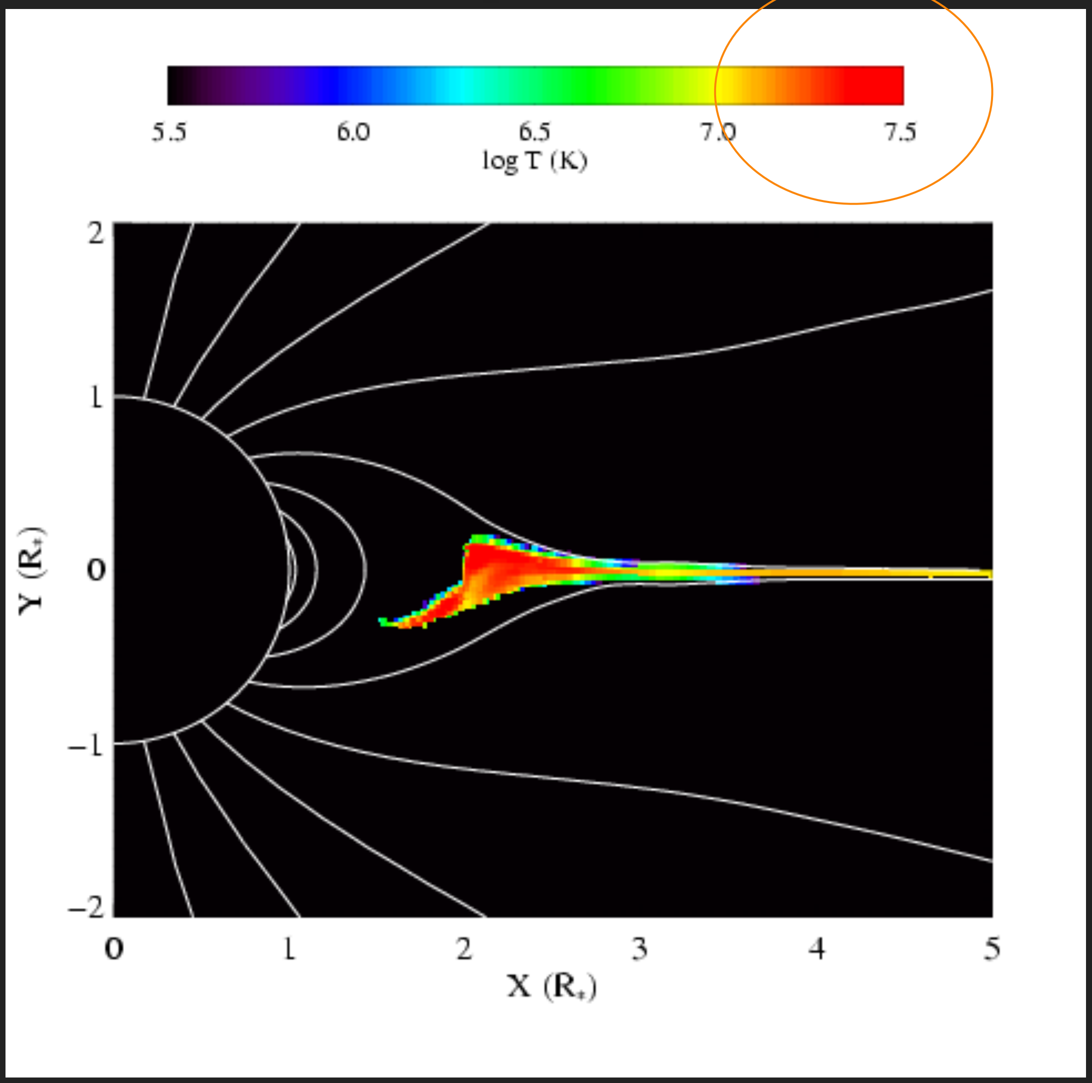

emission measure

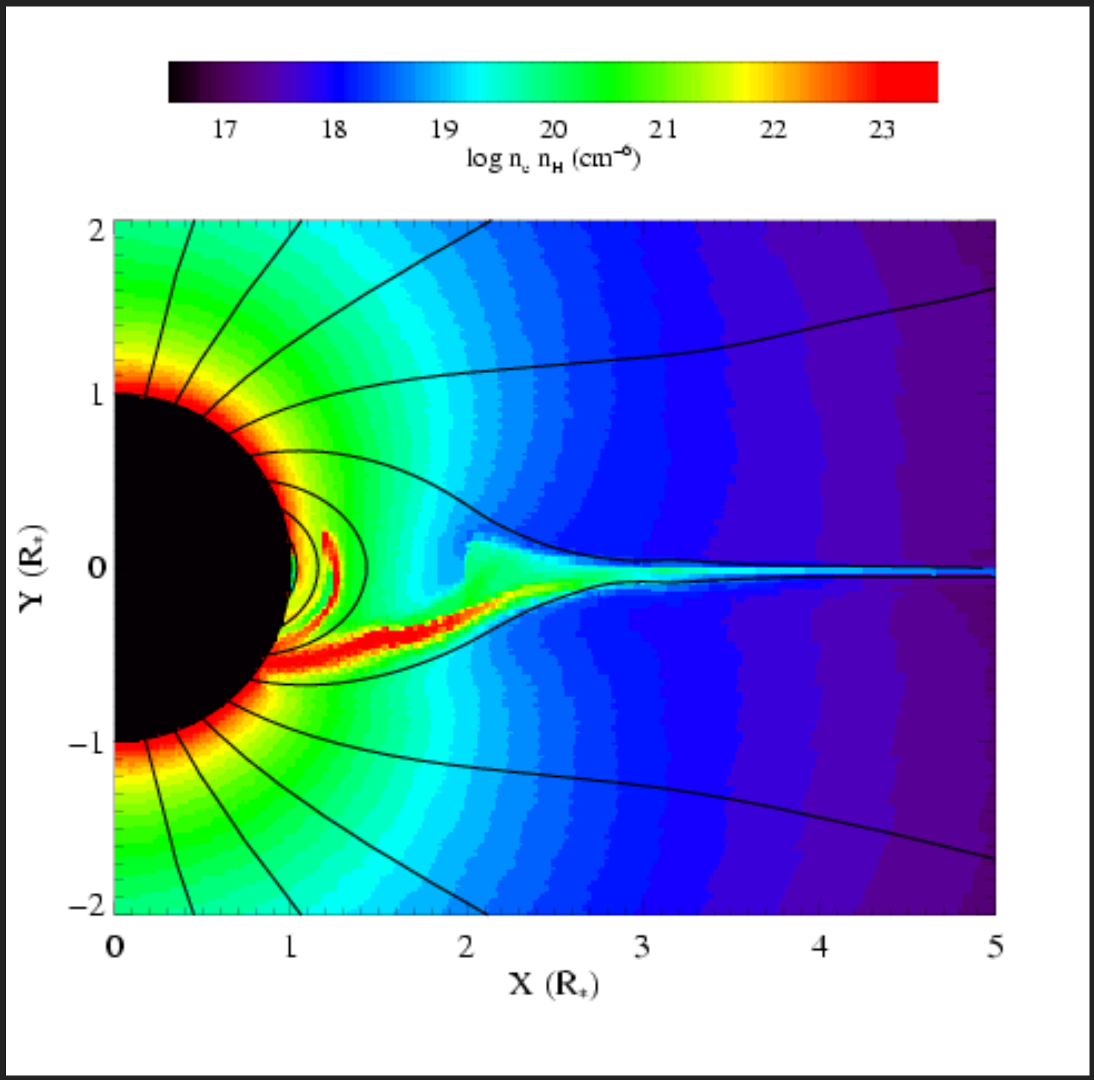

X-RAYS ARE HARDER AND LINES ARE NARROWER

shocked plasma is confined by the magnetic field

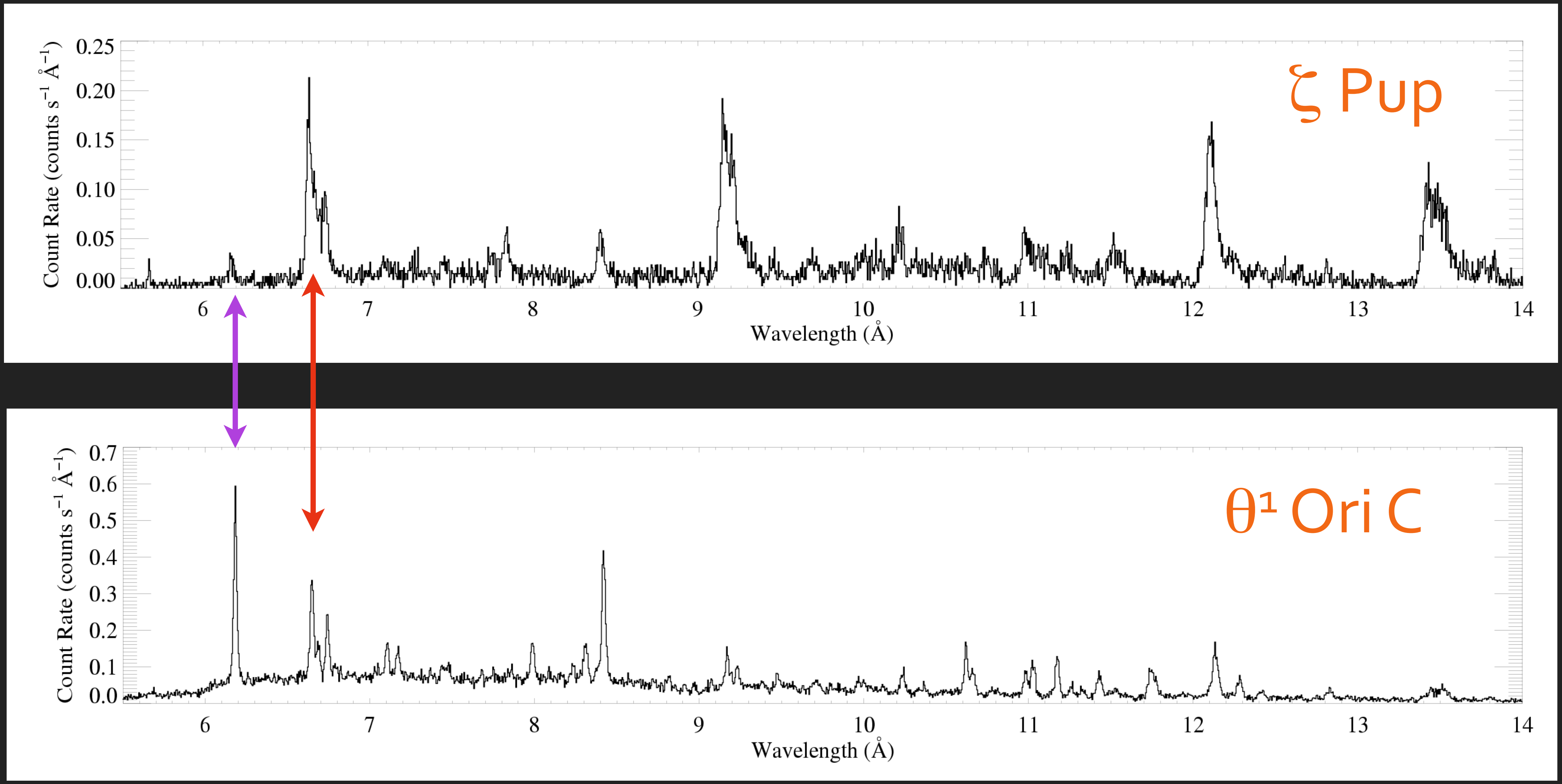

NGC 1624–2: O STAR WITH A GIANT MAGNETOSPHERE

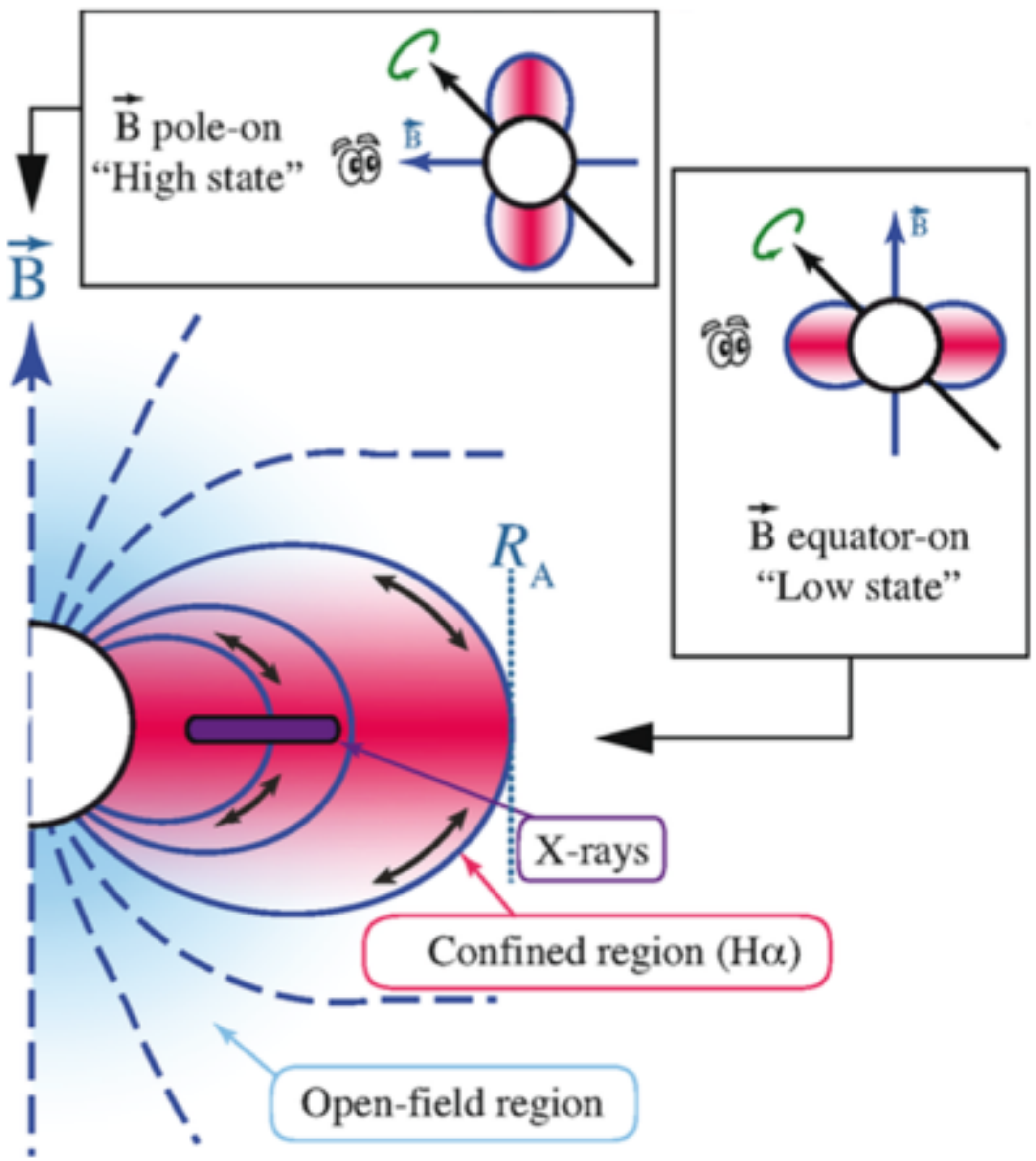

Figure 1. Schematic of a magnetic massive star dynamical magnetosphere (e.g. Sundqvist et al. 2012; Petit et al. 2013). Solid blue lines indicate regions below the last closed magnetic loop that confine the wind, located near the Alfvén radius R_A. Most of the Hα emission originates here. Dashed lines indicate regions where the momentum of the wind results in open field lines. The bulk of the X-rays are produced in the region indicated in purple; see Section 6. The insets illustrate the view of an observer as the star's rotation changes the orientation of the magnetosphere. It is important to note that due to the long rotation periods of magnetic O-type stars, the dynamical effects of rotation on the magnetospheric structure are negligible (ud-Doula, Owocki & Townsend 2008).

Monthly Notices of the ROYAL ASTRONOMICAL SOCIETY
MNRAS 453, 3288–3299 (2015) doi:10.1093/mnras/stv1741

X-ray emission from the giant magnetosphere of the magnetic O-type star NGC 1624-2

V. Petit,[1★] D. H. Cohen,[2] G. A. Wade,[3] Y. Nazé,[4†] S. P. Owocki,[5] J. O. Sundqvist,[5] A. ud-Doula,[6] A. Fullerton,[7] M. Leutenegger[8,9] and M. Gagné[10]

[1] *Department of Physics and Space Sciences, Florida Institute of Technology, Melbourne, FL 32904, USA*
[2] *Department of Physics and Astronomy, Swarthmore College, Swarthmore, PA 19081, USA*
[3] *Department of Physics, Royal Military College of Canada, PO Box 17000, Stn Forces, Kingston, Ontario K7K 7B4, Canada*
[4] *GAPHE, Université de Liège, Quartier Agora, Allée du 6 Août 19c, Bat. B5C, B-4000 Liège, Belgium*
[5] *Department of Physics and Astronomy, University of Delaware, Bartol Research Institute, Newark, DE 19716, USA*
[6] *Penn State Worthington Scranton, Dunmore, PA 18512, USA*
[7] *Space Telescope Science Institute, 3700 San Martin Dr, Baltimore, MD 21218, USA*
[8] *NASA/Goddard Space Flight Center, Code 662, Greenbelt, MD 20771, USA*
[9] *CRESST and University of Maryland, Baltimore County, Baltimore, MD 21250, USA*
[10] *Department of Geology and Astronomy, West Chester University, West Chester, PA 19383, USA*

Accepted 2015 July 28. Received 2015 July 6; in original form 2015 May 15

ABSTRACT

We observed NGC 1624-2, the O-type star with the largest known magnetic field ($B_p \sim 20$ kG), in X-rays with the Advanced CCD Imaging Spectrometer (ACIS-S) camera on-board the Chandra X-ray Observatory. Our two observations were obtained at the minimum and maximum of the periodic Hα emission cycle, corresponding to the rotational phases where the magnetic field is the closest to equator-on and pole-on, respectively. With these observations, we aim to characterize the star's magnetosphere via the X-ray emission produced by magnetically confined wind shocks. Our main findings are as follows. (i) The observed spectrum of NGC 1624-2 is hard, similar to the magnetic O-type star θ^1 Ori C, with only a few photons detected below 0.8 keV. The emergent X-ray flux is 30 per cent lower at the Hα minimum phase. (ii) Our modelling indicated that this seemingly hard spectrum is in fact a consequence of relatively soft intrinsic emission, similar to other magnetic Of?p stars, combined with a large amount of local absorption (~1–3× 10^{22} cm^{-2}). This combination is necessary to reproduce both the prominent Mg and Si spectral features, and the lack of flux at low energies. NGC 1624-2 is intrinsically luminous in X-rays (log $L_X^{em} \sim 33.4$) but 70–95 per cent of the X-ray emission produced by magnetically confined wind shocks is absorbed before it escapes the magnetosphere (log $L_X^{ISMcor} \sim 32.5$). (iii) The high X-ray luminosity, its variation with stellar rotation, and its large attenuation are all consistent with a large dynamical magnetosphere with magnetically confined wind shocks.

NGC 1624-2: O STAR WITH A GIANT MAGNETOSPHERE

magnetospheric X-ray absorption in the edge-on view

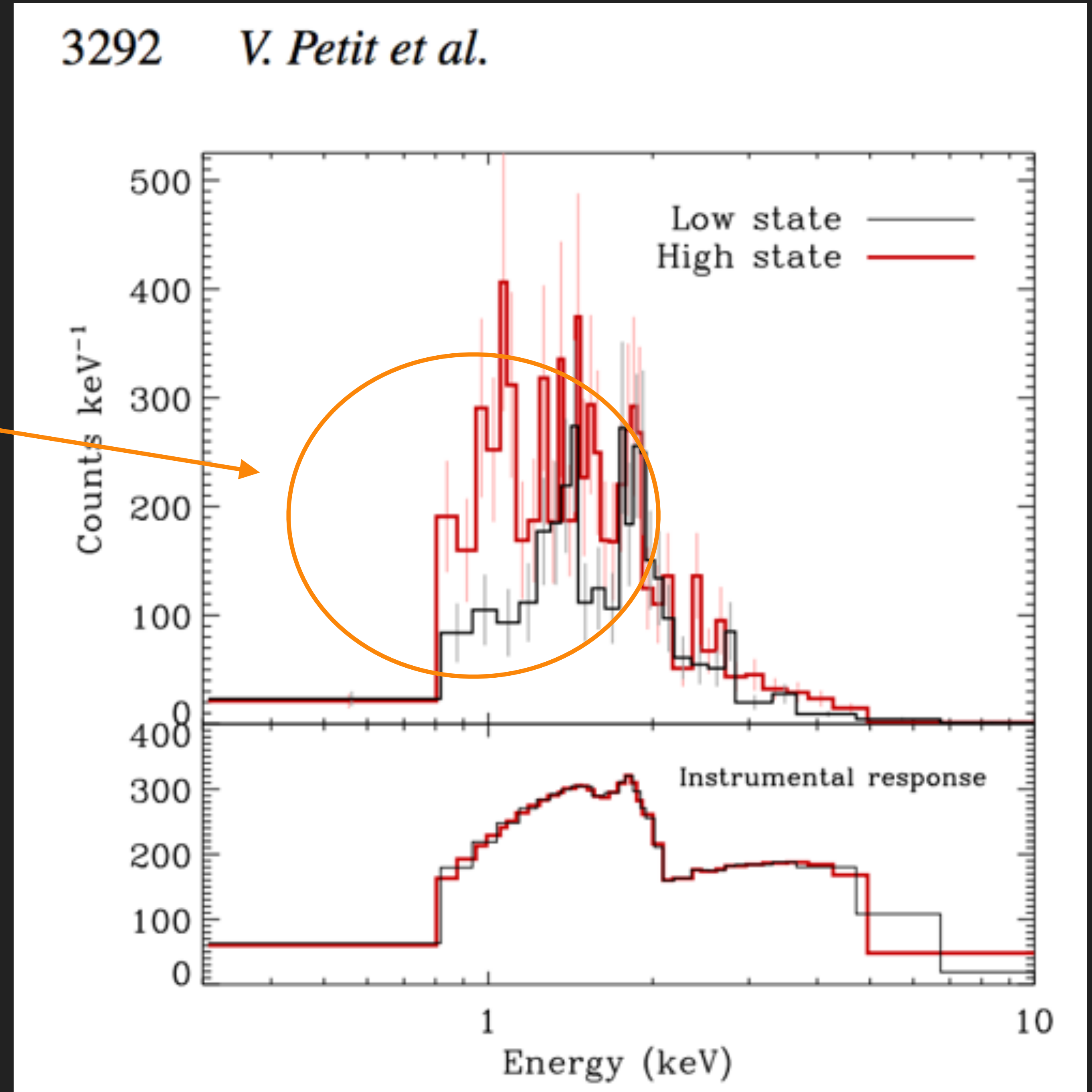

Figure 5. ACIS-S spectra of NGC 1624-2 during the low state (thin black) and the high state (thick red). The bottom panel shows a representation of the instrumental response, i.e. the spectra that would be observed if the emission model was flat. The small differences between the two epochs are caused by slight variations in response and adaptive signal-to-noise binning.

CAN LARGE SCALE MAGNETIC FIELDS EXPLAIN MASSIVE BLACK HOLES?

Just submitted!

Mon. Not. R. Astron. Soc. **000**, 1–10 (2010) Printed 25 October 2016 (MN LaTeX style file v2.2)

Magnetic massive stars as progenitors of “heavy” stellar-mass black holes

Petit, V. [1*], Keszthelyi, Z.[2,3], MacInnis, R.[1], Cohen, D. H.[4], Townsend, R. H. D.[5], Wade, G. A.[2], Thomas, S. L.[1], Owocki, S. P.[6], Puls, J.[7], ud-Doula, A.[8]

[1] *Department of Physics and Space Sciences, Florida Institute of Technology, 150 W. University Blvd, Melbourne, FL 32904*
[2] *Department of Physics, Royal Military College of Canada, PO Box 17000 Station Forces, Kingston, ON, Canada K7K 0C6*
[3] *Department of Physics, Engineering Physics and Astronomy, Queen's University, 99 University Avenue, Kingston, ON K7L 3N6, Canada*
[4] *Department of Physics and Astronomy, Swarthmore College, Swarthmore, PA 19081, USA*
[5] *Department of Astronomy, University of Wisconsin-Madison, 5534 Sterling Hall, 475 N Charter Street, Madison, WI 53706, USA*
[6] *Department of Physics and Astronomy, University of Delaware, Newark, DE, 19711, USA*
[7] *LMU Munich, Universitäts-Sternwarte, Scheinerstr. 1, 81679, München, Germany*
[8] *Penn State Worthington Scranton, Dunmore, PA 18512, USA*

Accepted ?. Received 2016 October 24; in original form 2016 October 24

ABSTRACT

The groundbreaking detection of gravitational waves produced by the inspiralling and coalescence of the black hole (BH) binary GW150914 confirms the existence of “heavy” stellar-mass BHs with masses $> 25\,M_\odot$. Initial modelling of the system by Abbott et al. (2016a) supposes that the formation of black holes with such large masses from the evolution of single massive stars is only feasible if the wind mass-loss rates of the progenitors were greatly reduced relative to the mass-loss rates of massive stars in the Galaxy, concluding that heavy BHs must form in low-metallicity ($Z \lesssim 0.25 - 0.5\ Z_\odot$) environments. However, strong surface magnetic fields also provide a powerful mechanism for modifying mass loss and rotation of massive stars, independent of environmental metallicity (ud-Doula & Owocki 2002; ud-Doula et al. 2008). In this paper we explore the hypothesis that some heavy BHs, with masses $> 25\,M_\odot$ such as those inferred to compose GW150914, could be the natural end-point of evolution of magnetic massive stars in a solar-metallicity environment. Using the MESA code, we developed a new grid of single, non-rotating, solar metallicity evolutionary models for initial ZAMS masses from 40-80 $M_\odot$ that include, for the first time, the quenching of the mass loss due to a realistic dipolar surface magnetic field. The new models predict TAMS masses that are significantly greater than those from equivalent non-magnetic models, reducing the total mass lost by a strongly magnetized 80 $M_\odot$ star during its main sequence evolution by 20 $M_\odot$. This corresponds approximately to the mass loss reduction expected from an environment with metallicity $Z = 1/30\,Z_\odot$.

CAN LARGE SCALE MAGNETIC FIELDS EXPLAIN MASSIVE BLACK HOLES?

closed field regions trap wind material, reducing mass loss

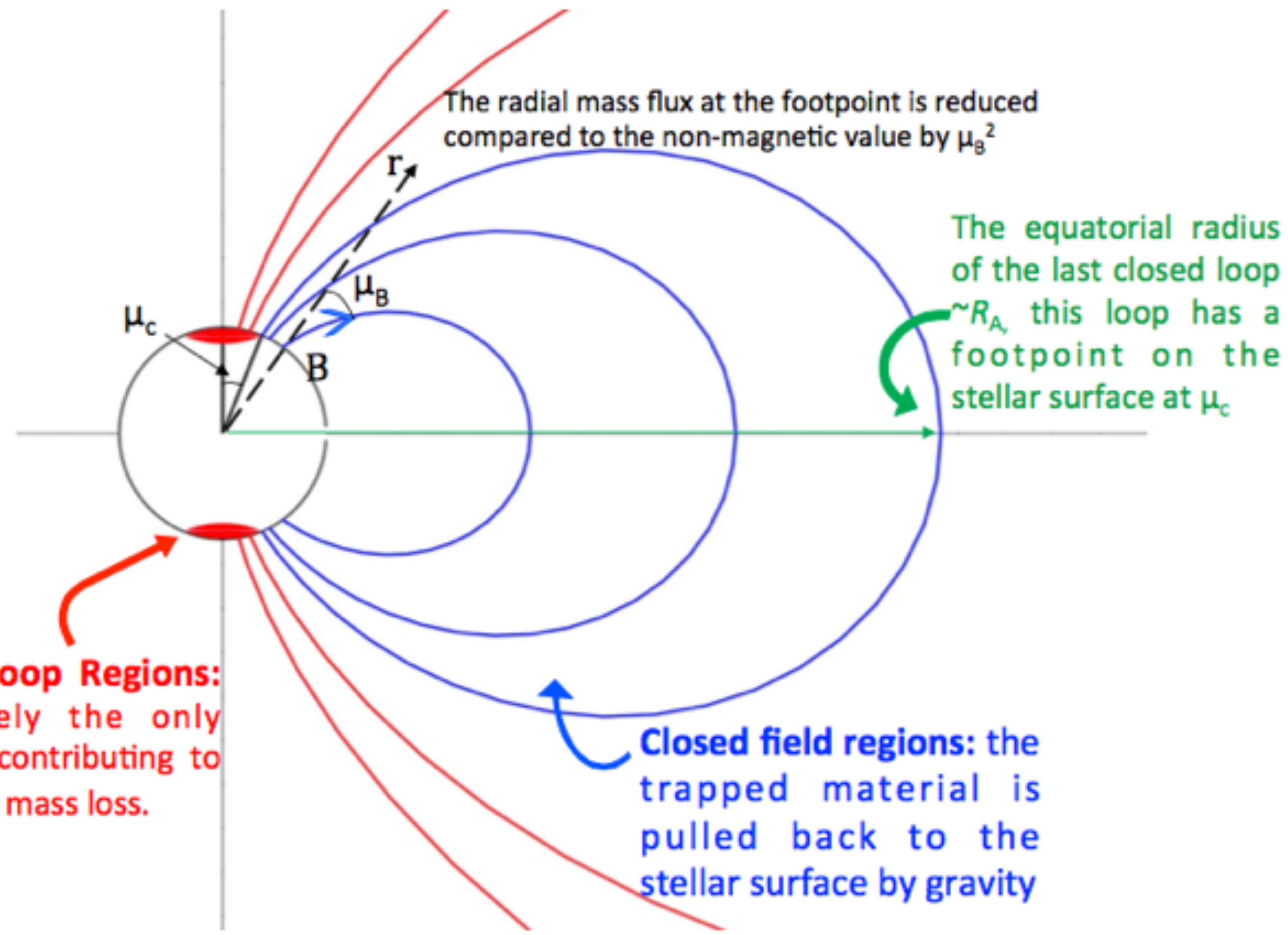

Figure 1. Schematic representation of the circumstellar magnetosphere of a slowly-rotating magnetic massive star, based on the description of ud-Doula & Owocki (2002); ud-Doula et al. (2008). The equatorial radius of the last closed loop is given by the closure radius R_c, which is on the order of the Alfvén radius R_A where the magnetic energy density balances the wind kinetic energy density.

CAN LARGE SCALE MAGNETIC FIELDS EXPLAIN MASSIVE BLACK HOLES?

strong field cause up to 20 additional solar masses to be retained

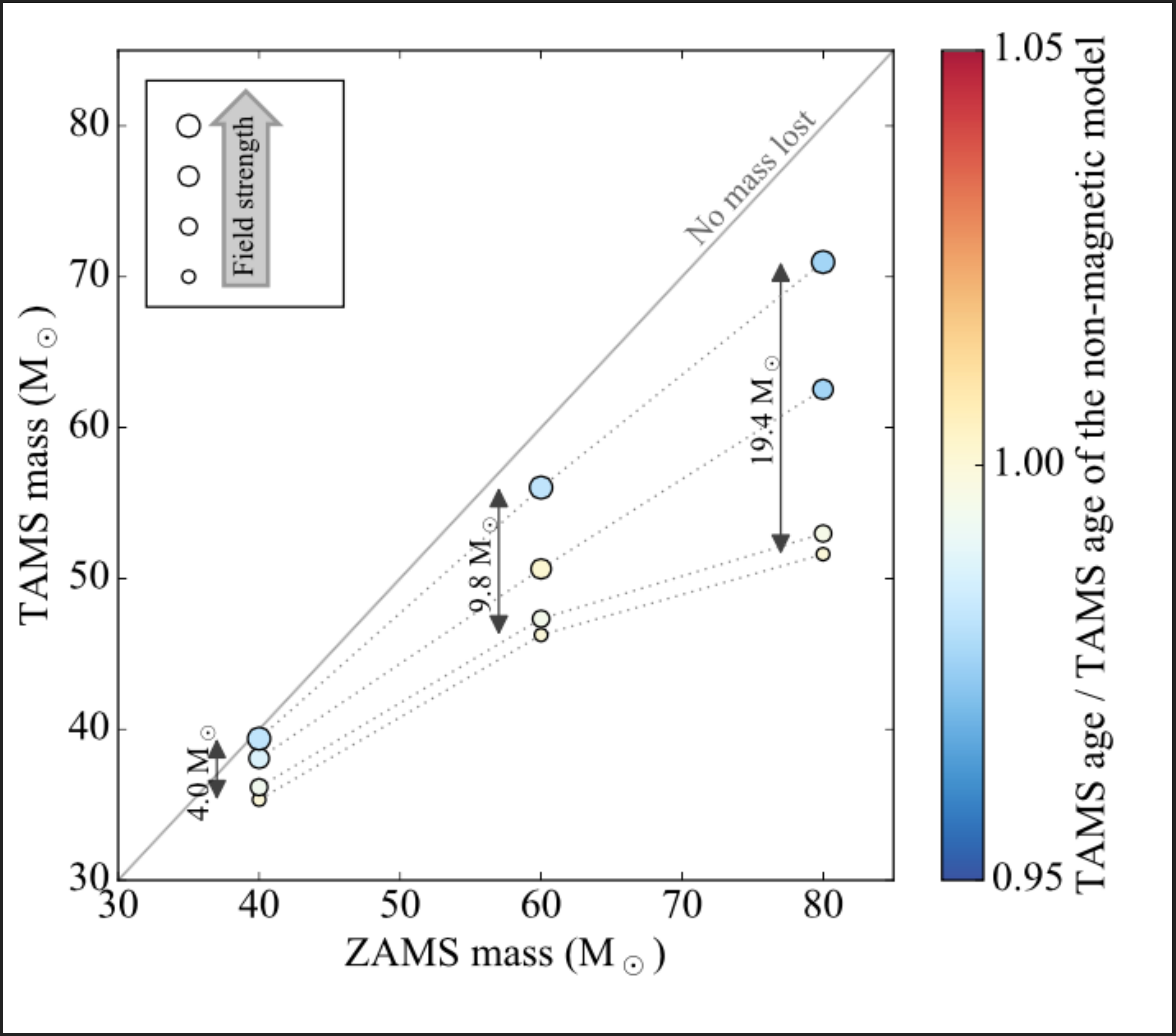

MASSIVE STAR WINDS VIA X-RAY SPECTROSCOPY

wind *plus magnetic fields* have significant effects

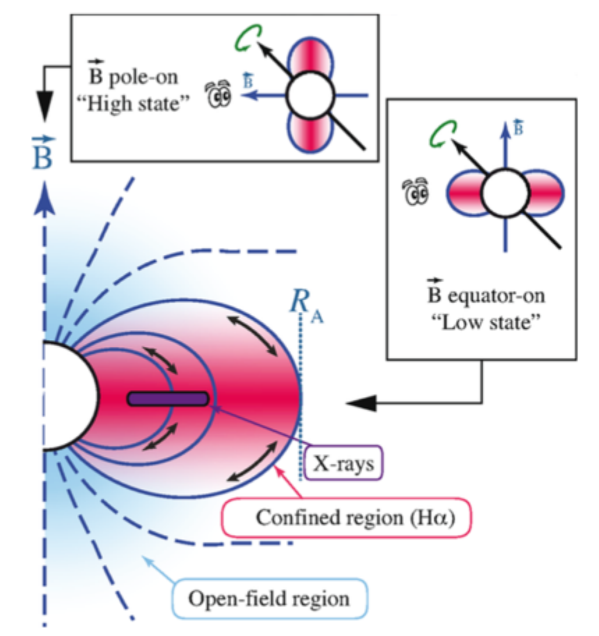

Figure 1. Schematic of a magnetic massive star dynamical magnetosphere (e.g. Sundqvist et al. 2012; Petit et al. 2013). Solid blue lines indicate regions below the last closed magnetic loop that confine the wind, located near the Alfvén radius R_A. Most of the Hα emission originates here. Dashed lines indicate regions where the momentum of the wind results in open field lines. The bulk of the X-rays are produced in the region indicated in purple; see Section 6. The insets illustrate the view of an observer as the star's rotation changes the orientation of the magnetosphere. It is important to note that due to the long rotation periods of magnetic O-type stars, the dynamical effects of rotation on the magnetospheric structure are negligible (ud-Doula, Owocki & Townsend 2008).

3292 *V. Petit et al.*

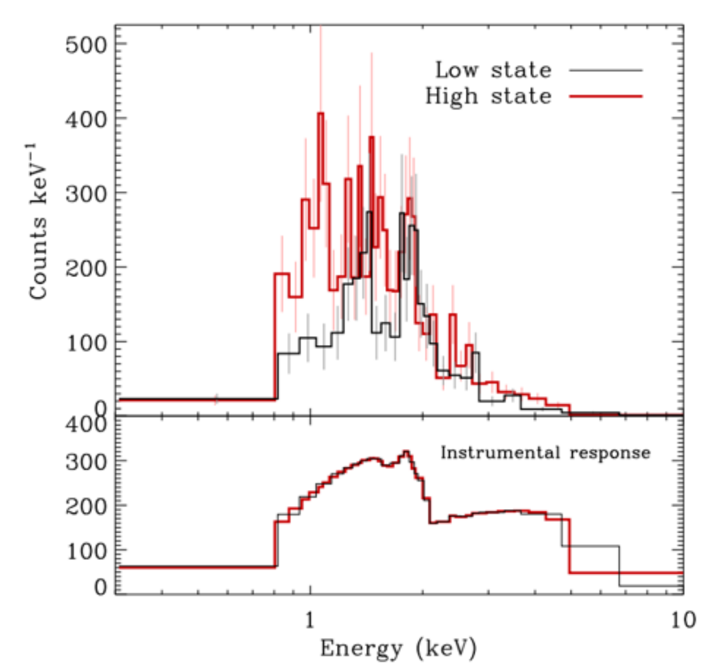

Figure 5. ACIS-S spectra of NGC 1624-2 during the low state (thin black) and the high state (thick red). The bottom panel shows a representation of the instrumental response, i.e. the spectra that would be observed if the emission model was flat. The small differences between the two epochs are caused by slight variations in response and adaptive signal-to-noise binning.